

BALTON SEA SCALES





Database Search Index Thesaurus Logout Help

GeoRef Disc 5: 1997-1999/06 GeoRef Disc 4: 1993-1996 GeoRef Disc 3: 1985-1992 GeoRef Disc 2: 1975-1984 GeoRef Disc 1: 1785-1974 GeoRef Serials

Results: 1 to 4 of 4

Search: (Darrell Gallup) in AU,CA

Gallup Refs

Previous 10 Next 10 Show Marked Print... Save... Change Display

Copyright Information

Record 1 of 4 in GeoRef Disc 5: 1997-1999/06

TITLE

Aluminum silicate scale formation and inhibition; (2), Scale solubilities and laboratory and field inhibition tests.

AUTHORS

Gallup-Darrell-L

SOURCE

Geothermics.27; 4, Pages 485-501. 1998. .

PUBLISHER

Pergamon Press. Oxford - New York, International. 1998.

PUBLICATION YEAR

1998

ACCESSION NUMBER

99-02764 .

Record 2 of 4 in GeoRef Disc 5: 1997-1999/06

TITLE

Geochemistry of geothermal fluids and well scales, and potential for mineral recovery.

AUTHORS

Gallup-Darrell-L

SOURCE

Ore Geology Reviews.12; 4, Pages 225-236. 1998. .

PUBLISHER

Elsevier. Amsterdam, International. 1998.

PUBLICATION YEAR

1998

ABSTRACT

Although the potential use of geothermal brines for simultaneous energy and mineral production is significant, only a few mineral recovery systems are currently in commercial operation. Selected metal concentrations reported in fluids and scale deposits that are of interest to economic geologists include the following. Geothermal fluids and scale deposits vary considerably in composition. Hyper-saline geothermal fluids encountered primarily in sedimentary basins exhibit significant concentrations of minerals. In many locations near active volcanoes, concentrations of valuable metals are too low to be detected or have not been reported. Metal transport and mobility in geothermal fluids is commonly constrained by concentrations of ligands, temperatures, pH and redox state. Natural or controlled precipitation of minerals from geothermal fluids commonly occurs by decreasing temperature/boiling, dilution, increasing pH, reaction with sulfides and redox reactions. To date, the vast majority of mineral recovery projects have been conducted at the laboratory and pilot scale. New processes and technologies to recover minerals from geothermal fluids may be developed in the future in an effort to improve the economics, development and

sustainability of geothermal resources.

ACCESSION NUMBER

98-69761 .

Record 3 of 4 in GeoRef Disc 1: 1785-1974

TITLE

Soil development related to glacial outwash near Gilmore, Idaho.

AUTHORS

Gallup-Darrell-L

SOURCE

Tebiwa.5; 2, Pages 18-22. 1962. .

PUBLISHER

[Idaho State University Museum of Natural History]. [Pocatello, ID], United States. 1962.

PUBLICATION YEAR

1962

ACCESSION NUMBER

62-11337 .

Record 4 of 4 in GeoRef Disc 1: 1785-1974

TITLE

Soil development related to glacial outwash near Gilmore, Idaho.

AUTHORS

Gallup-Darrell-L

SOURCE

Tebiwa.5; 2, Pages 18-22. 1962. .

PUBLISHER

[Idaho State University Museum of Natural History]. [Pocatello, ID], United States. 1962.

PUBLICATION YEAR

1962

ACCESSION NUMBER

66-13565 .

Previous 10	Next 10	Show Marked	Print...	Save...	Change Display
-------------	---------	-------------	----------	---------	----------------



Database	Search	Index	Thesaurus	Logout	Help
----------	--------	-------	-----------	--------	------

GeoRef Disc 5: 1997-1999/06
 GeoRef Disc 4: 1993-1996
 GeoRef Disc 3: 1985-1992
 GeoRef Disc 2: 1975-1984
 GeoRef Disc 1: 1785-1974
 GeoRef Serials



Copyright 1996, 1997, SilverPlatter International NV, *WebSPIRS* Version 3.1.
 Send your comments to WebSPIRS@SilverPlatter.com, referencing "Search".

TITLE

Characterization of geothermal scale deposits by Fe-57 Moessbauer spectroscopy and complementary X-ray diffraction and infra-red studies.

AUTHORS

Gallup-D-L; Reiff-W-M

SOURCE

Geothermics.20; 4, Pages 207-224. 1991. .

PUBLISHER

Pergamon Press. Oxford - New York, International. 1991.

PUBLICATION YEAR

1991

ACCESSION NUMBER

91-56778 .

 Record 4 of 5 in GeoRef Disc 3: 1985-1992
TITLE

The solubility of amorphous silica in geothermal brines.

AUTHORS

Gallup-D-L

BOOK TITLE

In: The Geysers; three decades of achievement; a window on the future.

BOOK AUTHORS

Von-Hoene-Jack (chairperson)

SOURCE

Transactions - Geothermal Resources Council. 13; Pages 241-245. 1989. .

PUBLISHER

Geothermal Resources Council. Davis, CA, United States. 1989.

PUBLICATION YEAR

1989

ACCESSION NUMBER

90-15293 .

 Record 5 of 5 in GeoRef Disc 2: 1975-1984
TITLE

Idaho case study; existing monitoring activities and research.

AUTHORS

Marcus-Linda-Graves-(compiler); MacDonald-S-B; Hancock-A; Hagius-C-F; Thomas-C-A; Moreland-J-A; Roberson-C-E; LaSala-A-M Jr.; Mehrhoff-L-A; Frandsen-O-A; Bradley-G; Kelly-D; Platts-W-S; Dalton-A-E; Primbs-E-R-J; Gallup-D-L; Debruyne-D; Schmidt-B; Geran-E-E; Ralston-D-R; Oldenburg-L-E; Boothe-G-F; Perry-J; Hopson-G-J; Stolz-R-K

BOOK TITLE

In: A methodology for post-EIS monitoring.

BOOK AUTHORS

Marcus-Linda-Graves (compiler)

SOURCE

Pages; variously paginated. 1976. .

PUBLICATION YEAR

1976

ACCESSION NUMBER

88-34866 .

TASK 4 : CHEMICAL, MINERALOGICAL, AND TEXTURAL CHARACTERIZATION OF SCALES FROM SALTON SEA WELLS

PROJECT DESCRIPTION AND OBJECTIVES

Before an effective, and possibly expensive, scale mitigation program can be designed or implemented, the processes that cause the formation of the scales must be well understood. The first step in this understanding is to examine the scales themselves and to document in detail their mineralogical, chemical and textural characteristics. These characteristics may vary depending upon where the wells are located in the Salton Sea geothermal field and at what depth the scales formed within the wells. Scales also form in some of the surface and power production facilities. This project is directed towards understanding the zinc-rich scales at CalEnergy's East Mesa plant.

We propose to carry out a detailed characterization of the metal-rich scales using X-ray diffraction (XRD) and electron microprobe analyses to characterize the mineralogy and mineralogic zoning, inductively coupled plasma (ICP) analyses to determine the chemistry and elemental abundances, and scanning electron microscopy (SEM) and thin-section analyses to document and describe the textural/mineralogical relationships. Once these characteristics are known, some inferences can be made concerning the chemical processes that caused their formation, and an appropriate scale mitigation program can be designed.

WORK PLAN - COSTS

Outside Analyses / Costs

10 samples for ICP	@ \$100 = \$1000
10 samples for microprobe & SEM	@ \$200 = \$ 2000
20 thin-sections	@ \$ 20 = \$ 400

Personnel

Susan Lutz (XRD, SEM, microprobe analyses)	10%
Joe Moore (sample collection, geochem interp)	10%?
Louise Spann (XRD)	5%

DELIVERABLES

The results of this study will be incorporated into a descriptive report for CEC, and may also be presented to the general geothermal community at next year's GRC conference.

Scale proposal
- See Lists.

Project Title: Chemical, Mineralogical, and Textural Characterization of Scales from Salton Sea Wells

Objective:

Before an effective, and possibly expensive, scale mitigation program can be designed or implemented, the processes that cause the formation of the scales must be well understood. The first step in this understanding is to examine the scales themselves and to document in detail their mineralogical, chemical and textural characteristics. These characteristics may vary depending upon where the wells are located in the Salton Sea geothermal field and at what depth the scales formed within the wells. Scales also form in some of the surface and power production facilities.

Scales deposited in the upper portions of wells and in surface plumbing are dominated by an amorphous iron silicate phase similar to hisingerite [$\text{Fe}(\text{OH})_3 \cdot \text{SiO}_2$] (Gallup, 1989, 1993; Gallup and Reiff, 1991), along with lesser galena and other sulfides (McKibben et al., 1990). Scales deposited on downhole steel liners near the flashpoint (point of initiation of steam + liquid flow in the well) consist largely of magnetite and loellingite (FeAs_2) and may contain up to 40 wt % As, 2 wt % Bi, 1 wt % U, 0.1 wt % Au, as well as high concentrations of other heavy metals (McKibben et al., 1990). The flashpoint deposits suggest that significant fractions of the trace Au and U in the brines are transported as complexes that become rapidly destabilized by gas loss during phase separation, such as Au-HS^- , U-CO_3^{2-} , and possibly, Au-As or Au- NH_3 complexes.

McKibben lists the chemical composition of magnetite-loellingite downhole liner scales that formed at or near the flashpoint in two SSGS wells (CW-11 and CW-14). He notes that platinum group elements (PGE) are present in the brines at concentrations similar to Au but that PGEs are not found in the flashpoint scales. He suggests that the PGE are transported by complexes that are not affected by gas loss (such as Cl^-) and/or that PGE precipitation is inhibited kinetically compared with Au. McKibben concludes that this contrast in behavior of Au and PGE remains as strong empirical evidence that very different complexes are transporting these two types of metals in the SSGS brines.

Although the genesis of the metalliferous brines in the Salton Sea geothermal system has been extensively studied (especially by McKibben), the chemistry of the scales themselves has not. However, before we can understand the processes of formation of the different kinds of scales, it is necessary to understand what kinds of minerals the scales contain and in which order they were precipitated. We propose to carry out a detailed characterization of the metal-rich scales using X-ray diffraction (XRD) and electron microprobe analyses to characterize the mineralogy and mineralogic zoning, inductively coupled plasma (ICP) analyses to determine the chemistry and elemental abundances, and scanning electron microscopy (SEM) and thin-section analyses to document and describe the textural/mineralogical relationships. Once these characteristics are known, some inferences can be made concerning the chemical processes that caused their formation, and an appropriate scale mitigation program can be designed.

Description:

We will perform a variety of analytical techniques upon scale samples provided to us by CalEnergy. A half-dozen to a dozen samples will be analyzed; these may represent mineralogically-different scales from a variety of depositional environments, or multiple scales from a particularly troublesome area (depending upon the needs of CalEnergy). We will study the chemical, mineralogical and textural characteristics of these scales using XRD, ICP, SEM, microprobe and petrographic techniques. If possible, we may also carry out some fluid inclusion analyses.

This project may be considered Phase I of a larger study that would address the geochemistry of the scales and would, presumably, entail a considerable amount of geochemical modelling of the scale formation based on both the fluid and scale chemistry.

Schedule:

After we receive the samples from CalEnergy and depending upon how many samples are to be described and the mineralogical complexity of the scales, it will take about a year to fully analyze these scales. At that point, either more scales from a different area could be described, or if enough mineralogical/chemical data had been obtained, we could move into Phase II, the geochemical modelling study.

Performers:

Susan Lutz
Joe Moore
EGI- University of Utah

References:

Gallup, D.L., 1989, Iron silicate scale formation and inhibition at the Salton Sea geothermal field, *Geothermics*, v. 18, p. 97-103.

Gallup, D.L., and W.M. Reiff, 1991, Characterization of geothermal scale deposits by 57 Fe Mossbauer spectroscopy and complementary X-ray diffraction and infra-red studies: *Geothermics*, v. 20, p. 207-224.

Lutz, S.J., 1994, Petrographic analysis of scale and formation drill cuttings from the Salton Sea field, Injection Well Sinc-22: proprietary report for Joe Hickey and Alex Schriener Jr, Magma Power Company, March 1994, 6 pg. report with 44 photomicrographs and thin-section descriptions.

McKibben, M.A., Williams, A.E., and G.E.M. Hall, 1990, Solubility and transport of platinum-group elements and Au in saline hydrothermal fluids: constraints from geothermal brine data: *Econ. Geol.*, v. 85, p. 1926-1934.

Subject: Salton Sea Scale Study

Date: Fri, 08 Jan 1999 10:09:01 -0600

From: mark.walters@calenergy.com

To: sjlutz@esri.esri.utah.edu

Sue-

Your proposal for the study of scales at the Salton Sea is approved and I will be preparing an "official" letter from CalEnergy to document this.

Samples will be provided to you on the condition that you handle them as you would "hazardous" ore materials. We will need to set up a date to get together to determine the specific samples sets and accompanying reservoir data.

I will be talking to you shortly on this matter.

Cheers,
Mark

Mineralogy, Approx. Wt.% (or) Relative Abundance

Salton Sea -
scale samples
carbon steel well
liner scale

Sample No.

Safflorite, syn
Loellingite, syn
Palladobismuth
arsenide, syn
Bismuth, syn
Sphalerite
Chalcopyrite
*1.45A phase
Amorphous/
Below Detection

RR-18 outside

* M M tr 4 tr m -

RR-18 inside

* M M tr tr 4 tr m -

Safflorite, syn:
(Co, Fe) As₂
Loellingite, syn:
Fe As₂
Palladobismutharsenide, syn:
Pd₁₀ As₄ Bi
Bismuth, syn:
Bi
* 1.45 angstrom phase may
represent carbon steel.

** Pattern near-
identical to
Loellingite -
strongly suspect
cobaltian
loellingite
instead - need*

MM = Predominant M = Major m = Minor Tr = Trace ? = Tentative Identification



ineer. Marcasite group. $a = 5.72$, $c = 3.60$, $Z = 2$, $d_{110} = 4.43$, $d_{100} = 1.02$. Small idiomorphic, metallic luster. $H = 6$. Isotropic. La Sal mine, Harz, Germany; San Francisco, California. *JMM:133(1955)*, *AM*

ORTH *Pnmm*. $a = 5.312$, $d_{110} = 14.8$, $d_{100} = 2.82$, $d_{111} = 2.71$, $d_{112} = 2.07$. Violet, metallic luster. Weakly pleochroic. *PQ*, Canada. *BM CM*

Norwegian-U.S. mineral (2.12.1.4). ORTH *Pnmm*. $d_{110} = 3.12$, $d_{100} = 2.94$, $d_{111} = 2.64$, $d_{112} = 2.55$. Light gray, metallic luster. *Kuu*

ORTH *Pnmm*. $a = 5.409$, $d_{110} = 4.07$, $d_{100} = 3.09$, $d_{111} = 2.69$, $d_{112} = 2.63$. Steel-gray, metallic luster; distinctly anisotropic. Fine deposit. *BM AM*

as a series with omeite. $d_{110} = 8.25$. *33-1144*: 2.005. Fine grains and granular luster. One cleavage. *t*, China. *BM AM*

substitution of Co for As has been

recorded. ORTH *Pnmm*. $a = 5.300$, $b = 5.983$, $c = 2.882$, $Z = 2$, $D = 7.47$. *25-249*: 2.62₃ 2.57₁₀ 2.40₈ 1.97₄ 1.87₇ 1.85₃ 1.66₇ 1.64₃. Prismatic crystals, or massive; twinned on {011}, sometimes trillings. Silver-white to steel-gray, gray-black streak, metallic luster. Cleavage {010} and {101}, sometimes distinct; uneven fracture; brittle. $H = 5-5\frac{1}{2}$, $VHN_{100} = 859-920$. $G = 7.4-7.5$. $R = 53.1-53.6$ (540 nm); strongly anisotropic. Occurs with calcite and sulfides of Fe and Cu in veins; also in pegmatites. Auburn, ME, and Center Strafford, NH, in pegmatites; Franklin and Sterling Hill, NJ, in skarn; Black Hills, SD, in many pegmatites (300-kg masses at Ingersoll mine); Gunnison Co., CO, in several mines; Pala, CA, in pegmatites; Cobalt, ON, Canada, in many mines; Andreasberg, Harz Mts., Germany; Lölling, Carinthia, Austria; Varuträsk, Sweden, in pegmatite; Guadalcanal, Sierra Morena, Spain; Broken Hill, NSW, Australia. *BM DI:303*, *AM 53:1856(1968)*, *R:854*, *P&J:242*, *ABI:300*.

2.12.2.10 Seinäjokite FeSb₂

Named in 1976 for the locality. Marcasite group. Contains up to 6% Ni and 8% As. ORTH *Pnmm*. $a = 5.810$, $b = 6.490$, $c = 3.190$, $Z = 2$, $D = 8.27$. *29-129*: 2.81₁₀ 2.59₉ 2.03₈ 1.79₆ 1.63₂ 1.52₂ 1.21₃ 1.17₃. Small grains. Light gray, metallic luster. $H = 4\frac{1}{2}$, $VHN_{30} = 332$. $R = 60.8$ (540 nm). *Seinäjoki*, Vaasa, Finland, in native antimony; Ilimaussaq intrusion, near Narssaq, Greenland; Zolotaya Gora, Urals, Russia. *BM ZVMO 105:617(1976)*, *AM 62:1059(1977)*, *ABI:467*.

2.12.2.11 Safflorite (Co,Fe)As₂

Named in 1835 from *Zaffer*, a German term for cobalt pigments. Marcasite group. Contains up to 16% Fe. ORTH *Pnmm*. $a = 5.173$, $b = 5.954$, $c = 2.999$, $Z = 2$, $D = 7.46$. *23-88*: 2.96₁ 2.60₆ 2.57₈ 2.38₁₀ 1.86₅ 1.85₂ 1.65₂ 1.64₂. Prismatic crystals but commonly massive with radiating fibrous structure. Cyclic twinning twins with {011} as twin plane, also cruciform twins with {101} as twin plane. Tin-white, tarnishing to dark gray, black streak, metallic luster. Cleavage {100}, distinct; uneven to conchoidal fracture. $H = 4\frac{1}{2}-5$, $VHN_{100} = 792-882$. $G = 7.1-7.4$. $R = 53.5-54.5$ (540 nm); strongly anisotropic. Quartzburg district, Grant Co., OR; Cobalt and South Lorrain, ON, Eldorado mine, Great Bear Lake, NWT, Hedley, BC, Canada; Batopilas, Chihuahua, Mexico; Schneeberg and Annaberg, Saxony, Bieber, Hesse, Wittichen, Baden, Germany; Tunaberg, Sweden; Sarrabus, Sardinia, Italy; Almalyk, Uzbekistan; Broken Hill, NSW, Australia; Bou Azzer, Morocco. *BM DI:307*, *AM 53:1856(1968)*, *R:347*, *P&J:332*, *ABI:457*.

2.12.2.12 Rammelsbergite NiAs₂

Named in 1854 for Karl F. Rammelsberg (1813-1899), German mineral chemist. Marcasite group. Trimorphous with krutovite and pararammelsbergite. ORTH *Pnmm*. $a = 4.759$, $b = 5.797$, $c = 3.539$, $Z = 2$, $D = 7.09$. *15-441*: 2.82₁₀ 2.52₉ 2.42₆ 2.00₃ 1.84₇ 1.75₃ 1.66₃ 1.21₁₀. Prismatic crystals rare, usually mas-

2.12.2.4 Hastite CoSe₂

Named in 1955 for P. F. Hast, German mining engineer. Marcasite group. Dimorphous with trogtalite. ORTH *Pnmm*. $a = 4.84$, $b = 5.72$, $c = 3.60$, $Z = 2$, $D = 7.23$. 10-408: 2.9₃ 2.58₁₀ 2.47₁₀ 1.90₁₀ 1.61₃ 1.44₃ 1.02₁₀. Small idiomorphic grains and radiating aggregates. Red-brown, metallic luster. $H = 6$. $R = 46.9-52.2$ (540 nm); strongly pleochroic and anisotropic. La Sal mine, Montrose Co., CO; Trogtal quarry, near Lauenenthal, Harz, Germany; San Francisco mine, La Rioja Prov., Argentina. BM *NJMM:133(1955)*, *AM 41:164(1956)*, *R:845*, *P&J:192*, *ABI:204*.

2.12.2.5 Mattagamite CoTe₂

Named in 1973 for the locality. Marcasite group. ORTH *Pnmm*. $a = 5.312$, $b = 6.311$, $c = 3.889$, $Z = 2$, $D = 8.00$. 11-553(syn): 3.14₈ 2.82₁₀ 2.71₁₀ 2.07₁₀ 1.94₈ 1.86₈ 1.58₈ 1.55₈. Microscopic grains. Gray-violet, metallic luster. $H = 4\frac{1}{2}-5\frac{1}{2}$, $VHN_{25} = 383-404$. $R = 47.9-53.9$ (540 nm); weakly pleochroic and anisotropic. Mattagami Lake mine, Galinee Twp., PQ, Canada. BM *CM 12:55(1973)*, *AM 59:382(1974)*, *P&J:260*, *ABI:317*.

2.12.2.6 Kullerudite NiSe₂

Named in 1964 for Gunnar Kullerud (1921-1989), Norwegian-U.S. mineralogist. Marcasite group. Dimorphous with penroseite (2.12.1.4). ORTH *Pnmm*. $a = 4.89$, $b = 5.96$, $c = 3.67$, $Z = 2$, $D = 6.73$. 18-886: 3.12₂ 2.94₃ 2.64₁₀ 2.55₁₀ 1.93₈ 1.84₈ 1.69₄ 1.65₆. Massive, fine-grained. Lead-gray, metallic luster. *Kuusamo, Finland*. BM *AM 50:519(1965)*, *R:846*, *ABI: 279*.

2.12.2.7 Omeiite OsAs₂

Named in 1978 for the locality. Marcasite group. ORTH *Pnmm*. $a = 5.409$, $b = 6.167$, $c = 3.021$, $Z = 2$, $D = 11.19$. 34-336(syn): 4.07₉ 3.09₃ 2.69₃ 2.63₁₀ 2.01₄ 1.93₃ 1.91₆ 1.70₃. Microscopic tabular crystals. Steel-gray, metallic luster. Cleavage parallel to elongation. $R = 39.2$ (546 nm); distinctly anisotropic. *Omeishan, Sichuan Prov., China*, in a Cu-Ni sulfide deposit. BM *AM 64:464(1979)*, *ABI:361*.

2.12.2.8 Anduoite RuAs₂

Named in 1979 for the locality. Marcasite group. Forms a series with omeiite. ORTH *Pnmm*. $a = 5.41$, $b = 6.206$, $c = 3.01$, $Z = 2$, $D = 8.25$. 33-1144: 2.00₅ 1.92₁₀ 1.50₉ 1.21₇ 1.19₇ 1.13₈ 1.10₉ 1.08₄. Microscopic grains and granular aggregates. Lead-gray, gray-black streak, metallic luster. One cleavage, brittle. $H = 6\frac{1}{2}-7$, $VHN_{50} = 1078$. *Anduo, Tibet, China*. BM *AM 65:808(1980)*, *ABI:13*.

2.12.2.9 Löllingite FeAs₂

Named in 1845 for the locality. Marcasite group. Minor substitution of Co for Fe (up to 6.5%) and S (up to 6.7%) and Sb (up to 5.6%) for As has been

recorded

2.12.2.6

massive;

gray-black

distinct;

75; R =

sulfides (

Stratford

Black H

Gunnison

Cahada,

Carinthia

Morena,

187856(

187856(

187856(

187856(

2.12.2.1

Named in

8% As. (

2.81₁₀ 2.5

lic luster

land, in

Zolotaya

ABI: 467

ABI: 467

2.12.2.1

Named in

group. Co

Z = 2, D

matic cry

staling t

twin plan

Cleavage

VHN₁₀₀ =

pic. Quar

Eldorado

OHII, M

Baden, G

Uzbekista

AM 53:18

2.12.2.1

2.12.2.1

2.12.2.1

2.12.2.1

Named in

list. Mar

ORTH *Pn*

2.52, 2.42

2.52, 2.42

luster. No cleavage, uneven fracture, $d = 71$. $R = 25.8$ (540 nm). Occurs with urora, Mineral Co., NV; Pinky Fault, Canada; *Skrikerum, near Tryserum*, Norge, and Clausthal, Harz, Germany; Republic; Kalgoorlie, WA, and El Shardo, La Rioja, Argentina. *BM DI:182*,

$P4/nmm$. $a = 3.990$, $c = 6.09$, $Z = 2$, $d_{100} = 1.99$, $d_{110} = 1.67$, $d_{111} = 1.42$, $d_{112} = 1.17$. Fine-grained on fresh fractures, metallic luster. Anisotropic. $H = 4$, $VHN_{50} = 216-249$. Occurs in sodalite syenite; Långban mine; Zolotaya Gora, Urals, Russia. *BM DI:14(88); ABI:123*.

(1819), English chemist, who discovered. *Ag*. *TET I4*. $a = 10.40$, $c = 3.93$, $d_{100} = 2.32$, $d_{110} = 2.11$, $d_{111} = 1.84$, $d_{112} = 1.78$. Finely crystalline aggregates. Gray, metallic luster. Two cleavages at right angles. $G = 6.90$. $R = 31.5-36.5$ (540 nm). Occurs in hydrothermal deposits with other minerals; Lake Athabaska, SK, Canada; Bukov, near Tisnov, Czech Republic. *BM P&J:135, ZK 181:241(1987)*.

(1857), French mineralogist. *TET P4*. $a = 3.09$, $c = 2.71$, $d_{100} = 3.09$, $d_{110} = 2.71$, $d_{111} = 2.53$, $d_{112} = 2.25$. Crystalline aggregates. Gray, metallic luster. Two cleavages at right angles. $G = 30.6$ (540 nm); strongly anisotropic. *BM BM 101:557(1978), ZK 181:241(1987), ABI:456*.

(1857), French mineralogist. *TET P4*. $a = 12.12$, $c = 18.175$, $Z = 27$, $d_{100} = 1.51$, $d_{110} = 1.20$, $d_{111} = 1.08$, $d_{112} = 0.916$. Crystalline aggregates. Gray, metallic luster. Cleavages at right angles. $G = 8.1$, $VHN_{50} = 23.5$. Occurs in carbonaceous

limestone in the *Carlín mine, Eureka Co., NV*. *BM AM 60:559(1975), R:167, ABI:81*.

2.4.14.1 Palladoarsenide Pd_2As

Named in 1974 for the composition. *MON P2/m*. $a = 9.24$, $b = 8.47$, $c = 10.45$, $\beta = 94.00^\circ$, $Z = 18$, $D = 10.54$. *17-227(syn)*: $d_{100} = 2.89$, $d_{110} = 2.60$, $d_{111} = 2.35$, $d_{112} = 2.31$, $d_{113} = 2.22$, $d_{114} = 2.15$, $d_{115} = 2.13$, $d_{116} = 1.96$. Microscopic grains. Steel-gray, metallic luster. Cleavage perfect in two directions, brittle. $H = 5$, $VHN_{100} = 390$. $R = 52.5-54.8$ (540 nm); moderately anisotropic. Stillwater Complex, MT, in heavy-mineral concentrates; Lac des Iles Complex, ON, Canada; *Oktyabr mine, Talnakh, Norilsk, Russia*; *Merensky Reef, Transvaal, South Africa*. *BM ZVMO 105:104(1974), AM 60:162(1975), CM 13:321(1975), ABI:377*.

2.4.15.1 Palladobismutharsenide $Pd_2(As,Bi)$

Named in 1976 for the composition. *ORTH Pmcn* or *P2₁cn*. $a = 7.467$, $b = 18.946$, $c = 6.797$, $Z = 20$, $D = 10.8$. *29-962(syn)*: $d_{100} = 2.59$, $d_{110} = 2.49$, $d_{111} = 2.38$, $d_{112} = 2.26$, $d_{113} = 2.23$, $d_{114} = 2.20$, $d_{115} = 2.13$, $d_{116} = 2.08$. Microscopic grains. Cream-white, metallic luster. $H = 6$, $VHN_{25} = 429-483$. $R = 52.1-53.0$ (546 nm); weakly to distinctly anisotropic. Stillwater Complex, MT, in heavy-mineral concentrates. *BM CM 14:410(1976), ABI:378*.

2.4.16.1 Majakite $PdNiAs$

Named in 1976 for the locality. *HEX* Space group unknown. $a = 6.066$, $c = 7.20$, $Z = 6$, $D = 10.42$. *29-965*: $d_{100} = 3.04$, $d_{110} = 2.65$, $d_{111} = 2.40$, $d_{112} = 2.30$, $d_{113} = 2.19$, $d_{114} = 1.19$, $d_{115} = 1.80$, $d_{116} = 1.75$. Microscopic grains. Gray-white, metallic luster. $H = 6$, $VHN_{50} = 520$. $G_{syn} = 9.33$. $R = 52.8$ (540 nm); weakly anisotropic. *Majak mine, Talnakh, Norilsk, Russia*, intergrown with chalcopyrite and platinum-group minerals. *BM ZVMO 105:698(1976), AM 62:1260(1977), ABI:307*.

2.4.17.1 Petrovskaita $AuAgS$

Named in 1984 for Nina Petrovskaya (b.1910), Russian mineralogist. Contains up to 1.3% Se. *MON* Space group unknown. $a = 4.943$, $b = 6.670$, $c = 7.221$, $\beta = 95.68^\circ$, $Z = 4$, $D = 9.44$. *38-396*: $d_{100} = 7.25$, $d_{110} = 3.87$, $d_{111} = 2.77$, $d_{112} = 2.63$, $d_{113} = 2.39$, $d_{114} = 2.25$, $d_{115} = 1.80$, $d_{116} = 1.47$. Microscopic rims on gold. Dark gray to black, dark gray streak, dull metallic luster. $H = 2-2\frac{1}{2}$, $VHN = 40-48$. Occurs with gold in the *Maikain gold deposit, Kazakhstan*. *BM ZVMO 113:602(1984), AM 70:1331(1985), ABI:401*.

2.4.18.1 Novakite $(Cu,Ag)_2As_{10}$

Named in 1961 for Jiri Novak (1902-1971), Czech mineralogist. *MON* Space group uncertain, probably *C2/m*. $a = 16.269$, $b = 11.711$, $c = 10.007$, $\beta = 112.7^\circ$, $Z = 4$, $D = 8.01$. *39-370*: $d_{100} = 3.15$, $d_{110} = 2.52$, $d_{111} = 2.38$, $d_{112} = 2.00$, $d_{113} = 1.96$, $d_{114} = 1.88$, $d_{115} = 1.18$. Granular aggregates or veinlets. Steel-gray, tarnishing to black, black streak, metallic luster. $H = 3-3\frac{1}{2}$. $R = 50.6-55.6$ (540 nm);

often polysynthetic or in complex groups; very brittle. $H = 3-3\frac{1}{2}$, $VHN_{100} = 50-69$. $G = 6.6-6.7$. $R = 70.0-71.6$ (540 nm); weakly pleochroic and anisotropic. Occurs in veins with silver, antimony, and arsenic minerals, often with stibnite or stibarsen. Surcease mine, near Las Plumas, Butte Co., and Antimony Peak deposit and Tom Moore mine(*), Kern Co., CA; Lake George mine(*), York Co., NB, Canada; Moctezuma, SON, Mexico; Allemont, Isere, France; *Sala, Västmanland, Sweden*; Seinäjoki, Finland; Andreasberg(*), Harz, Germany; Příbram, Czech Republic; Sarawak, Borneo; Consols mine(*), Broken Hill, NSW, Australia; Huasco, Atacama, Chile; Quime, La Paz, Bolivia. BM *DI:132*, *R:373*, *P&J:69*, *ABI:16*, *MR 22:263(1991)*.

1.3.1.3 Stibarsen SbAs

Named in 1941 for the composition. Arsenic group. Allemontite is stibarsen intergrown with either arsenic or antimony. HEX-R $R\bar{3}m$. $a = 4.02$, $c = 10.80$, $Z = 3$, $D = 6.48$. *31-80*: 3.60_3 2.92_{10} 2.13_8 2.01_7 1.66_4 1.47_2 1.28_4 1.01_2 . Usually massive, reniform or mammillary, or fine granular. Tin-white, tarnishing to gray, metallic luster. Cleavage {0001}, perfect. $H = 3-4$. $G = 5.8-6.2$. $R = 61.6-66.3$ (540 nm). Occurs in hydrothermal veins and granite pegmatites. Ophir mine, Comstock Lode, NV; Bernic Lake, MB, and Atlin and Alder Is., BC, Canada; *Varuträsk, Västerbotten, Sweden*; Mine des Chalanches, near Allemont, France; Andreasberg, Harz, Germany; Příbram, Czech Republic; Broken Hill, NSW, Australia. BM *DI:130*, *AM 26:456(1941)*, *R:371*, *P&J:352*, *ABI:496*.

1.3.1.4 Bismuth Bi

Known since the Middle Ages. Arsenic group. HEX-R $R\bar{3}m$. $a = 4.546$, $c = 11.860$, $Z = 6$, $D = 9.75$. *5-519(syn)*: 3.95_1 3.28_{10} 2.37_4 2.27_4 1.97_1 1.87_2 1.49_1 1.44_2 . Indistinct crystals, often in parallel groupings; also arborescent, foliated, or granular. Silver-white with a reddish hue, iridescent tarnish; silver-white streak, metallic luster. Cleavage {0001}, perfect and easy; {10 $\bar{1}$ 1}, good; {10 $\bar{1}$ 4}, poor; sectile; brittle. $H = 2-2\frac{1}{2}$, $VHN_{100} = 16-18$. $G = 9.7-9.8$. $R = 62.6-63.8$ (540 nm); distinctly anisotropic. Easily fusible, $MP = 270^\circ$. Occurs in hydrothermal veins and in pegmatites. Monroe, CT; Chesterfield district, SC; French Creek and Las Animas mines, Boulder Co., CO; Pala, San Diego Co., CA; Cobalt, ON, and Great Bear Lake, NWT, Canada; Dolcoath and other mines, Cornwall, England; Meymac, Correze, France; Altenberg, Schneeberg(*), and Annaberg, Saxony, Germany; Jachymov, Czech Republic; Ikuno(*), Hyogo Pref., Japan; Wolfram Camp(*), Q, and Kingsgate(*), NSW, Australia; Uncia, Chorolque, Llallagua, Tazna(*), Colquechaca(*), and Potosi(*), Bolivia; Bogueiraa(*), Parelhas, RN, Brazil. BM *DI:134*, *R:374*, *P&J:91*, *ABI:55*.

1.3.1.5 Sti

Named in 190...
HEX-R $R\bar{3}m$. $a = 2.16_3$ 1.78_1 1.1 .
metallic luster
dan R., Uzbe.
from placer
NJMM:117(

1.3.2.1 Ars

Named in 188...
its luster. D:
 $a = 3.65$, $b =$
 1.88_1 1.74_3 $1.$
white, tarnish
one direction
pic. Ste.-Ma
Black Forest
land; Jachym
CE 20:71(198

1.3.3.1 Pa

Named in 1...
 $b = 4.172$, $c =$
 2.09_7 1.73_4 1
streak, met:

Salton Sea - scale samples carbon steel well liner scale Sample No.	Mineralogy, Approx. Wt.% <input checked="" type="checkbox"/> (or) Relative Abundance <input checked="" type="checkbox"/>									
	Safflorite, syn	Loellingite, syn	Palladobismuth arsenide, syn	Bismuth, syn	Sphalerite	Chalcopyrite	*1.45A phase	Amorphous Below Detection		
RR-18 outside	M	M	tr		4	tr	m	-		
RR-18 inside	M	M	tr	tr	4	tr	m	-		
<div style="border: 1px solid black; padding: 10px; width: fit-content; margin: auto;"> <p>Safflorite, syn: (Co, Fe) As₂ Loellingite, syn: Fe As₂ Palladobismutharsenide, syn: Pd₁₀ As₄ Bi Bismuth, syn: Bi * 1.45 angstrom phase may represent carbon steel.</p> </div>										
MM = Predominant M = Major m = Minor Tr = Trace ? = Tentative Identification										



Salton Sea - scale samples from geothermal wells	Mineralogy, Approx. Wt.% <input checked="" type="checkbox"/> (or) Relative Abundance <input checked="" type="checkbox"/>													
	Quartz	Plagioclase	K-feldspar	Calcite	Halite	Loellingite	Magnetite	Chlorite	Illite+/-Mica	Nontronite-15A	Smectite	*Amorphous Silica	Amorphous Below Detection	
Sample No.														
Injection wells:														
Sinclair-26	1	tr				1	tr	7			MM			
Sinclair-26 black	tr			1		1		2			M	M		tr sphalerite?
Elmore-101	2	2	2	1		tr	2	1	2		MM			
Production wells:														
Sinclair-10								52				M		
Sinclair-11	1					2		36				M		
Elmore-12	tr			tr	18			40				M		

*The presence of amorphous silica is characterized by a broad hump in the diffraction pattern centered at about 3.90 angstroms. Apparently, the amorphous iron silicate (hisingerite?) leaves no signature on the diffractograms.

Nontronite-15A has a general formula of: $Na_{0.3} Fe_2 Si_4 O_{10} (OH)_2 \cdot x H_2O$, and is characterized by broad peaks at: 14.3 (air-dried) to 16.4 (glycolated), 4.48, 2.61, and 1.53 angstroms.

Loellingite ($Fe As_2$) exhibits peaks at 2.61, 2.54, 2.42, 2.34, 2.21, 1.86, 1.69, and 1.64 angstroms.

MM = Predominant M = Major m = Minor Tr = Trace ? = Tentative Identification



SUMMARY OF X-RAY DIFFRACTION ANALYSIS
Energy & Geoscience Institute at the University of Utah

S. Lutz
 2-2000
 801 585 188

Petrographic Analysis
of
Scale and Formation Drill Cuttings
from the
Salton Sea Field
Injection Well S-22

for

Alex Schriener Jr.
Joe Hickey
Magma Power Company

by
Susan J. Lutz
University of Utah Research Institute

March 1994

The relative amount of magnetite, pyrrhotite and pyrite in the banded scale is tentative because their presence is based on approximate differences in the color of reflectance in the unpolished sections. In general, the magnetite is concentrated along the bands and reflects whitish. The pyrrhotite and pyrite are more commonly found in aggregates. The pyrrhotite has a slight bronzy reflectance. The pyrite reflects a brassy color but doesn't form nice euhedral crystals (could be marcasite?). There may also be compositional zoning in the scales with depth; pyrrhotite is more common from 4000-5200' and pyrite is more common in the scale below 5900'. This relationship may indicate that pyrite is the more stable phase at higher temperatures.

Magnetite, hematite, pyrite and pyrrhotite are among the most commonly-occurring minerals in geothermal scales. Other sulfides that could be present, such as chalcopyrite and sphalerite, were not observed. Without a chemical analysis of the scale, their presence can not be confirmed. For positive identification of the mineralogy of the iron oxides and sulfides in the scale, X-ray diffraction and chemical analyses are highly recommended.

Scaling in the Formation

The formation consists of a variety of weakly metamorphosed sedimentary rocks and some intrusive rocks. Siltstones predominate to 4400' and calcite-cemented sandstones are common from 4600-4765'. The depth interval from 4900' to 5900' contains fine-grained, clayey sandstones and siltstones interbedded with some coarser calcite-cemented sandstones and shales, and minor amounts of granophyre. Potassium feldspar-epidote-chlorite-pyrite-sphene veins are common from 4900' to 5900'. Below 6000', the calcareous sandstones are brecciated and contain thick calcite-epidote-chlorite veins.

Petrographically, there does not appear to be much, if any, impregnation of the formation by scale solids. Where the contact between scale and wallrock can be observed, the contact is sharp. In some places, the color of the scale and the color of the sandstone matrix is similar. On close examination, the sandstone matrix is composed of its initial components; that is, chlorite, pyrite and leucoxene. The clayey matrix appears slightly iron-stained at the contact with the scale but is still fully intact (not actually replaced by the scale). In fact, none of the calcareous or clayey sandstones or other formation lithologies appear to have any significant matrix porosity that could be filled by scale-forming material.

4) Fine Crystalline Material in Scale. The barite that precipitated from the injection fluids was previously (mistakenly) described as crystalline quartz. More detailed petrographic analysis of the very fine crystalline material in the granular scale revealed the presence of tiny euhedral barite crystals lacking hexagonal shapes and with relief that is too high for quartz. X-ray diffraction analysis of the scale could confirm the presence of barite and/or other sulfates, and also determine whether the fibrous carbonate is indeed calcite or some other carbonate (such as aragonite or siderite).

Summary

The geochemistry of the injection fluid and the precipitation mechanisms that result in scale formation are complex issues that can't be solved by petrographic means alone. The modeling is complicated by changes in temperature, oxidation potential, sulfur and metal content, and pH of the injection fluid as it moves along a reaction pathway away from the point of injection. From this petrographic study, there is some indication of depth zoning in the scale mineralogy related to some or all of these geochemical factors. To summarize the textural information gained from this petrographic study, scaling of the wallrock appears to be a much greater factor in areas with high initial fracture permeability (that could take the injection fluid) rather than in the sandstones pores themselves. Characteristic mineralogically and textural features of the scale and the formation are documented with photomicrographs.

FIGURE 2: WELL SINC-22 FORMATION		lithology										alteration mineralogy						
		shale	siltstone	cc-cement sandstone	clayey sandstone	granophyre	vein fragments	gouge	magnetite	leucoxene	sphene	pyrite	pyrrhotite	chlorite	epidote			
S22fc:	1200	tr					tr											
	2000	tr					tr											
	3000	tr		tr									x					po in ss and scale
	5300-5600		tr				tr						x					lots of po in ss some in scale
	5600-5900																	
	5900-6200	tr			tr		tr											
S22ur:	4000		MM	m			tr	tr	x	x								tr casing cement
	4200		MM	m	m		tr		x	x			x		m	x		
	4400	m	MM	m			m		x	x	x	x	x					kf-ep-sph veins
	4600	M		M			m	tr		x	x	m						kf-cc veins
	4765	m	m	M					x	x		x	x					lots of py and po in ss
	4900	m			M	m				x	x	x		M				
	5100	m	tr		MM	tr	tr			x	x	m						lots of py
	5200		M	tr	M		tr	tr	x	x		x						
	5400	m	M	m	m	tr	m			x		x					x	kf-ep veins
	5600	m	M	m	m		M	m		x		x		x	x			kf-ep-chl-py-sph and ep-chl veins
	5700	M	m	m	m		m	tr		x		x						
	5900	tr	m	M	m	tr	tr	tr		x				x				cc-chl vein
	6100		M	M			tr	m	x	m	x						x	sulfides in scale oxides in ss
S22sw:	3835		M		M													very fine cuttings
	5017		m	M	M		tr	tr		x	x	x		M				
	5063			MM						x		x		M				
	5345		MM				tr		x	m		x						siltstone to very fine gr. sandstone
	5416			MM			m	^m		x	x	x		M	x			kf-ep vein
	5563			MM			tr	^m		x		x		M				cc veins ^ red corrosion
	6120						*MM	M						M	x			cc-sph-ep veins; gouged, late chl veins

tr trace
m minor
M major
MM predominant

* common, small fluid inclusions
in calcite, 225-250°C

often polysynthetic or in complex groups; very brittle. $H = 3-3\frac{1}{2}$, $VHN_{100} = 50-69$. $G = 6.6-6.7$. $R = 70.0-71.6$ (540 nm); weakly pleochroic and anisotropic. Occurs in veins with silver, antimony, and arsenic minerals, often with stibnite or stibarsen. Surcease mine, near Las Plumas, Butte Co., and Antimony Peak deposit and Tom Moore mine(*), Kern Co., CA; Lake George mine(*), York Co., NB, Canada; Moctezuma, SON, Mexico; Allemont, Isere, France; *Sala, Västmanland, Sweden*; Seinäjoki, Finland; Andreasberg(*), Harz, Germany; Příbram, Czech Republic; Sarawak, Borneo; Consols mine(*), Broken Hill, NSW, Australia; Huasco, Atacama, Chile; Quime, La Paz, Bolivia. *BM DI:132, R:373, P&J:69, ABI:16, MR 22:263(1991)*.

1.3.1.3 Stibarsen SbAs

Named in 1941 for the composition. Arsenic group. Allemontite is stibarsen intergrown with either arsenic or antimony. *HEX-R $R\bar{3}m$. $a = 4.02$, $c = 10.80$, $Z = 3$, $D = 6.48$. 31-80: 3.60₃ 2.92₁₀ 2.13₆ 2.01₇ 1.66₄ 1.47₂ 1.28₄ 1.01₂*. Usually massive, reniform or mammillary, or fine granular. Tin-white, tarnishing to gray, metallic luster. Cleavage {0001}, perfect. $H = 3-4$. $G = 5.8-6.2$. $R = 61.6-66.3$ (540 nm). Occurs in hydrothermal veins and granite pegmatites. Ophir mine, Comstock Lode, NV; Bernic Lake, MB, and Atlin and Alder Is., BC, Canada; *Varuträsk, Västerbotten, Sweden*; Mine des Chalanches, near Allemont, France; Andreasberg, Harz, Germany; Příbram, Czech Republic; Broken Hill, NSW, Australia. *BM DI:130, AM 26:456(1941), R:371, P&J:352, ABI:496*.

1.3.1.4 Bismuth Bi

Known since the Middle Ages. Arsenic group. *HEX-R $R\bar{3}m$. $a = 4.546$, $c = 11.860$, $Z = 6$, $D = 9.75$. 5-519(syn): 3.95₁ 3.28₁₀ 2.37₄ 2.27₄ 1.97₁ 1.87₂ 1.49₁ 1.44₂*. Indistinct crystals, often in parallel groupings; also arborescent, foliated, or granular. Silver-white with a reddish hue, iridescent tarnish; silver-white streak, metallic luster. Cleavage {0001}, perfect and easy; {10 $\bar{1}$ 1}, good; {10 $\bar{1}$ 4}, poor; sectile; brittle. $H = 2-2\frac{1}{2}$, $VHN_{100} = 16-18$. $G = 9.7-9.8$. $R = 62.6-63.8$ (540 nm); distinctly anisotropic. Easily fusible, $MP = 270^\circ$. Occurs in hydrothermal veins and in pegmatites. Monroe, CT; Chesterfield district, SC; French Creek and Las Animas mines, Boulder Co., CO; Pala, San Diego Co., CA; Cobalt, ON, and Great Bear Lake, NWT, Canada; Dolcoath and other mines, Cornwall, England; Meymac, Correze, France; Altenberg, Schneeberg(*), and Annaberg, Saxony, Germany; Jachymov, Czech Republic; Ikuno(*), Hyogo Pref., Japan; Wolfram Camp(*), Q, and Kingsgate(*), NSW, Australia; Uncia, Chorolque, Llallagua, Tazna(*), Colquechaca(*), and Potosi(*), Bolivia; Bogueiraa(*), Parelhas, RN, Brazil. *BM DI:134, R:374, P&J:91, ABI:55*.

1.3.1.5 Sti

Named in 19th century. *HEX-R $R\bar{3}m$. $a = 2.16_3$ 1.78₁ 1.1. metallic luster. dan R., Uzbe. from placer NJMM:117(*

1.3.2.1 Ars

Named in 18th century. *D: its luster. $D: a = 3.65$, $b = 1.88_1$ 1.74₃ 1. white, tarnish one direction pic. Ste.-Ma Black Forest land; Jachym CE 20:71(19*

1.3.3.1 Pa

Named in 1st century. *b = 4.172*, $c = 2.09_7$ 1.73₄ 1 streak, met:

lic luster. No cleavage, uneven fracture, $d = 6.71$. $R = 25.8$ (540 nm). Occurs with Aurora, Mineral Co., NV; Pinky Fault K, Canada; *Skrikerum*, near *Tryserum*, Zorge, and Clausthal, Harz, Germany; Republic; Kalgoorlie, WA, and El Sharngo, La Rioja, Argentina. BM *DI:182*, 50.

TET $P4/nmm$. $a = 3.990$, $c = 6.09$, $Z = 2$, $d = 1.99_4$ 1.67_2 1.42_3 1.17_4 . Fine-grained luster on fresh fractures, metallic luster. Fracture. $H = 4$, $VHN_{50} = 216-249$. Anisotropic and anisotropic. Franklin, NJ; in vein in sodalite syenite; *Långban* dolomite; *Zolotaya Gora*, Urals, Russia. (2), *J* (1988); *ABI:123*.

(182-1919), English chemist, who discovered 1% Ag. TET $I4$. $a = 10.40$, $c = 3.93$, $d = 2.60_{10}$ 2.32_3 2.11_5 1.84_4 1.78_4 . Finely luster. Two cleavages at right angles. $G = 6.90$. $R = 31.5-36.5$ (540 nm). Hydrothermal deposits with other minerals, Lake Athabaska, SK, Canada; *Aden*; *Bukov*, near *Tisnov*, Czech Republic. BM *P&J:135*, *ZK 181:241*(1987).

(1823), French mineralogist. TET $P4/nmm$. $d = 4.1-14.58$ (syn): 3.09_{10} 2.71_6 2.53_2 . Polycrystalline aggregates. Gray, luster. $R = 9-30.6$ (540 nm); strongly anisotropic. Republic. BM *BM 101:557*(1978), 987), *ABI:456*.

$a = 12.12$, $c = 18.175$, $Z = 27$, $d = 1.75_1$ 1.51_1 1.20_1 1.08_1 0.916_1 . Metallic luster. Cleavage. $H = 1$, $VHN_{50} = 23.5$. $G = 8.1$. Occurs in carbonaceous

limestone in the *Carlin mine*, *Eureka Co.*, NV. BM *AM 60:559*(1975), *R:467*, *ABI:81*.

2.4.14.1 Palladoarsenide Pd_2As

Named in 1974 for the composition. MON $P2/m$. $a = 9.24$, $b = 8.47$, $c = 10.45$, $\beta = 94.00^\circ$, $Z = 18$, $D = 10.54$. $17-227$ (syn): 2.89_3 2.60_7 2.35_5 2.31_5 2.22_{10} 2.15_{10} 2.13_4 1.96_4 . Microscopic grains. Steel-gray, metallic luster. Cleavage perfect in two directions, brittle. $H = 5$, $VHN_{100} = 390$. $R = 52.5-54.8$ (540 nm); moderately anisotropic. Stillwater Complex, MT, in heavy-mineral concentrates; *Lac des Iles Complex*, ON, Canada; *Oktyabr mine*, *Talnakh*, *Norilsk*, *Russia*; *Merensky Reef*, *Transvaal*, *South Africa*. BM *ZVMO 108:104*(1974), *AM 60:162*(1975), *CM 13:321*(1975), *ABI:377*.

2.4.15.1 Palladobismutharsenide $Pd_2(As, Bi)$

Named in 1976 for the composition. ORTH $Pm\bar{c}n$ or $P2_1cn$. $a = 7.467$, $b = 18.946$, $c = 6.797$, $Z = 20$, $D = 10.8$. $29-962$ (syn): 2.59_8 2.49_9 2.38_4 2.26_4 2.23_{10} 2.20_8 2.13_5 2.08_9 . Microscopic grains. Cream-white, metallic luster. $H = 6$, $VHN_{25} = 429-483$. $R = 52.1-53.0$ (546 nm); weakly to distinctly anisotropic. *Stillwater Complex*, *MT*, in heavy-mineral concentrates. BM *CM 14:410*(1976), *ABI:378*.

2.4.16.1 Majakite $PdNiAs$

Named in 1976 for the locality. HEX Space group unknown. $a = 6.066$, $c = 7.20$, $Z = 6$, $D = 10.42$. $29-965$: 3.04_4 2.65_{10} 2.40_4 2.30_5 2.19_7 1.19_{10} 1.80_4 1.75_3 . Microscopic grains. Gray-white, metallic luster. $H = 6$, $VHN_{50} = 520$. $G_{syn} = 9.33$. $R = 52.8$ (540 nm); weakly anisotropic. *Majak mine*, *Talnakh*, *Norilsk*, *Russia*, intergrown with chalcopyrite and platinum-group minerals. BM *ZVMO 105:698*(1976), *AM 62:1260*(1977), *ABI:307*.

2.4.17.1 Petrovskaita $AuAgS$

Named in 1984 for *Nina Petrovskaya* (b.1910), Russian mineralogist. Contains up to 1.3% Se. MON Space group unknown. $a = 4.943$, $b = 6.670$, $c = 7.221$, $\beta = 95.68^\circ$, $Z = 4$, $D = 9.44$. $38-396$: 7.25_3 3.87_3 2.77_{10} 2.63_5 2.39_4 2.25_4 1.80_3 1.47_4 . Microscopic rims on gold. Dark gray to black, dark gray streak, dull metallic luster. $H = 2-2\frac{1}{2}$, $VHN = 40-48$. Occurs with gold in the *Maikain gold deposit*, *Kazakhstan*. BM *ZVMO 113:602*(1984), *AM 70:1331*(1985), *ABI:401*.

2.4.18.1 Novakite $(Cu, Ag)_{21}As_{10}$

Named in 1961 for *Jiri Novak* (1902-1971), Czech mineralogist. MON Space group uncertain, probably $C2/m$. $a = 16.269$, $b = 11.711$, $c = 10.007$, $\beta = 112.7^\circ$, $Z = 4$, $D = 8.01$. $39-370$: 3.15_6 2.52_7 2.38_5 2.00_9 1.96_8 1.91_7 1.88_{10} 1.18_8 . Granular aggregates or veinlets. Steel-gray, tarnishing to black, black streak, metallic luster. $H = 3-3\frac{1}{2}$. $R = 50.6-55.6$ (540 nm);

2.12.2.4 Hastite CoSe₂

Named in 1955 for P. F. Hast, German mining engineer. Marcasite group. Dimorphous with trogtalite. ORTH *Pnmm*. $a = 4.84$, $b = 5.72$, $c = 3.60$, $Z = 2$, $D = 7.23$. 10-408: 2.9₃ 2.58₁₀ 2.47₁₀ 1.90₁₀ 1.61₃ 1.44₃ 1.02₁₀. Small idiomorphic grains and radiating aggregates. Red-brown, metallic luster. $H = 6$. $R = 46.9-52.2$ (540 nm); strongly pleochroic and anisotropic. La Sal mine, Montrose Co., CO; Trogtal quarry, near Lauenthal, Harz, Germany; San Francisco mine, La Rioja Prov., Argentina. BM *NJMM:133(1955)*, *AM 41:164(1956)*, *R:845*, *P&J:192*, *ABI:204*.

2.12.2.5 Mattagamite CoTe₂

Named in 1973 for the locality. Marcasite group. ORTH *Pnmm*. $a = 5.312$, $b = 6.311$, $c = 3.889$, $Z = 2$, $D = 8.00$. 11-553(syn): 3.14₈ 2.82₁₀ 2.71₁₀ 2.07₁₀ 1.94₈ 1.86₈ 1.58₈ 1.55₈. Microscopic grains. Gray-violet, metallic luster. $H = 4\frac{1}{2}-5\frac{1}{2}$, $VHN_{25} = 383-404$. $R = 47.9-53.9$ (540 nm); weakly pleochroic and anisotropic. Mattagami Lake mine, Galinee Twp., PQ, Canada. BM *CM 12:55(1973)*, *AM 59:382(1974)*, *P&J:260*, *ABI:317*.

2.12.2.6 Kullerudite NiSe₂

Named in 1964 for Gunnar Kullerud (1921-1989), Norwegian-U.S. mineralogist. Marcasite group. Dimorphous with penroseite (2.12.1.4). ORTH *Pnmm*. $a = 4.89$, $b = 5.96$, $c = 3.67$, $Z = 2$, $D = 6.73$. 18-886: 3.12₂ 2.94₈ 2.64₁₀ 2.55₁₀ 1.93₈ 1.84₈ 1.69₄ 1.65₆. Massive, fine-grained. Lead-gray, metallic luster. Kullerud, Finland. BM *AM 50:519(1965)*, *R:846*, *ABI: 279*.

2.12.2.7 Omeiite OsAs₂

Named in 1978 for the locality. Marcasite group. ORTH *Pnmm*. $a = 5.409$, $b = 6.167$, $c = 3.021$, $Z = 2$, $D = 11.19$. 34-336(syn): 4.07₉ 3.09₃ 2.69₃ 2.63₁₀ 2.01₄ 1.93₃ 1.91₆ 1.70₃. Microscopic tabular crystals. Steel-gray, metallic luster. Cleavage parallel to elongation. $R = 39.2$ (546 nm); distinctly anisotropic. Omeishan, Sichuan Prov., China, in a Cu-Ni sulfide deposit. BM *AM 64:464(1979)*, *ABI:361*.

2.12.2.8 Anduoite RuAs₂

Named in 1979 for the locality. Marcasite group. Forms a series with omeiite. ORTH *Pnmm*. $a = 5.41$, $b = 6.206$, $c = 3.01$, $Z = 2$, $D = 8.25$. 33-1144: 2.00₅ 1.92₁₀ 1.50₉ 1.21₇ 1.19₇ 1.13₈ 1.10₉ 1.08₄. Microscopic grains and granular aggregates. Lead-gray, gray-black streak, metallic luster. One cleavage, brittle. $H = 6\frac{1}{2}-7$, $VHN_{50} = 1078$. Anduo, Tibet, China. BM *AM 65:808(1980)*, *ABI:13*.

2.12.2.9 Löllingite FeAs₂

Named in 1845 for the locality. Marcasite group. Minor substitution of Co for Fe (up to 6.5%) and S (up to 6.7%) and Sb (up to 5.6%) for As has been

recorded
249: 2.6
massive;
gray-black
distinct;
75: R =
sulfides c
Stratford
Black H
Gunnison
Canada,
Carinthia
Morena,
59:1856(

2.12.2.1

Named in
8% As. c
2.81₁₀ 2.5
lic luster
land, in
Zolotaya
ABI: 467

2.12.2.1

Named in
group. Co
 $Z = 2$, D
matic cry
twinning t
twin plan
Cleavage
 $VHN_{100} =$
pic. Quar
Eldorado
CHIH, M
Baden, G
Uzbekista
AM 53:18

2.12.2.1

Named in
mist. Mar
ORTH *Pnn*
2.52, 2.42

neer. Marcasite group. $a = 5.72$, $c = 3.60$, $Z = 2$, $D = 7.47$. $25-249$: 2.62_3 2.57_{10} 2.40_8 1.97_4 1.87_7 1.85_3 1.66_7 1.64_3 . Prismatic crystals, or massive; twinned on {011}, sometimes trillings. Silver-white to steel-gray, gray-black streak, metallic luster. Cleavage {010} and {101}, sometimes distinct; uneven fracture; brittle. $H = 5-5\frac{1}{2}$, $VHN_{100} = 859-920$. $G = 7.4-7.5$. $R = 53.1-53.6$ (540 nm); strongly anisotropic. Occurs with calcite and sulfides of Fe and Cu in veins; also in pegmatites. Auburn, ME, and Center Stfafford, NH, in pegmatites; Franklin and Sterling Hill, NJ, in skarn; Black Hills, SD, in many pegmatites (300-kg masses at Ingersoll mine); Gunnison Co., CO, in several mines; Pala, CA, in pegmatites; Cobalt, ON, Canada, in many mines; Andreasberg, Harz Mts., Germany; Lölling, Carinthia, Austria; Varuträsk, Sweden, in pegmatite; Guadalcanal, Sierra Morena, Spain; Broken Hill, NSW, Australia. BM *DI:303*, *AM 53:1856(1968)*, *R:854*, *P&J:242*, *ABI:300*.

ORTH *Pnmm*. $a = 5.312$, $b = 5.983$, $c = 2.882$, $Z = 2$, $D = 7.47$. $25-249$: 2.62_3 2.57_{10} 2.40_8 1.97_4 1.87_7 1.85_3 1.66_7 1.64_3 . Prismatic crystals, or massive; twinned on {011}, sometimes trillings. Silver-white to steel-gray, gray-black streak, metallic luster. Cleavage {010} and {101}, sometimes distinct; uneven fracture; brittle. $H = 5-5\frac{1}{2}$, $VHN_{100} = 859-920$. $G = 7.4-7.5$. $R = 53.1-53.6$ (540 nm); strongly anisotropic. Occurs with calcite and sulfides of Fe and Cu in veins; also in pegmatites. Auburn, ME, and Center Stfafford, NH, in pegmatites; Franklin and Sterling Hill, NJ, in skarn; Black Hills, SD, in many pegmatites (300-kg masses at Ingersoll mine); Gunnison Co., CO, in several mines; Pala, CA, in pegmatites; Cobalt, ON, Canada, in many mines; Andreasberg, Harz Mts., Germany; Lölling, Carinthia, Austria; Varuträsk, Sweden, in pegmatite; Guadalcanal, Sierra Morena, Spain; Broken Hill, NSW, Australia. BM *DI:303*, *AM 53:1856(1968)*, *R:854*, *P&J:242*, *ABI:300*.

ORTH *Pnmm*. $a = 5.312$, $b = 5.983$, $c = 2.882$, $Z = 2$, $D = 7.47$. $25-249$: 2.62_3 2.57_{10} 2.40_8 1.97_4 1.87_7 1.85_3 1.66_7 1.64_3 . Prismatic crystals, or massive; twinned on {011}, sometimes trillings. Silver-white to steel-gray, gray-black streak, metallic luster. Cleavage {010} and {101}, sometimes distinct; uneven fracture; brittle. $H = 5-5\frac{1}{2}$, $VHN_{100} = 859-920$. $G = 7.4-7.5$. $R = 53.1-53.6$ (540 nm); strongly anisotropic. Occurs with calcite and sulfides of Fe and Cu in veins; also in pegmatites. Auburn, ME, and Center Stfafford, NH, in pegmatites; Franklin and Sterling Hill, NJ, in skarn; Black Hills, SD, in many pegmatites (300-kg masses at Ingersoll mine); Gunnison Co., CO, in several mines; Pala, CA, in pegmatites; Cobalt, ON, Canada, in many mines; Andreasberg, Harz Mts., Germany; Lölling, Carinthia, Austria; Varuträsk, Sweden, in pegmatite; Guadalcanal, Sierra Morena, Spain; Broken Hill, NSW, Australia. BM *DI:303*, *AM 53:1856(1968)*, *R:854*, *P&J:242*, *ABI:300*.

ORTH *Pnmm*. $a = 5.312$, $b = 5.983$, $c = 2.882$, $Z = 2$, $D = 7.47$. $25-249$: 2.62_3 2.57_{10} 2.40_8 1.97_4 1.87_7 1.85_3 1.66_7 1.64_3 . Prismatic crystals, or massive; twinned on {011}, sometimes trillings. Silver-white to steel-gray, gray-black streak, metallic luster. Cleavage {010} and {101}, sometimes distinct; uneven fracture; brittle. $H = 5-5\frac{1}{2}$, $VHN_{100} = 859-920$. $G = 7.4-7.5$. $R = 53.1-53.6$ (540 nm); strongly anisotropic. Occurs with calcite and sulfides of Fe and Cu in veins; also in pegmatites. Auburn, ME, and Center Stfafford, NH, in pegmatites; Franklin and Sterling Hill, NJ, in skarn; Black Hills, SD, in many pegmatites (300-kg masses at Ingersoll mine); Gunnison Co., CO, in several mines; Pala, CA, in pegmatites; Cobalt, ON, Canada, in many mines; Andreasberg, Harz Mts., Germany; Lölling, Carinthia, Austria; Varuträsk, Sweden, in pegmatite; Guadalcanal, Sierra Morena, Spain; Broken Hill, NSW, Australia. BM *DI:303*, *AM 53:1856(1968)*, *R:854*, *P&J:242*, *ABI:300*.

ORTH *Pnmm*. $a = 5.312$, $b = 5.983$, $c = 2.882$, $Z = 2$, $D = 7.47$. $25-249$: 2.62_3 2.57_{10} 2.40_8 1.97_4 1.87_7 1.85_3 1.66_7 1.64_3 . Prismatic crystals, or massive; twinned on {011}, sometimes trillings. Silver-white to steel-gray, gray-black streak, metallic luster. Cleavage {010} and {101}, sometimes distinct; uneven fracture; brittle. $H = 5-5\frac{1}{2}$, $VHN_{100} = 859-920$. $G = 7.4-7.5$. $R = 53.1-53.6$ (540 nm); strongly anisotropic. Occurs with calcite and sulfides of Fe and Cu in veins; also in pegmatites. Auburn, ME, and Center Stfafford, NH, in pegmatites; Franklin and Sterling Hill, NJ, in skarn; Black Hills, SD, in many pegmatites (300-kg masses at Ingersoll mine); Gunnison Co., CO, in several mines; Pala, CA, in pegmatites; Cobalt, ON, Canada, in many mines; Andreasberg, Harz Mts., Germany; Lölling, Carinthia, Austria; Varuträsk, Sweden, in pegmatite; Guadalcanal, Sierra Morena, Spain; Broken Hill, NSW, Australia. BM *DI:303*, *AM 53:1856(1968)*, *R:854*, *P&J:242*, *ABI:300*.

ORTH *Pnmm*. $a = 5.312$, $b = 5.983$, $c = 2.882$, $Z = 2$, $D = 7.47$. $25-249$: 2.62_3 2.57_{10} 2.40_8 1.97_4 1.87_7 1.85_3 1.66_7 1.64_3 . Prismatic crystals, or massive; twinned on {011}, sometimes trillings. Silver-white to steel-gray, gray-black streak, metallic luster. Cleavage {010} and {101}, sometimes distinct; uneven fracture; brittle. $H = 5-5\frac{1}{2}$, $VHN_{100} = 859-920$. $G = 7.4-7.5$. $R = 53.1-53.6$ (540 nm); strongly anisotropic. Occurs with calcite and sulfides of Fe and Cu in veins; also in pegmatites. Auburn, ME, and Center Stfafford, NH, in pegmatites; Franklin and Sterling Hill, NJ, in skarn; Black Hills, SD, in many pegmatites (300-kg masses at Ingersoll mine); Gunnison Co., CO, in several mines; Pala, CA, in pegmatites; Cobalt, ON, Canada, in many mines; Andreasberg, Harz Mts., Germany; Lölling, Carinthia, Austria; Varuträsk, Sweden, in pegmatite; Guadalcanal, Sierra Morena, Spain; Broken Hill, NSW, Australia. BM *DI:303*, *AM 53:1856(1968)*, *R:854*, *P&J:242*, *ABI:300*.

recorded. ORTH *Pnmm*. $a = 5.300$, $b = 5.983$, $c = 2.882$, $Z = 2$, $D = 7.47$. $25-249$: 2.62_3 2.57_{10} 2.40_8 1.97_4 1.87_7 1.85_3 1.66_7 1.64_3 . Prismatic crystals, or massive; twinned on {011}, sometimes trillings. Silver-white to steel-gray, gray-black streak, metallic luster. Cleavage {010} and {101}, sometimes distinct; uneven fracture; brittle. $H = 5-5\frac{1}{2}$, $VHN_{100} = 859-920$. $G = 7.4-7.5$. $R = 53.1-53.6$ (540 nm); strongly anisotropic. Occurs with calcite and sulfides of Fe and Cu in veins; also in pegmatites. Auburn, ME, and Center Stfafford, NH, in pegmatites; Franklin and Sterling Hill, NJ, in skarn; Black Hills, SD, in many pegmatites (300-kg masses at Ingersoll mine); Gunnison Co., CO, in several mines; Pala, CA, in pegmatites; Cobalt, ON, Canada, in many mines; Andreasberg, Harz Mts., Germany; Lölling, Carinthia, Austria; Varuträsk, Sweden, in pegmatite; Guadalcanal, Sierra Morena, Spain; Broken Hill, NSW, Australia. BM *DI:303*, *AM 53:1856(1968)*, *R:854*, *P&J:242*, *ABI:300*.

2:12.2.10 Seinäjokite $FeSb_2$

Named in 1976 for the locality. Marcasite group. Contains up to 6% Ni and 8% As. ORTH *Pnmm*. $a = 5.810$, $b = 6.490$, $c = 3.190$, $Z = 2$, $D = 8.27$. $29-129$: 2.81_{10} 2.59_9 2.03_8 1.79_6 1.63_2 1.52_2 1.21_3 1.17_3 . Small grains. Light gray, metallic luster. $H = 4\frac{1}{2}$, $VHN_{30} = 332$. $R = 60.8$ (540 nm). *Seinäjoki, Vaasa, Finland*, in native antimony; Ilimaussaq intrusion, near Narssaq, Greenland; Zolotaya Gora, Urals, Russia. BM *ZVMO 105:617(1976)*, *AM 62:1059(1977)*, *ABI:467*.

2:12.2.11 Safflorite $(Co,Fe)As_2$

Named in 1835 from *Zaffer*, a German term for cobalt pigments. Marcasite group. Contains up to 16% Fe. ORTH *Pnmm*. $a = 5.173$, $b = 5.954$, $c = 2.999$, $Z = 2$, $D = 7.46$. $23-88$: 2.96_1 2.60_6 2.57_8 2.38_{10} 1.86_5 1.85_2 1.65_2 1.64_2 . Prismatic crystals but commonly massive with radiating fibrous structure. Cyclic twinning twins with {011} as twin plane, also cruciform twins with {101} as twin plane. Tin-white, tarnishing to dark gray, black streak, metallic luster. Cleavage {100}, distinct; uneven to conchoidal fracture. $H = 4\frac{1}{2}-5$, $VHN_{100} = 792-882$. $G = 7.1-7.4$. $R = 53.5-54.5$ (540 nm); strongly anisotropic. Quartzburg district, Grant Co., OR; Cobalt and South Lorrain, ON, Eldorado mine, Great Bear Lake, NWT, Hedley, BC, Canada; Batopilas, CHIH, Mexico; *Schneeberg* and *Annaberg, Saxony*, Bieber, Hesse, Wittichen, Baden, Germany; Tunaberg, Sweden; Sarrabus, Sardinia, Italy; Almalyk, Uzbekistan; Broken Hill, NSW, Australia; Bou Azzer, Morocco. BM *DI:307*, *AM 53:1856(1968)*, *R:347*, *P&J:332*, *ABI:457*.

2.

2:12.2.12 Rammelsbergite $NIAs_2$

Named in 1854 for Karl F. Rammelsberg (1813-1899), German mineral chemist. Marcasite group. Trimorphous with krutovite and pararammelsbergite. ORTH *Pnmm*. $a = 4.759$, $b = 5.797$, $c = 3.539$, $Z = 2$, $D = 7.09$. $15-441$: 2.82_{10} 2.52_3 2.42_6 2.00_3 1.84_7 1.75_3 1.66_3 1.21_{10} . Prismatic crystals rare, usually mas-



August 10, 1999

Dr. Susan Juch Lutz
Energy and Geoscience Institute
University of Utah
423 Wakara Way
Salt Lake City, UT 84108

Dear Sue,

Enclosed are the background documents I promised to send regarding past Salton Sea scale studies. Please keep these documents confidential and notify us prior to publishing on their content in accordance with the existing Technical Data Gathering agreement between CalEnergy and the University of Utah dated June 15, 1998.

Let me know if I can send you other data or information that may help with the study. Also let me know when you are ready for the scale samples.

Sincerely,

Melinda Wright
Geochemist

4 kinds of scale:

Melinda Wright
8-30-99

2 kinds of injection:

① pH mod - add HCl to brine - low pH at injection.

② C R C
crystallizer - reactor - clarifier

2 other production wells:

③ titanium-cased wells

④ reg. carbon-cased wells

has about 10 samples now
zoned samples - 3 about

Melinda at
GRC - ^{geochemical} geochemistry workshop

Melinda Wright 11-1-99:

3 production scales — sending

- downhole (not piped).
- titanium-cased wells
- small

2 from Site — low TDS (small samples)
1 from Region 3 — high salinity. } contrast diff. fluids.
(big samples).

- talked to Wil Osborn after GRC
- (she did go to geochemistry workshop)

DANA'S NEW MINERALOGY

The System of Mineralogy
of
James Dwight Dana and Edward Salisbury Dana

EIGHTH EDITION
ENTIRELY REWRITTEN AND GREATLY ENLARGED

RICHARD V. GAINES
EARLYSVILLE, VIRGINIA

H. CATHERINE W. SKINNER
YALE UNIVERSITY

EUGENE E. FOORD
UNITES STATES GEOLOGICAL SURVEY, DENVER

BRIAN MASON
CURATOR EMERITUS, THE SMITHSONIAN INSTITUTION

ABRAHAM ROSENZWEIG
ROSENZWEIG ASSOCIATES, TAMPA

With Sections by

VANDALL T. KING
ROCHESTER ACADEMY OF SCIENCE, ROCHESTER, NEW YORK

And with Illustrations by

ERIC DOWTY
SHAPE SOFTWARE



1997

JOHN WILEY & SONS, INC.

NEW YORK · CHICHESTER · WEINHEIM · BRISBANE · SINGAPORE · TORONTO

25°; birefringence = 0.018—can be slightly pleochroic series extends to nontronite using ^{IV}Al. Chromian montmorillonite true volkonskoite has wed, and the mean of 101 gave (Na_{0.01}Ca_{0.007}K_{0.004})₁₀(OH)₂ · nH₂O. Two-thirds tetrahedral sites, and few had). Low-Mg montmorillonite and high-Mg montmorillonite been distinguished [AM tetrahedral occupancy, but can be present in a single species (Cheto type) than the) values do not show enough g montmorillonite types as ng of types within a sample e also been subdivided into an (taylor types) based on ge contribution to net layer 5(1969). Mg may be helpful 5B(1945). Frequently found material, can be impure and es of major elements (wt %) Fe₂O₃, 0.00–13.61; FeO, 0.00–4.23; Na₂O, 0.00–3.74; K₂O, (ppm): Li₂O, 4–88; F, 7100) meq per 100 g. Interlayer A product of alkaline weatherment of altered ash flows and liminary environments. Also , and in hydrothermal mineral ay minerals, also with detrital localities: Only selected occur- am, Oxford Co., ME; Branch- MS; Helms Park, Gonzales; Rita, Grant Co., NM; Pierre ark, Casper; Clay Spur; J.C. ok Co., WY; Ely, NV; Cham- Garfield, Rosebud, and Horn sa Valley; Otay, CA; Umiat, B; Pembina, MAN, Canada; lots, Antigua; Giants Cause- urn Bedfordshire; Red Hill, le Charente Dept.; Plom-

bières, Ludes, Montjavoult, and Violet, *France*; Vallortigara-Posina, Schio, Venezia; Castiglignocello, Livorno; Cala Aqua mine, Ponza Is., Italy; Groschlattengrün, Fichtelgebirge, Bavaria, Germany; Cilly, Untersteiermark, Austria; Stritez, Bohemia, Czech Republic; Barataka, Transylvania, Romania; Selongin Daura, Russia; Malka River area, Caucasus Mts., Kazakhstan; Nahal Ayalon and Hatrurim formations, Israel; Emilia, Calingasta and Burreira mine, Jachal and El Retamito and Mario Don Fernando mine, Retimito, San Juan Prov.; Tala, Heras and Santa Elena, Potrerillos and San Gabriel, Mendoza Prov., Argentina; Taourirt, Morocco; Marnia, Fadli-Mostaganem, and Camp Berteaux, Algeria; Thies, Senegal; Youe, Chad; Iriba, Cameroon; Ankaratra, Malagasy; Reunion Is.; Itoigawa, Niigata Pref.; Usui and Hojun Mts., Gumma Pref.; Yakote and Hanaoka Mts., Akita Pref., Rokkaku, Yamagata Pref.; Tottori, Japan. VK, EF *MIN* 4(2):15(1992).

71.3.1a.3 Nontronite (Na,Ca_{0.5})_{0.33}(Fe³⁺,Al)₂(Si,Al)₄O₁₀(OH)₂ · nH₂O

Named in 1827 by Berthier for the locality. Smectite group. Also originally called chloropal. *MON* C2/m. *a* = 5.23–5.264, *b* = 9.06–9.18, *c* ~ 10, 14.80, 15.0–15.5, β = 90°, 99°, *Z* = 1, 2, *D* = 2.29–2.36. 29-1497(nat): 15.2₁₀ 4.48_{5.5} 3.58₂ 3.05₂ 2.564_{2.5} 2.560_{2.5} 1.51₁ 1.34₁; 34-842(nat): 14.6₁₀ 4.53₁₀ 3.67₂ 3.01₃ 2.60₅ 1.52₃ 1.31₃ 1.27₃. Typical smectite structure with air-dried basal spacings 13.6–15.0 Å normal. Rarely naturally found with collapsed spacings ~ 10 Å. Ethylene glycol causes expansion to 16.9–17.3 Å. Collapses on heating (550°) 9.6–10.4 Å. K-intersalination generally causes some collapse from air-dried spacings to 11.9–13.1 Å. Mössbauer studies show some ^{IV}Fe³⁺. *AM* 73:1346(1988). Nontronites can contain significant ^{IV}Al and parallel beidellite-like smectites: Ca_{0.18}(Fe³⁺1.94Mg_{0.10}Al_{0.06}Fe²⁺0.05)(Si_{3.55}Al_{0.45})₈₄O₁₀(OH)₂ · nH₂O. *AM* 31:294(1946). A pseudo-anhydrous nontronitelike mineral has been reported [Arkansas, *GSAPA* 18(6):528(1986)]. The Arkansas nontronite has a collapsed spacing (~ 10 Å), expands with glycol, but does not hydrate upon immersion in water, and has a near-end-member composition: one water molecule per formula is apparently ordered within the opening of the tetrahedral ring of the silicate layer, yet does not contribute to non-mica-like spacings, (Ca, Mg, Mn)_{0.135} (Fe³⁺1.785Fe²⁺0.185V⁵⁺0.04)_{Σ2.01}(Si_{3.8}Fe³⁺0.18Al_{0.02})_{Σ4}O₁₀(OH)₂ · H₂O. **Physical properties:** Pale to dark yellow-green to olive, also bright yellow-green, resinous to waxy luster with conchoidal fracture to earthy, sometimes fibrous. *H* = 1–2. *G* = 2.06–2.32. Cleavage {001}, perfect. Decomposed or gelatinized by common acids. **Optics:** Biaxial (–); *Y* = *b*, *Z* ~ *c*, high RI material has *X* ~ *c*; *N_x* = 1.545–1.625, *N_y* = 1.569–1.650, *N_z* = 1.570–1.655; 2*V* moderate, 33–40°, ranges 25–70°; *n_x* < *v*; birefringence = 0.035–0.044 (0.010 low Fe); very strong increase in RI with increasing Fe³⁺; positive elongation; usually pleochroic in yellowish (001) to brownish greens parallel to (001); pleochroic. *X*, pale yellow; *Y*, olive-green; *Z*, yellow-green. **Chemistry:** Forms a series with montmorillonite and Fe³⁺ exchange with Al; most compositions yield < 1.0 wt % Al₂O₃, SiO₂,

40.8–48.8; Fe₂O₃, 20.4–32.4; FeO usually < 0.50; MgO, 0.61–2.1; CaO, 0.77–2.2; Na₂O, 0–0.29; K₂O, 0–0.24; TiO₂, 0.08–1.72; P₂O₅, 0–0.02; H₂O⁺, 7.8–11.4; H₂O⁻, 7.1–14.75; H₂O (total), 14.5–23.0; CEC = 60 meq per 100 g. Can replace olivine, chlorite, or pyroxene or be replaced by chlorite. Occurrence: Found with other clay minerals, including kaolinite, glauconite, chlorite, and vermiculite. Found in weathered basalts, ophiolites, basic and ultrabasic rocks, and fractures therein, also in basalt vesicles. Abundant in vertisols, also in submarine sediments, usually authigenic. As a sediment on sea mounts, also around midocean-ridge hydrothermal vents. As a coating in fractures in some granite pegmatites. Localities: Topsham, Sagadahoc Co., ME; Lehigh Mt., Mountainville; Bethlehem(I), PA; Chevy Chase, MD; North Garden, Albemarle Co., VA; Sugar Grove, Pendleton Co., WV; Sandy Ridge; Spruce Pine, Mitchell Co., NC; Wilson mine, Potash Sulphur Springs, AR; Green River Fm, Shirley Basin, WY; Bingham, UT; Santa Rita, NM; Miami, Gila Co., AZ; Woody, Kern Co.; Crestmore, Riverside Co., CA; Garfield(I) and Colfax, Whitman Co., Spokane, Manito, Excelsior, and Valleyford, Spokane Co., WA; lower Cook Inlet, AK; Loihi submarine volcano, HI; Peace River deposit, ALB, Canada; Pinares de Mayari deposit, Oriente Prov., Cuba; Concepcion del Oro, ZAC; Santa Eulalia, CHIH, Mexico; Smallacombe, Devon, England; Isle MaGee, County Antrim, Northern Ireland; *Perigueux Mn mine, St. Pardoux, Nontron, Dordogne, France*; Froland, Norway; Starbo, Sweden; Tirschenreuth and Passau, Bavaria; Meenser Steinberg, Göttingen, Hanover; St. Andreasberg, Zwickau, and Wolkenstein, Saxony; Menzenberg, Siebengebirge, Rhineland, Germany; Uzhorod, Ruthenia (formerly Unghwar); Sitno complex, Pukanec; Sternberg, Moravia, Czech Republic; Urkut deposit, also Szekes-Fejevar, Hungary; Starog Cikatova, Kosovo; Goles, Yugoslavia; eastern Rhodopes Mt., Bulgaria; Troodos ophiolite, Cyprus; Suakin and Atlantis II deeps, Red Sea; Sary-Krym, near Mariupol; Petrovsk, Krivoi-Rog region; Kerch, Ukraine; Balkan mine, Ural Mts., Russia; Baltatarak, Kazakhstan; Galapagos Is., Ecuador; Niquelandia, Goias; Xanda mine, Virgem da Lapa, MG; Campo Formo, Bahia, Brazil; Lake Malawi, Malawi; Lake Chad, Chad; Black Rock and Hotazel, Cape Prov., South Africa; Faratsiho and Behenji, Malagasy; Shulan, Jilin Prov., China; Yamashiro-cho, Saga Pref., Japan; Mururoa Atoll, French Polynesia; Mariana Trench; Kasuga and other Pacific sea mounts; Burra Burra, SA, Australia; Waipiate, New Zealand; remotely sensed at *Viking* land site on Mars. VK, EF

71.3.1a.4 Volkonskoite (Ca_{0.5})_{0.33}(Cr³⁺, Mg, Fe³⁺)₂(Si, Al)₄O₁₀(OH)₂ · 4H₂O

Named in 1830 by Volkov for A. Volkonsky, Russian nobleman. Smectite group. Synonyms: wolchonskoite, volchonskoite. MON Space group unknown. $a = 5.16$, $b = 8.94$, $c = 14.40$, $Z = 2$; also HEX $a = 5.172$, $c = 15.12$, $Z = 1$. $D = 2.29$. *42-619(nat)*: 15.0₁₀ 5.02_{<1} 4.49₅ 3.05_{<1} 2.56_{3.5} 2.51_{<1} 1.69₁ 1.50_{3.5}. Volkonskoite is defined as a dioctahedral smectite with $Cr^{3+} \geq \sum[Al, Fe^{3+}, Mg, \text{etc.}]$. A structural formula of volkonskoite based on type

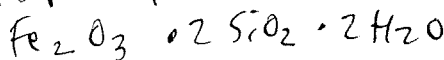
Material has been (Fe³⁺0.29Ca_{0.02})(Si_{3.50}beidellite. Volkon. *CCM 35:139(1987)*. I green; bluish green porous. Conchoidal f. slowly soluble in wa. Fösslbauer and TG. 1969, $N_z = 1.564-1$. refringence = 0.004 green. Refractive ind. volkonskoite usually requ. in a smectite mineral from listed chromophoric effect. relatively low amount. been misidentified a. slow. Volkonskoite: Fe₂O₃ is generally 1-5. Smectite has been de. the total trivalent el. nomenclature should with a possible series (*CCM 35:139(1987)*): Cu, 300; Ga, 30; Li. Okhansk). Sometime (*CCM 35:139(1987)*). (adka); MnO, 0.36 (an); NiO, 0.24 (olkonskoite was found fossil plants. Welkerman area, north adka, Kama area; *Maria, Perm Basin,*

71.3.1a.5 Swinefordite (OH, F)₂ · 2H₂O

Named in 1975 by T. list and professor of am, WA. Smectite probably C2/m. $a =$ (t): 12.96₁₀ 6.27₄ 4.5. hedral 13-Å ect. hues, which can deh.

SS scale formula

1432



only, 5% Al_2O_3

71.1.5.1 Allophane

71.1.5.1 Allophane

for Fe^{3+} . Slightly soluble in HCl and H_2SO_4 . On heating yields hematite and tripuhyite. Occurs as a hydrothermal or secondary mineral in Sb-As deposits and in gneisses with other Sb and As minerals. Found at the McDermitt mercury mine, Humboldt Co., NV; at Venesela Mt., AK; at the Keeley mine, Timiskaming district, South Lorraine Twp., ON, Canada; Velardeña, DGO, Mexico; La Bassade (Haute Loire) Vosges, France; at Freiberg, Braunsdorf, and Schneeberg, Saxony, Germany; Tafone, Tuscany, Italy; at Smilkov, Votice, and Borenov, Bohemia, Czech Republic; in the Kadamdzhai deposit, Kirgizia; Suzuyama mine, Kagoshima Pref., Japan. *EF AM 43:656(1958), 49:1499(1964); MIN 3(1):503(1972).*

ALLOPHANE GROUP

The allophanes are poorly crystallized or noncrystalline minerals with some ordering when viewed by electron microscopy. *CLM 18:21(1983), SRF(1988), MIN 29(1994).* Members of the group include the following:

ALLOPHANE GROUP

Mineral	
Allophane	71.1.5.1
Hisingerite	71.1.5.2
Imogolite	71.1.5.3
Neotocite	71.1.5.4

71.1.5.1 Allophane $Al_2Si_{1-2}O_{6-7} \cdot 2-3H_2O$

Named in 1816 by Stromeyer from the Greek to appear [as] another, in allusion to its change when blow-piped. Allophane group. Synonym: protoallophane. Amorphous or poorly crystalline. Space group unknown. $b = 9.0$, $c = 7.0$. *J8-449(nat)*: 3.3₁₀ 2.25₂ 1.86_{<1} 1.40₁ 1.23_{<1}. Allophane is generally amorphous to X-rays, and is a mineral that has a variable chemical composition. As many as four wide diffraction bands are occasionally observed [*AM 38:634(1953)*] which can disappear on heating to 400° [*CCM 29:124(1981)*] and ^{IV}Al and ^{VI}Al have been determined [*CS 2:1(1964)*], both suggesting some ordering. Numerous TEM studies show that it frequently consists of hollow spheres (~35–55 Å with walls 7–10 Å thick and an external water monolayer [*AM 56:465(1971)*], but which can quickly dehydrate and collapse in electron beams. The spheres might be composed of a phyllosilicate structure rolled to reduce bond distortions. *PICC 2:29(1969)*. Spherical halloysite can be mistaken for allophane by TEM. *CCM 11:169(1963)* and others. A defect kaolinite structure has been proposed [*DS 27:537(1979)*], but MAS-NMR studies suggest an octahedral sheet similar to that of 2:1 phyllosilicates, but different

ating yields hematite and secondary mineral in Sb-As als. Found at the McDermott Mt., AK; at the Keeley ON, Canada; Velardeña, es, France; at Freiberg, 'afone, Tuscany, Italy; at ublic; in the Kadamdzhai Pref., Japan. EF AM

alline minerals with some [18:21(1983), SRF(1988), following:

near [as] another, in allusion. Synonym: protoallophane. Known. $b = 9.0$, $c = 7.0$. 38° is generally amorphous to al composition. As many as served [AM 38:634(1959)] 9:124(1981)] and ^{IV}Al and suggesting some ordering. consists of hollow spheres nal water monolayer [AM 38:634(1959)] and collapse in electron yllsilicate structure rolled rical halloysite can be mis- and others. A defect kaoli-), but MAS-NMR studies hyllosilicates, but different

from that of kaolinite or gibbsite [CCM 42:276(1994)]. Dry grinding can affect allophane morphology [CM 18:101(1983)], as can electron beams [AM 61:379(1976)]. IR studies have been numerous [e.g., CCM 28:295,328(1980); 29:124(1981)] and are similar to those of imogolite. CCM 28:285(1980). Habit: Generally occurs as hyaline crusts, masses, and coatings; stalactites and rarely as flowstone. Physical properties: White to tan, also bright blue, green, or yellow; frequently stained brown; uncolored streak unless stained; waxy to earthy luster, can be unctuous; sometimes translucent. Conchoidal fracture and then showing a shining luster; brittle; sometimes stalactitic. $H = 3$. $G = 1.8-2.78$. Infusible. Gelatinizes in HCl. Chemistry: Chemistry is variable, in part due to impurities, and has been assigned a composition $Al_2Si_2O_7 \cdot 3H_2O$ to $Al_2SiO_5 \cdot 2H_2O$ [AM 52:690(1967)]; $SiO_2/R_2O_3 \approx$ to 2.0 but frequently near 1:1. Analysis (wt %): SiO_2 , 19.71-33.22 (34.80-41.29, Japan); Al_2O_3 , 28.24-50.5; Fe_2O_3 , generally 0.2-1.0 but to 5-6; MgO , 0-0.18; CaO , 0-2.86; P_2O_5 , 0-10.57 (Indiana); SO_3 , 0-0.44; H_2O^- , 19.26-22.52; H_2O^+ , 9.80-25.0. CEC 69-74 meq per 100 g, also 100 meq per 100 g and varies according to cation. PSSSA 23:210(1959). Optics: Isotropic; $N = 1.47-1.52$; RI increases with Fe_2O_3 . Occurrence: Principally a weathering product of volcanic ash; also a hydrothermal alteration product of feldspars. Allophane may be a precursor to halloysite, but halloysite has been observed to alter from allophane. CCM 9:315(1962). Citric and humic acids can inhibit the formation of allophane. PICC 221(1985). Frequently found with admixed halloysite, imogolite, limonite, opal, gibbsite, cristobalite, occasionally chrysocolla or evansite, but nearly pure material can occur in sulfide veins or as a coating. Found in sedimentary (sediments, laterites, weathered basalt, marl, chalk, limestone, coal beds, etc.) and hydrothermal (sulfide veins, replacement zones, etc.) environments. Variously abundant or insignificant in soils. Localities: Selected localities include: Richmond, MA; Bristol, CT; Morgantown, Berks Co.; Friedensville and Allentown, Lehigh Co.; Rohrs Cave, Lancaster Co., Cornwall, Lebanon Co., PA; Polk Co., TN; Lawrence Co., IN; Alabama Street mine and elsewhere, Saline Co., AR; Kelly mine, Socorro Co., NM; Bisbee, and the Maid of Sunshine mine, Gleeson, Cochise Co., AZ; Cerro Gordo, Inyo Co., CA; Trail Bridge and Crescent Lake, OR; Maui Is., HI; Derbyshire; Wheal Hamblyn, Devon; New Charleton, Kent; Hawkswood mine, North Hill, Cornwall, England; Chessy copper mine, Lyons, Rhône, France; Rosas mine, Sulsis, Sardinia; Calabona mine, Alghero; Cerro del Pasca, Mt. Amiata, Italy; Visé, Belgium; Gräfenenthal, near Saalfeld, Thuringia; Schneeberg, and Schwarzenberg, Saxony; Dehrn; in marl at Gräfenenthal, Thuringia, Germany; Jachymov and Chotina, Bohemia; Petrov, Moravia, Czech Republic; Boleslaw mine, Olkusz, Poland; Vyshkovo region, Transcarpathia, Ukraine; Central Aldan and Podolsk district; Cis-Baikal, Yakutia, Russia; Mbobo Mkulu Cave, Transvaal, South Africa; Alotenango, Guatemala; Guoshan deposit, Fujian Prov., China; northwestern Taiwan; Shishigayama, Mt. Chokai; Fukazawa and Iijima, Nagano Pref.; Kakino pumice, Hoyo, and Imogo soil, Hitoyoshi, Kumamoto Pref.; Kanuma and Hangadai, Tochigi Pref.; Oze, Gunma Pref.; Bihoro, Hokkaido Pref.; Kitikami, Iwate

Pref.; Kurayoshi, Tottori Pref.; Ando soil, Okamoto, Japan; Bandung, Java; Sulawesi, Celebes, Indonesia; Aoba, Vanuatu; Mt. Schank, South Australia, Australia; Bealey Spur, Silica Springs, and elsewhere, New Zealand. *VK, EF AM 59:1094(1974), CMB 12:289(1977)*.

71.1.5.2 Hisingerite $(\text{Fe,Mn})\text{SiO}_3, \text{Fe}_2^+ \text{Si}_2\text{O}_7 \cdot 2\text{H}_2\text{O}$

Named in 1828 by Berzelius for the eminent chemist Wilhelm Hisinger (1766–1852). Allophane group. Synonyms: canbyite, scotiolite, sturtite. Amorphous or *MON* $a = 5.40$, $b = 9.0\text{--}9.30$, $c = 14.99$, $\beta = 98.32^\circ$, $Z = 4$, $D = 3.23$. *26-1140(nat)*: 4.23_{10} 2.71_8 2.46_{10} 2.25_8 2.20_8 1.72_{10} 1.57_8 1.55_8 . Hisingerite is generally an amorphous substance which frequently yields a small set of wide or diffuse X-ray diffraction peaks. TEM studies [*CCM 35:29(1987)*] reveal that hisingerite consists of hollow spherical particles, generally 100–200 μm but up to 1000 μm in diameter. As sphere size increases, so does smectite content. *NJBM: 321(1982)*. The weak X-ray diffraction peaks observed have been variously attributed to those of a smectite [*CUSGM 19:1(1974)*], mica, or generalized phyllosilicate, but the longest basal spacings of smectite, micas, and so on, have been observed only rarely (Romania). Does not expand with ethylene glycol. Mössbauer and other more recent studies indicate that hisingerite does not have a layer structure. *CM 18:21(1983)*. IR, DTA, and TGA did not suggest the presence of hydroxyl. *CCM 32:272(1984)*. Hisingerite can be a mixture of amorphous and crystalline materials. *AM 9:1(1924)*. Hisingerite can recrystallize to a mixture of ferrian saponite or nontronite + hematite when heated to 180°. Habit: Commonly massive and compact. May be minutely spherical. Physical properties: Black to brownish black, amber-brown in thinnest slivers and a streak lighter than the massive material; rarely dark red or dark green and photosensitive; resinous to vitreous luster, rarely greasy. Conchoidal fracture but can have a platy parting. [Trace cleavage observed in canbyite (Brandywine).] $H = 3\text{--}3\frac{1}{2}$. $G = 2.3\text{--}3.0$. Decomposed by HCl. Infusible. Can be confused with ferrihydrite. Summary of IR, EPR, Mössbauer data: *MIN 4(2):620(1992)*. Optics: Isometric; $N = 1.44\text{--}1.73$; biaxial; $N_x = 1.562$ (maximum range 1.552–1.595), $N_y = 1.580$, $N_z = 1.582$; $2V(-)$ very small [also $N_x = 1.715$, $N_z = 1.730$, *PASP 44:279(1944)*]; birefringence = 0.020 (0.015); $r > v$, parallel extinction; $B \times O$ perpendicular to cleavage; orange to golden brown, generally nonpleochroic. Chemistry: Hisingerite is generally regarded to have $\text{SiO}_2/\text{Fe}_2\text{O}_3 = 2:1$ with minor substitutions [*CMB 2:294(1955)*], while attempts have been made at rationalizing the alkalis into exchangeable positions [*CCM 32:272(1984)*], frequently with the calculating of a smectite-like formula. Chemical analyses are variable [*DS 36:97(1981)*], but given some high values, such as MgO and/or Al_2O_3 , suggest that some materials, perhaps unrecognized as new to the group were included in the survey. Inability to distinguish X-ray amorphous mixtures (opal, etc.) and minor crystalline components could contribute to the uncertainty of some extreme analyses (wt %): SiO_2 , most commonly 40.35–49.90 ranging to 27.99–56.91; Fe_2O_3 , commonly 14.34–29.00, ranging to 4.80–

70; Al_2O_3 ,
95; MnO , (
10; H_2O^- ,
nally occurri
dently observ
microscopic
or glass. Sc
nygdules. Fr
mes siderite
alcöpyrite. A
observed in re
springs. A
eration rims.
rgite. Localit
icious in qua
cognize. Selec
NY; Gap r
DE; Alexa
y, and Silver
Steppe clai
ardinal mine,
ill, QUE; Wi
AS, Canada; I
ne, Elvestory
id; Tunaberg,
inland, Swede
mburg Sasbac
gul Cetatii, B
II Deep, Rec
mchorr, Khi
probleme, Kri
morsky Krai.
livia; Suzuya
; Sano mine
ll, NSW, Au
BBS 19:9(1
by a sharp 1'

71.1.5.3 Imogo

named in 1962
ce group unk
T 51:327(198
tively few X-
meter and 7-
illaments, usu
by a sharp 1'

Bandung, Java; South Australia, and. VK, EF AM

Hisinger (1766-
te. Amorphous

D = 3.23. 26-

Hisingerite is
a small set of

(1987)

generally 100-

reases, so does

fraction peaks

ite [CUSSGM

basal spacings

omania). Does

recent studies

(1983). IR,

(1984).

materials. AM

an saponite or

y massive and

ck to brownish

an the massive

esinous to vit-

platy parting.

$\frac{1}{2}$. G = 2.3-3.0.

rite. Summary

ics: Isometric;

1.552-1.595),

5, $N_z = 1.730$,

llet extinction;

rally nonpleo-

$2/Fe_2O_3 = 2:1$

ave been made

(1984),

mical analyses

1 as MgO and/

as new to the

ay amorphous

ntribute to the

monly 40.35-

nging to 4.80-

40.70; Al_2O_3 , ranging 0-22.65; TiO_2 , 0-1.88; FeO , 0-6.75 (24.64); MgO , 0-25.95; MnO , 0-3.72; CaO , 0-3.80; Na_2O , 0-2.90; K_2O , 0-1.44; H_2O^+ , 3.46-12.10; H_2O^- , 5.53-17.92. $CEC_{meas} = 20-74.5$ meq per 100 g. Occurrence: Originally occurring in large mammillary masses (to many centimeters) and frequently observed in obvious veins, coatings, or crusts. Increasingly observed as microscopic alterations of iron-bearing rocks, especially igneous rocks and ash or glass. Sometimes observed as a thin amber film or as amber globules in amygdules. Frequently veining fayalite, enstatite, and/or amphiboles, sometimes siderite or wollastonite; also alters from pyrrhotite and possibly from chalcopyrite. A component of chlorophaeite and probably in some iddingsite. Observed in recent sediments. Probably formed by meteoric water, also from hot springs. Alters to nontronite; large hisingerite spheres show nontronite alteration rims. *NJBM*: 321(1982). Also occurs as pseudomorphs after hedenbergite. Localities: Found in a wide variety of occurrences frequently inconspicuous in quantity and due to its nearly amorphous character difficult to recognize. Selected occurrences include: Tilley Foster mine, Brewster, Putnam Co., NY; Gap nickel mine, Lancaster Co., PA; Brandywine quarry, Wilmington, DE; Alexander Co., NC; Montreal mine, Iron Co., WI; Hibbing, Beaver Bay, and Silver Bay, MN; Castle Dome mine, Gila Co., and on the Mildren and Steppe claims, Cababi district, Pima Co., AZ; Bellvue, Blaine Co., ID; Cardinal mine, Stevens Co., WA; Tetrault mine, Montauban-les-Mines and Hull, QUE; Wilcox mine, Parry Sound, ONT; Nicholson mine, Goldfields, SAS, Canada; Lostwithiel and Wheal Jane, Kea, Cornwall, England; Solberg mine, Elvestorp; Brunjo(l), Västmanland; Sjöström mine, Hofors, Gästrikland; Tunaberg, Långban, and Vestra Silfberg, Värmland; *Riddarhyttan, Västmanland, Sweden*; Helsingfors, and Orijärvi; Degerö mine, Helsinki, Finland; Limburg Sasbach, Kaiserstuhl, Germany; Gallego and Aragon rivers, Spain; Fagul Cetatii, Balan, and Masca, Iara Valley, Apuseni Mts., Romania; Atlantis II Deep, Red Sea, Israel; Mt. Karnasurt, Lovozero massif, and Mt. Rasnuchorr, Khibiny massif, Kola Penin.; Ilmen Mts., Urals; Terny Astrobleme, Krivoy Rog, Russia; Zaval'ye, Bug region, Ukraine; Dalnegorsk, Primorsky Krai; Talnakh, Kazakhstan; Gran Canaria, Canary Is.; Llallagua, Bolivia; Suzuyama mine, Kagoshima Pref.; Kawayama mine, Yamaguchi Pref.; Sano mine, Wakayama Pref., Japan; Geelong, VIC; Cobar and Broken Hill, NSW, Australia; Aoba, Vanuatu. Remotely sensed on Mars. VK, EF *SUBBSC* 19:9(1974), *MIN* 4(2):620(1992).

1.1.5.3 Imogolite $Al_2SiO_3(OH)_4$

Named in 1962 by Yoshinaga and Aomine for the locality. Allophane group. Space group unknown. 38-447(nat): 21.0₃ 11.5₁₀ 7.9₈ 5.6₂ 4.4₁ 3.7_{1.5} 3.3₆ 2.25₃; *MM* 51:327(1987): 16₁₀ 7.9₇ 5.6_{3.5} 4.4₁ 4.1₁ 3.7₂ 3.3_{6.5} 2.25_{2.5}. Imogolite gives relatively few X-ray diffraction peaks, has a tubular structure (17-21 Å outer diameter and 7-10 Å inner diameter) and can appear as partial webs composed of filaments, usually in bundles, in TEM. Imogolite is sometimes characterized by a sharp 19.7 Å peak and broad peaks at 13.3, 7.6, 5.5-5.7, 3.7, 3.3-3.45,

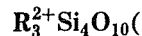
2.25, 2.1, and 1.40 Å. The main peak might be related to a close packing of tubes and the broad peaks relate to a scattering of single tubes. *DS* 27:547(1979). MAS-NMR studies suggest that imogolite has an octahedral sheet similar to that of 2:1 phyllosilicates but different from that of kaolinite or gibbsite. *CCM* 42:276(1994). Dry grinding can affect imogolite crystallinity. *CM* 16:139(1981). Imogolite has been synthesized [*DS* 27:547(1979)] and might form naturally from allophane. The IR of imogolite is similar to allophane [*CCM* 28:285(1980)] and might represent the crystalline equivalent of allophane. *AM* 61:379(1976). Earthy, composed of microscopic threadlike grains and bundles of fine tubes, each about 20 Å in diameter. Light brownish yellow, also tan to white, blue, green, brown. Conchoidal fracture, brittle. $H = 2-3$. $G = 2.7$. Isometric; $N = 1.47-1.51$ and similar to allophane. RI increases with Fe_2O_3 . Principally in soils derived from volcanic ash. Can be found with allophane, halloysite, vermiculite, goethite, gibbsite, quartz, and detrital minerals. Observed in cracks in weathered plagioclase. Citric and humic acids can inhibit the formation of imogolite. *PICC* 221(1985). Selected localities include: Adirondack Mts., NY; Hawaii Is., HI; Plastic Lake, ONT, Canada; Roudado basalt, Aurillac, Cantal, France; Luochan loess, Shensi Prov.; Guoshan deposit, Fujian Prov., China; Kitakami, Iwate Pref.; Kanto loam, Ibaroki Pref.; (Fukuwa) Kanumatsuchi ash bed, Kanuma and Hangadai, Tochigi Pref.; Kurayoshi, Tottori Pref.; Mitsutsuchi ash bed, Iijima, Nagano Pref.; Uemura, Choyo, and Imogo soil, Hitoyoshi, Kumamoto Pref., Japan; New Hebrides; Papua New Guinea; Tirau, Rangitaua, and Wharepaina, New Zealand. VK, EF *SSPN* 8:6(1962); *AM* 54:50(1969); *CM* 8:87(1969), 12:289(1977); *PCM* 12:342(1985).

71.1.5.4 Neotocite $Mn^{3+}SiO_3 \cdot H_2O$

Named in 1848 by Nordenskiöld from the Greek for *new origin*, in allusion to its paragenetic position. Allophane group. Synonyms: stratopeite, penwithite. Isostructural with hisingerite. Amorphous or MON Space group unknown. $b = 9.0-9.30$. 14-172(nat): 4.36₁₀ 3.59₁₀ 2.59_{<1} 1.54₁₀. Neotocite is generally an amorphous substance but has been observed to yield at least five X-ray diffraction reflections (6.4, 4.36-4.4, 3.5-3.59, 2.59-2.6, 1.54 Å). Neotocite forms 70- to 100-Å microspheroids as for hisingerite and allophane. *CM* 18:21(1983). When heated to 1000° for 5 minutes, usually yields braunite and minor jacobsite-magnetite and rarely hausmannite; or pyroxmangite (Påjsberg). Brown, brownish black, rarely dark red, amber brown in thinnest slivers, with a brown to dark brown streak. Generally massive and compact; resinous to greasy luster, rarely vitreous to adamantine. Can be photosensitive, changing from red to brown shades on exposure. Conchoidal fracture, brittle. Rarely shows a platy parting (Klapperud). $H = 4$. $G = 2.04-2.8$. Decomposed by HCl. Sensitive to relative humidity. DTA, IRA data: *MM* 42:279, *M26*(1978), *MIN* 4(2):633(1992). Isometric; $N = 1.475-1.654$, usually pale yellow to reddish brown; sometimes birefringent. 2V to 20°. The composition of neotocite is variable [*MM* 42:279, *M26*(1978)], especially with respect

on, and a series of
 Fe_2O_3 , 0.01-18%
 (Gastrikland); M
 SiO_2 , 0.02-0.3; K_2O
 (1). See also *MIN*
 quartz, mangane
 ers. Can have ad
 tings, or crusts. O
 ks or minerals, a
 thered manganese
 e. Found lining fra
 ese-bearing miner
 difficult to recognize
 ob, Alleghany Co.
 ne, Gogebic Range
 de district, OK; A
 tions in CA, inci
 inore area, Rivers
 Anacortes and el
 -Prov.; Polaris mi
 ov., Cuba; Bamboli
 les; Wheal Owles,
 evik, West Gothlar
 ne, Svärta, Söderm
 sberg, and Filipst
 eden; also in the B
 o, Finland; Herbc
 aveglia, Genoa, It
 omania; Malo-Sedeh
 n; Lafaiete district
 chi Pref.; Kawazu
 n, Japan. VK, EF Al

pyrophyllite talc;
 general formula



ere

$R = Al, Fe^{3+}$

$R = Mg, Fe^{2+}, Ni^{2+}$

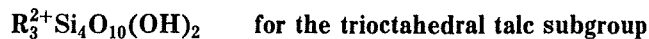
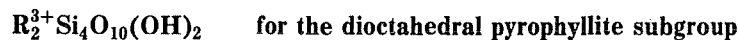
a close packing of single tubes. *DS* has an octahedral n that of kaolinite (ogolite crystallin-27:547(1979)) and is similar to allo- line equivalent of microscopic threadlike er. Light brownish l fracture, brittle. to allophane. RI canic ash. Can be bsite, quartz, and oclase. Citric and 21(1985). Selected lastic Lake, ONT, chan loess, Shensi wate Pref.; Kanto anuma and Hang- i ash bed, Iijima, Kumamoto Pref., taua, and Whare- 54:50(1969); *CM*

igin, in allusion to opeite, penwithite. e group unknown. otocite is generally at least five X-ray (1.54 Å). Neotocite and allophane. *CM* ly yields braunite or pyroxmangite brown in thinnest ssive and compact; Can be photosensi- onchoidal fracture, = 4. *G* = 2.04-2.8. Å, IRA data: *MM* 475-1.654, usually o 20°. The compo- sially with respect

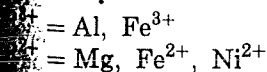
iron, and a series might extend to hisingerite. Analysis (wt %): SiO₂, 30.0-33.8; Fe₂O₃, 0.01-18.7; Al₂O₃, 0.10-2.9; Mn₂O₃, 0-33.2; FeO, usually 0, also 0.6 (Gastrikland); MnO, 10.4-37.2; TiO₂, 0.01; MgO, 0.5-9.6; CaO, 0.1-2.3; Na₂O, 0.02-0.3; K₂O, 0.01-0.3; CO₂, 2.2-7.4; H₂O⁺, 8.2-11.8; H₂O⁻, 7.04 (WI). See also *MIN 4(2):633(1992)*. Associated with rhodonite, rhodochro- site, quartz, manganese phosphates, spessartine, bementite, tephroite, and others. Can have admixed birnessite. Frequently observed in obvious veins, coatings, or crusts. Observed as microscopic alterations of manganese-bearing rocks or minerals, also manganese-bearing ophiolite. Frequently veining weathered manganese-bearing pyroxenes, especially rhodonite, and spessar- tine. Found lining fractures in granite pegmatite and in association with man- ganese-bearing minerals or rocks, but due to its nearly amorphous character, difficult to recognize. Selected occurrences include: Plainfield, MA; Bald Knob, Alleghany Co.; Foote mine, Kings Mt., Cleveland Co., NC; Montreal mine, Gogebic Range, Iron Co., WI; Batesville, Independence Co., AR; Bro- mide district, OK; Aravaipa district, Graham Co. and Ajo, AZ; in several locations in CA, including Johe Ranch mine, San Luis Obispo Co., Lake Placerville area, Riverside Co., and in the Charles Mt. deposit, Humboldt Co.; Anacortes and elsewhere, Olympic Penin., WA; El Fino mine, Pinar del Rio Prov.; Polaris mine, Candelaria district and elsewhere, Bueycito, Oriente Prov., Cuba; Bambolita mine, Moctezuma, SON, Mexico; Llanfaerhys, Rhiw, Wales; Wheal Owles, Penwith, and Geevor mine, St. Just, Cornwall, England; Brevik, West Gothland, Norway; Klapperud, Dalsland; Delecarlia; Gillinge mine, Svärta, Södermanland; at Långban, Jakobsberg, and the Harstig mine, Pajsberg, and Filipstad, Värmland; *Erik-Ers mine, Torsåker, Gästrikland, Sweden*; also in the Brunnsjö mine, near Grythyttan, Örebro; Wittingi, Stor- tyro, Finland; Herborn, Dillenberg, Germany; Chiavari, Liguria, and Val Graveglia, Genoa, Italy; Litosice, Iron Mts., Czech Republic; Yakobeni, Romania; Malo-Sedelnikovsk, Middle Ural Mts., Russia; Tien Shan, Kirghiz- tan; Lafaiete district, MG, Brazil; Broken Hill, NSW, Australia; Shidara, Aichi Pref.; Kawazu mine, Shizuoka Pref., Noda-Tamagawa mine, Iwate Pref., Japan. *VK, EF AM 46:1412(1961), MIN 4(2):633(1992)*.

PYROPHYLLITE TALC GROUP

The pyrophyllite talc group minerals are phyllosilicates corresponding to the general formula



where



Chemical, Mineralogical, and Textural Characterization of Scales from Salton Sea Wells

Progress/Results

At the request of CalEnergy, we have begun a study of scales from the Salton Sea geothermal system. The objective is to understand the scale mineralogy and precipitation mechanisms in both injection and production wells. In injection wells, the scale build up plugs the boreholes and is deleterious to the injection program. In contrast, zinc-bearing scales in production wells are actually a good thing. The zinc in the production fluids and in scales from both the wellbore and surface facilities is being mined at a profit. Before an effective, and possibly expensive, zinc recovery or scale mitigation program can be designed for these wells, the processes that cause the formation of the scales must be well understood. The first step in this understanding is to examine the scales themselves and to document in detail their mineralogical, chemical and textural characteristics. These characteristics may vary depending upon where the wells are located in the Salton Sea geothermal field and at what depth the scales formed within the wells. Scales also form in some of the surface and power production facilities.

There have been a few studies on the formation of the production scales. Scales deposited in the upper portions of wells and in surface plumbing are dominated by an amorphous iron silicate phase similar to hisingerite [$\text{Fe}(\text{OH})_3 \cdot \text{SiO}_2$] (Gallup, 1989, 1993; Gallup and Reiff, 1991), along with lesser galena and other sulfides (McKibben et al., 1990). Scales deposited on downhole steel liners near the flashpoint (point of initiation of steam + liquid flow in the well) consist largely of magnetite and loellingite (FeAs_2) and may contain up to 40 wt % As, 2 wt % Bi, 1 wt % U, 0.1 wt % Au, as well as high concentrations of other heavy metals (McKibben et al., 1990). McKibben lists the chemical composition of magnetite-loellingite downhole liner scales that formed at or near the flashpoint in two SSGS wells (CW-11 and CW-14).

With samples provided by Mark Walters, and Melinda Wright, and Alex Schriener (all formerly of CalEnergy), we have started our investigation by performing X-ray diffraction (XRD) and petrographic analyses of three scales from injection wells Sinclair-21, Sinclair-26, and Elmore-101, and three samples from production wells Sinclair-10, Sinclair-11 and Elmore-12. The results of the XRD analyses indicate that the injection wells are predominantly amorphous silica which is characterized on the diffractogram by a broad hump centered at about 3.90 angstroms. Minor amounts (2-7 wt %) of nontronite (an iron-bearing smectite) and other smectitic clays are also present in these injection scales, as well as about 1 wt % magnetite. The production scales contain between 40 and 52 wt % nontronite. The scale from production well Elmore-12 contains 18 wt % loellingite along with the nontronite. Botryoidal, brownish iron-silicate scale (composed of hisingerite?) observed in thin-sections of the production scales is apparently completely amorphous, leaving no signature on the diffractograms. In thin-section, the amber orange-brown hisingerite is observed to be altered to fine-grained,



November 2, 1999

Susan Juch Lutz
Energy and Geoscience Institute
423 Wakara Way
Salt Lake City, UT 84108

Dear Sue,

Enclosed are three scale samples we talked about on the phone Monday.

Well	Well Type	Date	Depth	Comments
Sinclair-10	Production	7/21/99	?	Sample collected from survey tool
Sinclair-11	Production	2/24/99	?	"
Elmore-12	Production	4/30/99	?	"

Sinclair-10 and Sinclair-11 are located in the Region 1 area of the field (southwest) and Elmore-12 is located in the Region III area (north). The brine produced from the Sinclair wells contains about 23 wt.% TDS and Elmore-12 produces about 30 wt.%. I will provide brine analyses from these wells at a later date.

Let me know if you need additional information or have any questions.

Sincerely,

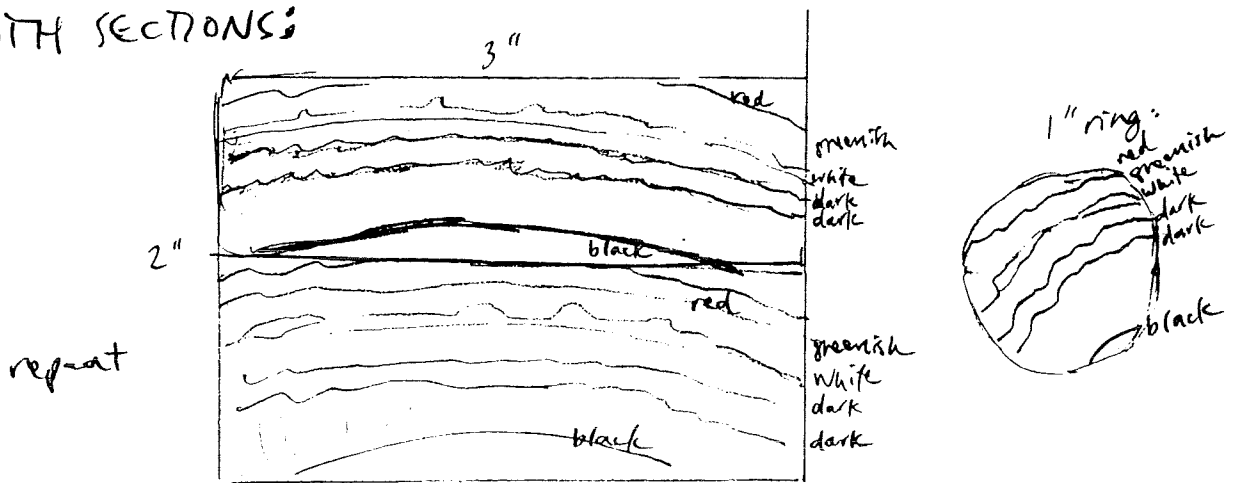
Melinda Wright
Geochemist

10-15-99

TO BE DONE..

SALTON SEA INJECTION SCALES	COVERED OVERSIZED THIN-SECTION 2x3"	POLISHED SECTION 1" ring mounted w/epoxy
SINC-26 9/2/98	X	X X MAKE TWO THIN SECTIONS TO GET ALL THE ZONING
ECMORE-101 6/14/99	COVERED STANDARD THIN-SECTION	X

AL -
FOR SINC-26, PLEASE TRY TO GET SOME OF THE BLACK MATERIAL ON THE INSIDE OF THE PIPE SCALE FOR BOTH SECTIONS. WISH TO HAVE ALL THE BANDS REPRESENTED IN BOTH SECTIONS;
ZONING



I'M SURE YOU'LL DO YOUR USUAL BEAUTIFUL JOB. THANKS. SUE

SECTIONS TO ME:

SUE LUTZ
EGU - UNIV. OF UTAH
423 WAKARA WAY

INVOICE TO:

DEE PETTY
(SAME ADDRESS)

USE P.O. # 18343



September 17, 1999

Susan Juch Lutz
Energy and Geoscience Institute
423 Wakara Way
Salt Lake City, UT 84108

Dear Sue,

Enclosed are two scale samples to start off the project.

Well	Type	Date	Process	Depth (ft)
Sinclair 26	Injection	9/2/98	pH mod	3602
Elmore 101*	Injection	6/14/99	pH mod	4250-4500

*Elmore 101 is an unwashed cutting sample. If you need more sample I can send an adjacent depth interval.

I thought we would begin with pH mod wellbore injection scale. That way we can focus on our worst scale problem from the reservoir standpoint. Sinclair 26 and Elmore 101 are located in the Region 1 area of the field (southwest). The brine injected into these wells contain about 26wt.% TDS and have a pH between 3 and 4. I can send injection brine analyses taken prior to the well clean out if needed. I'm still looking through our storage for additional samples. I'll send those along as soon as I can.

Let me know if you need additional information or have any questions.

Sincerely,

Melinda Wright
Geochemist

Re: scale study

Subject: Re: scale study

Date: Tue, 21 Dec 1999 12:18:21 -0700

From: "Sue J. Lutz" <sjlutz@egi.utah.edu>

Organization: Energy & Geoscience Institute

To: Melinda.Wright@calenergy.com

Howdy Melinda,

I just got the thin-sections and polished sections (for future microprobe work) back yesterday for the production scales. I looked at them briefly and am kind of dissappointed- they appear to be predominantly amorphous banded iron silicate without much sulfides or other opaques. The scales from Elmore-12 and Sinclair-10 are all orange-brown (oxidized-ferric?) iron silicate with some patches of green (reduced-ferrous?) similar-looking stuff. The scale from Sinc-11 may actually be more interesting- it consists of fragments of the iron silicate scale that are cemented by a very fine opaque material. (And, of course, it's the one I didn't get made into a polished section because it looked so grungy as a hand sample.)

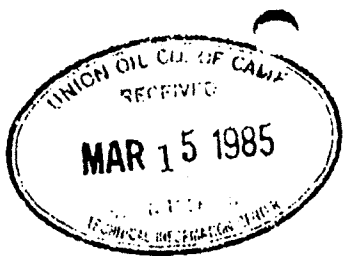
So, that's as far as I've gotten. We can do the XRD easily, but I'm not expecting any great results from the bulk mineralogy (mostly amorphous anyway). I'm guessing that the most variation within the scales and the best characterization will be at the elemental level, and that we will need to do the microprobe work on the very fine-grained opaques.

Hope things are going well for you down in the desert. It's snowing here, but just flurries, the skiing's still no good (I'm a powder hound).

Lunatics will enjoy the big, bright moon tonight,
Sue

Melinda.Wright@calenergy.com wrote:

> Hi Sue,
> How are things going in SLC? It's a balmy 75 here! I just wanted to get
> an update from you on the scale project. No rush, just wanted to see
> what's been accomplished, and if you have a tentative schedule.
> Have a good Christmas and a happy and safe Y2K
> Melinda



Technical Memorandum
Union Science & Technology Division
Union Oil Company of California



CONFIDENTIAL

To: D. P. McArthur, AD

Memo: REF: 85-20M

From: D. L. Gallup, I

Date: February 14, 1985

Department: Refining and Products Research

Project: 745-83401

Subject: Iron Silicate Geothermal Scale
Deposition Mechanism

Supervisor: L. D. Krenzke, A

cc: Library (2)
Patent

S. K. Alley, AD
W. E. Amend, B
G. R. Andersen, R
K. Baron, A
R. V. Bertram, R
C. J. Cron, A
A. A. Dickman, R
J. L. Featherstone, Brawley
G. A. Gritters, Indio
M. M. Hatter, R
P. F. Helfrey, R
D. Hopgood, D
J. W. Jost, AD

W. C. Lieffers, AD
S. D. Light, AD
J. Dave Miller, E1
J. W. Miller, A
B. M. Smith, E1
O. D. Whitescarver, Indio (4)
C. F. Wong, R
M. M. Wong, I
R. A. Dondanville, Santa Rosa
V. E. Sutter, UOC
Circ cc: Alternative Energy and
Minerals Resources Personne

CONFIDENTIAL

SUMMARY

A formation mechanism of iron-rich amorphous silica scale deposited from Salton Sea and Brawley geothermal brine has been tentatively elucidated. The scale arises from a two-step reaction involving the production of ferric iron in the brine via oxidation and subsequent reaction of ferric iron with silicic acid to yield a non-stoichiometric solid. The production of ferric iron is a thermodynamically-controlled process, while the precipitation of scale is kinetically-controlled. Tracer studies show that iron in the scale derives from iron in brine, not iron piping. Brine acidification is shown to inhibit formation of the scale. Reducing agents are shown to be rather ineffective in inhibiting ferric iron production in the brine. The scale has been characterized by elemental analysis and by IR, NMR, Mossbauer, and electron diffraction spectroscopy. Analysis of the scale characterization data supports the proposed mechanism and assists in assigning structure.

INTRODUCTION

Iron-rich amorphous silica scale has plagued smooth operation of Union Oil Co. geothermal steam gathering facilities in the Imperial Valley. Although two processes, crystallization-clarification and pH modification, have been successfully developed to mitigate this scale, no completely satisfactory description of its structure or deposition mechanism has evolved. For several years, we have attempted to understand the scaling mechanism and several hypotheses have been presented(1,2). However, a "uniform theory" of scale deposition that completely satisfies all experimental observations has proven to be most elusive. The objective of this report is to present the results of scale characterization studies conducted over the past few years which support and clarify the actual deposition mechanism. Included in this study is a description of the mechanism of inhibition of this scale.

DISCUSSION

Scale Characterization

Iron-rich amorphous silica scale is deposited from hypersaline brines produced at the Salton Sea and Brawley geothermal fields (see Table 1). Generally, the scale is observed in surface brine handling equipment operating below about 425°F. A typical scale composition is presented in Table 2. The scale is comprised primarily of hydrated silica and iron oxide exhibiting various iron to silicon ratios. Minor constituents present in the scale include transition metal oxides or sulfides and alkaline-earth oxides. A possible empirical formula for the scale is $\text{Fe}_2\text{O}_3 \cdot 2\text{SiO}_2 \cdot 2\text{H}_2\text{O}$.

This iron-rich silica scale does not exhibit an x-ray diffraction pattern and therefore is termed "amorphous." The scale is a non-stoichiometric compound exhibiting iron to silicon mole ratios ranging from about 0.2 to 1.0. The iron-silicon ratio is temperature dependent, decreasing with decreasing temperature (see Table 3). Scale deposited at Brawley in the high temperature brine re-injection mode typically exhibits an iron-silicon mole ratio of 0.8 (four iron to five silicon atoms). By contrast, scale deposited at Salton Sea in the low temperature brine re-injection mode exhibits a ratio near 0.2 (one iron to five silicon atoms).

Infrared spectra of iron silicate scales exhibit bands characteristic of inorganic silicates (Figure 1). Medium intensity bands centered near 3 microns are assigned to silanol O-H groups, weak bands near 6 microns to water, strong-broad bands near 10 microns to Si-O stretching vibrations and strong-broad bands in the far infrared to Si-O and Si-O-Fe groups(3). There appears to be several weak bands between 12 and 15 microns that may be attributable to OH groups bound directly to iron. The spectra could be ascribed to hydrated silica containing chemically bound iron, with iron being bound to silica through oxygen bridges, viz., Fe-O-Si with SiO_4 groups.

By leaching the scale with concentrated hydrochloric acid, all iron in the scale can essentially be removed. The infrared spectrum of the leached scale exhibits bands characteristic of hydrated silica, $\text{SiO}_2 \cdot x\text{H}_2\text{O}$ (Figure 2). The spectrum is very similar to the iron silicate spectra, except for minor shifting of bands to higher frequency, the resolution of weak bands at 10.5 and 12.6 microns and a loss of band intensity in the far infrared. The loss of band intensity and the shifting of bands is evidence for the existence of Fe-O-Si groups (chemically-bound iron) or substitution of iron in a silicate matrix.

High resolution ^{29}Si NMR spectra of iron silicate scales cannot be obtained. The scale is magnetic to paramagnetic which will not allow the sample to be spun at magic angle in the applied magnetic field. However, the iron-free scale (acid leached) can be spun and a typical spectrum obtained by cross polarization-magic angle spinning and high-power proton decoupling is shown in Figure 3. There are several broad resonances in the spectrum between -90 and -110 ppm (relative to TMS). The spectrum resembles that reported for silica gel and clearly shows Q_2 - $(\text{HO})_2\text{Si}^*(\text{OSi})_2$ at -90 ppm, Q_3 - $(\text{HO})\text{Si}^*(\text{OSi})_3$ at -100 ppm, and fully cross-linked Q_4 - SiO_4 groups at -109 ppm(4). The strongest resonance at -100 ppm is evidence for $(\text{HO})\text{Si}^*(\text{OSi})_3$ or if iron were present, $(\text{FeO})\text{Si}^*(\text{OSi})_3$. While the NMR spectrum is rather difficult to interpret due to peak broadening by an inhomogeneous material (scale), peak heights imply a ratio of 1 Q_2 and 1 Q_4 type silicon environment to 4 Q_3 . The scale must contain silicate (SiO_4) groups with random Fe-O-Si linkages. The scale is a three-dimensional polymer of silica containing bound iron. It cannot be a single tetrahedron or a single chain. Figure 4 shows a hypothetical scale structure with the Q groups linked to obtain the ratios observed in the spectrum. Although the structure in Figure 4 is not shown in three dimensions, it is important to note that the Q groups are all tetrahedra with OH and OFe groups located at apices. Figure 4 does not show the complete environment around the ferric iron. Mossbauer spectroscopy shows the ferric iron is high spin and paramagnetic. Ferric iron is octahedral, likely exhibiting an oxide, hydroxide and/or silicate ligand environment, vide post.

Iron-57 Mossbauer spectroscopy has proven to be a very useful tool over the past four years for characterization of iron silicate scale. Figure 5 is a typical Mossbauer spectrum of high temperature scale. The major resonances centered near 0 mm/sec are attributed to iron bound to silica with iron present in the ferric (+3) oxidation state(5a). Weak bands near +2 mm/sec are due to traces of ferrous (+2) iron. Mossbauer spectroscopy conclusively shows that primarily ferric iron is chemically bound to silica in scale. Iron is not present as a chloride or an oxide.

Mossbauer spectroscopy of iron-rich silica sludge deposited from low temperature brine at Salton Sea has also been performed (Figure 5A). In contrast to the scale, the sludge is shown to consist of both ferric and ferrous iron, as silicates. Integration of resonances indicates that iron in the sludge is 46% ferric and 54% ferrous. There is significantly more ferrous iron in sludge than in scales. Wong has titrated iron leached from sludge by acid and found that nearly equal amounts of ferrous and ferric were present, confirming the Mossbauer result(5b).

Transmission Electron Microscopy coupled with Electron Diffraction was recently employed to characterize iron silicate scale from Brawley and siliceous sludge from Salton Sea. Micrographs of scale showed a fibrous, plate-like structure exhibiting a diffraction pattern in good agreement with fayalite, Fe_2SiO_4 (Figure 6A). Fayalite is an olivine group ortho-silicate containing SiO_4 tetrahedra. The electron diffraction result conclusively shows that iron in iron silicate is chemically bound to silica. On the other hand, sludge consisted primarily of microspheres exhibiting a diffraction pattern entirely consistent with $\alpha\text{-SiO}_2$, low cristobalite exhibiting SiO_4 tetrahedra (Figure 6B). Fibrous iron silicate structure is also present in sludge in minor amounts. The TEM analysis confirms that sludge is comprised of a mixture of iron silicate and a rather pure silica phase. Additional analyses of scales and sludges by TEM/ED to define structural changes with deposition variables is planned.

Spectroscopic studies of scale are internally consistent in defining a structure for iron-rich amorphous silica. The scale is a three-dimensional, microcrystalline polymer of silica containing iron (+3) in random positions. Some of the iron is present on surfaces of the polymer network. The iron is chemically bound to the silicate via oxygen bridges to yield a ferric-substituted fayalite-like crystal. The silica is hydrated and contains some silanol surface groups. Ferrous iron (+2) is also present in the scale in minor amounts. Ferrous iron is less tightly bound to the silicate, as it is readily leached from the scale with acid before appreciable ferric iron is displaced from the structure. After leaching iron from the scale, the structural integrity of the particulate scale is maintained, implying that a significant amount of iron is present on the surface.

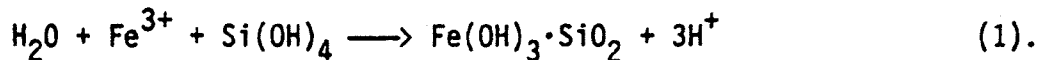
Low temperature sludge differs from high temperature scale in that a significant amount of ferrous iron is present in the silicate matrix. Since silica polymerization dominates the sludge precipitation process, a microcrystalline, three-dimensional polymer likely exists that consists of more Q_4 and Q_2 groups than scale. That ferrous iron is an important constituent in the sludge suggests that ferrous silicate is more soluble in brine than ferric silicate. As the deposition temperature decreases from $\sim 350^\circ\text{F}$ to 220°F , ferrous iron deposition increases dramatically. It appears that ferrous silicate solubility is <10 mg/kg brine at 350°F and at least 60 mg/kg brine at 220°F . Ferrous iron in the scale is in a high spin state implying an oxide (octahedral) environment similar to ferric iron.

Scale Deposition

Iron silicate scale deposits from a complex hypersaline brine containing ~ 500 ppm silica and 500-4000 ppm total iron. The brine in the geothermal reservoir is in contact with minerals such as chlorite, quartz, calcite, pyrite, epidote and clays, from which the species in the brine are probably derived(6). Epidote, pyrite, hematite and magnetite are potential sources of ferric and ferrous iron in the brine. Iron in the brine is primarily present in the ferrous (+2) state as a result of reducing conditions provided especially by H_2S . Ferric iron is always detected in the brine in trace (1-6 ppm) quantities by various analytical methods including, Mossbauer spectroscopy of evaporites, stannous chloride titration, and thiocyanate and pyridylazo-resorcinol colorimetry. Dissolved silica in brine is assumed to be present as monosilicic acid, $\text{Si}(\text{OH})_4$.

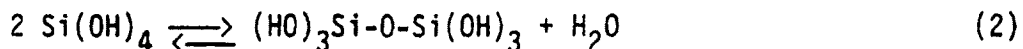
Oxygen appears to be present in the brine in minute quantities (<100 ppb). Oxygen fugacities for geothermal brine have been calculated, as have ferric/ferrous ratios(7). Due to the reducing conditions existing in the brine (Eh of separated brine is usually <+200 mv relative to NHE), ferric iron levels are anticipated to be very low, for example, <1 ppm. Although it has been postulated that 25 to 60 ppm of ferric iron are present in the brine, we have no evidence to support this claim.

Scale material balance calculations have indicated that in the absence of scale control measures, up to 150 mg of scale can be deposited from 1 kg of brine during high temperature re-injection operations. The iron in the scale translates to 25-50 mg/kg brine and silica to 30-70 mg/kg brine. This would seemingly indicate that at least 25-50 ppm of ferric iron are present in the brine and that up to 10-15 % of the total silica in the brine precipitates as scale. In low temperature re-injection operations, much more silica and a little more iron are purposefully precipitated from the brine. Based upon these results and scale characterization data, we earlier proposed a scale forming reaction between ferric iron and silica(8):



This reaction is not exactly correct since varying iron-silicon ratios result in a non-stoichiometric scale.

Scale containing pure silica is not observed in Imperial Valley geothermal operations. It is always associated with ferric iron. The deposition of pure silica arises from polymerization of silicic acid, a condensation reaction:



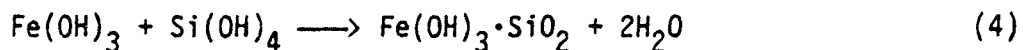
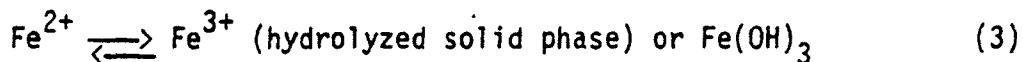
Further polymerization reaction leads to larger oligomers until large particles develop that precipitate as scale. This scale forms as an amorphous solid due to supersaturation as brine cools. (See Ref. 9 for a thorough discussion of silica scaling.) Due to the unique precipitation of amorphous silica from a solution in equilibrium with quartz, Union Oil Co. has attempted to control this scale by re-injecting brine above or near the supersaturation temperature of silica at Brawley or by precipitating silica by seed crystallization at low temperature (sludge) at Salton Sea.

Iron silicate scale generally begins to form at 425°F, which is a much higher temperature than that which results in pure silica scale. Cations in the hypersaline brines decrease silica solubility(10), but still iron silicate forms as much as 75°F higher than pure silica. The Brawley Steam Gathering System, initially designed to re-inject brine above the saturation temperature of silica, scaled deleteriously with iron silicate, not pure silica. At that time, we did not understand the solubility or deposition mechanism of this novel scale.

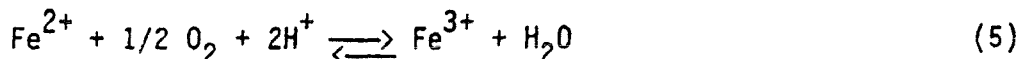
Scale Deposition Mechanism

During the course of silica solubility studies conducted last year in a laboratory autoclave, scale deposition was observed when iron was present in the solvent system. This scale was shown to consist of ferric iron by Mossbauer spectroscopy, in spite of efforts to maintain iron in solution in the ferrous state and to preclude oxygen. Recently a series of tests was conducted to confirm the earlier result. Silica was allowed to dissolve in a synthetic brine containing ferrous iron at 400-500°F in a stirred autoclave. Oxygen was precluded from the system and in some tests, oxygen scavenger/reducing agents were present in high dosages to insure reducing conditions. Resultant scales from the dissolution reaction were retrieved and analyzed by Mossbauer spectroscopy under an inert atmosphere. The spectra of the synthetic scales are strikingly similar to those obtained for scales deposited in piping at the Brawley and Salton Sea Steam Gathering Systems. The spectra show iron in the scales is present primarily in the ferric state as a silicate. This is the first reported case where synthetic laboratory conditions produced similar results to those observed in the field, confirming that ferric silicate scale can derive from brine containing essentially only ferrous iron(11).

The results of these studies lead us to propose a new scale formation mechanism theory which is entirely consistent with characterization studies and the observation that 25-50 ppm of iron in scale is deposited from brine containing <5 ppm ferric iron. The reaction involves two steps; the continuous production of a hydrolyzed ferric iron specie followed by available iron precipitating with silica:



Reaction 3 is an equilibrium between ferrous and ferric iron and is likely the rate-determining step of the overall reaction. The reaction is thermodynamically-controlled. A constant ferrous/ferric ratio is maintained by the brine as the redox potential remains constant. The oxidizing agent in the brine required to continuously generate ferric iron has not been identified conclusively. Possible oxidants might include oxygen and metal ions. Oxygen may be produced by the decomposition of water at high temperature. We have observed various oxidation states of metals in scales. Reduced species observed include elemental silver, lead, arsenic, antimony and hydrogen. Sufficient quantities of the above metals and oxygen are detected in the brine to easily account for the production of 25-60 ppm ferric iron. Cobble(12) has reported the following temperature dependent reaction that yields ferric iron below about 360°F:



A reaction like (5) above could account for the results observed in the field where ferric silicate scale is produced in the presence of <1 ppm oxygen, as the brine temperature is reduced during energy extraction. Ferrous iron would exist above ~360°F (in brine production piping) and hydrolyzed ferric iron would exist below ~360°F (in brine re-injection piping).

In contrast to the field results, autoclave studies of the system, Na-Fe²⁺-Cl-SiO₂ (11), where oxygen was rigidly excluded, produced ferric silicate and ferric oxide (magnetite or iron oxyhydroxide, FeOOH). Even in the presence of reducing agents, ferric iron precipitation continued. In this simple system where the oxidant cannot be oxygen or the metals, lead, silver or antimony, the oxidant would have to arise from the available components, viz., silicic acid, sodium ion, chloride ion, or hydrogen ion (water). Hydrogen ion is the most plausible oxidant in the system; hydrogen ion is available at pH 4, the resultant natural pH of the system. The reduced specie of hydrogen ion oxidation is hydrogen. Hydrogen is observed in the field brine, but is too low in concentration to be observed in the autoclave. In the field, the deposition of 25-60 ppm ferric iron from brine only requires the production of 1-2 ppm hydrogen gas.

Thus, it would appear that hydrogen ion is a likely oxidant in the geothermal system, particularly in the acidic pH range. During brine acidification, silver and antimony metals are precipitated suggesting that the ions may also be potential oxidants. We have observed in the field that increasing the brine pH above 6 results in the formation of lead hydroxychloride. Lead hydroxychloride subsequently corrodes (oxidizes) steel pipe and deposits elemental lead via a redox reaction(13). Thus, increasing the brine pH to inhibit oxidation of ferrous iron by H⁺ is not feasible.

That hydrogen ion may oxidize ferrous iron in the brine is not surprising based on a study of corrosion mechanisms in geothermal systems conducted several years ago by Marsh(14). In an autoclave, corrosion of steel was described by Reaction 6:



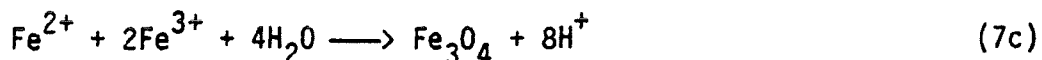
The oxidant of steel was determined to be hydrogen ion. The anodic reaction is the release of iron ions (including ferric iron) and electrons:



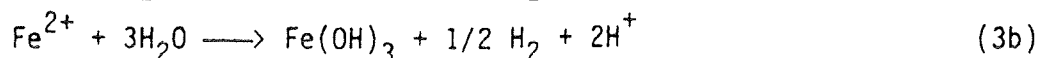
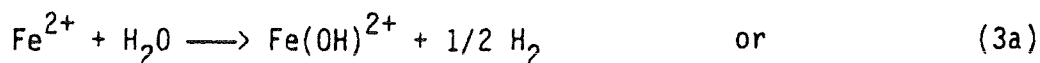
The cathodic reaction is the liberation of hydrogen gas:



The reaction is complicated by the fact that additional hydrogen ions are released as the iron ions react with water to form the corrosion product, magnetite:



The summation of Reactions 7a, 7b, and 7c yields Reaction 6. The abundance of hydrogen ions in the acidic brine forces the cathodic and anodic reaction to the right. Since hydrogen ion can generate ferric ion from elemental iron (presumably ferrous iron is always an intermediate specie) during corrosion, it seems entirely plausible that hydrogen ion (water) is involved in the equilibrium conversion of ferric iron in Reaction 3:

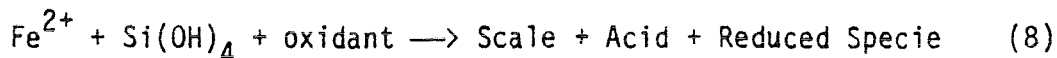


The oxidation reaction product is always hydrolyzed ferric iron. Ferric oxyhydroxides in scales have been detected by x-ray diffraction.

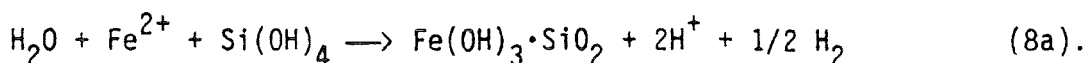
Whenever hydrogen or hydroxyl ions appear in half-reactions (3b), the redox potential varies with pH. The relation between potential and pH is often depicted graphically in the form of Pourbaix diagrams. Figure 7 shows a Pourbaix diagram for a simple iron system. We have not attempted to construct a Pourbaix diagram of geothermal brine due to the complexity of the system. However, we know that in brine exhibiting Eh = +200 mV and pH = 5.5, oxidation of ferrous iron occurs that leads to formation of Fe(OH)₃ (not free ferric ion) predicted by Figure 7. Although standard redox potentials show the iron half reaction occurs at +770 mV and hydrogen at 0mV, the brine is sufficiently complex that hydrogen ion (water) could oxidize iron. Pourbaix diagrams can also show that a ferric iron-containing solid can coexist with ferrous iron in aqueous solution. This result is not unexpected. (Note that free ferric iron only exists at low pH and very oxidizing conditions.) For example, the redox-pH diagrams of sulfur systems can show a little sulfate coexisting in the presence of H₂S. At the Salton Sea Steam Gathering System, we indeed observe barite precipitation in crystallizers containing brines exhibiting traces of sulfide.

Reaction 4 is the scale-forming reaction. It is kinetically-controlled. The reaction is believed to be quite fast because ferric iron is known to have a strong affinity for silica. This is especially true for Fe(OH)₃, which is used to coagulate many colloids in waste waters. Hydrolyzed ferric iron is a well-known coagulant of silica dispersions. At intermediate pH levels (typically pH 4-7), aggregation of silica particles is accomplished by the interaction of positively charged hydrolyzed ferric iron with negatively charged silica surfaces. In this regard, the zero point of charge is about pH 7 for iron hydroxide and about pH 2 for silica. Destabilization of silica colloids by hydrolyzed ferric iron occurs readily at room temperature(15). Thus, the iron silicate rate and formation constants are assumed to be large in the brine environment. As the reaction proceeds, together with the silica polymerization reaction (2), nucleation occurs in the supersaturated (with respect to iron silicate) brine. Scale can become enriched in silica (lower Fe-Si ratio) if Reaction (2) competes with Reaction (4) effectively, especially at lower temperatures. The scale particles grow until outright precipitation occurs. That the scale is amorphous is evidence that a supersaturation with respect to iron silicate exists in the brine. Figure 8 shows a representation of the reaction of ferric hydroxide with silica (Reaction 4).

In the two step process, adding reactions (3) and (4), ferrous iron in brine produces a trace of hydrolyzed ferric iron (solid?) which subsequently precipitates silica as iron silicate (Reaction 8):



and for oxidant = H⁺:



This process, or a similar reaction, allows very little ferric iron to exist at a given time in brine, and accounts for the deposition of ferric silicate containing 25-60 ppm iron. This means that there exists a continuous sink of iron in brine to deposit scale equal to the ferrous iron content. This two step reaction is entirely consistent with observations, scale characterization studies, and autoclave results.

To conclusively determine the source of iron in the scale, we conducted stable isotope (Fe-57) tracer studies in the presence of silica in the autoclave. These experiments were performed similar to those discussed previously(11), by heating silicic acid powder to 500°F in 20% sodium chloride solution containing 1500 ppm ferrous iron as ferrous chloride. In the first experiment, iron-57 foil was added to the mixture and the resultant solid was analyzed by Mossbauer spectroscopy (Table 4 and Figure 9). The Mossbauer spectrum indicates that iron-57 was not concentrated in the resultant iron silicate scale. Iron-57 appears to be concentrated in a trace of the corrosion product, magnetite. In the second experiment, iron-57 foil was dissolved in hydrochloric acid to enrich the ferrous chloride in iron-57. Figure 10, the Mossbauer spectrum of the resultant iron silicate scale, shows an enrichment in the tracer. These results conclusively show that the source of iron in ferric silicate scale is primarily ferrous iron in the brine. Only a small contribution of iron piping to scale is possible.

Scale Inhibition

To inhibit the deposition of iron silicate scale from brine, several chemical treatments have been proposed and field tested, viz., pH modification by acid, reducing agents and dispersants. Acid addition to brine has proven to be an effective scale control procedure. Acid addition drives the scale-forming Reaction (8a) to the left so that ferric iron and silica remain dissociated or iron is leached away in Reaction (4). Acid may also effect Reaction (3) depending on the oxidant. We know that acid inhibits ferrous oxidation especially below pH 2. Whether the amount of acid employed inhibits Reaction (3) or Reaction (3b) is not known, but after inhibiting Reaction (8), the brine continues to establish a trace of ferric iron in the brine. We do not observe an increase in ferric iron in brine upon acidification, indicating re-equilibration via Reaction (3) to yield mostly ferrous iron or inhibition of Reaction (3b). At any rate, acid addition effectively inhibits the overall reaction that precipitates scale. Acid could also restabilize colloidal silica by dehydrolyzing ferric iron. Acidification is also known to inhibit pure silica polymerization kinetics (Reaction 4).

Reducing agents have been extensively studied to inhibit iron silicate formation(12). Reducing agents were selected to drive Reaction (3) to the left. If ferric iron can be totally eliminated by reducing agents, Reaction (4) could not proceed. In all of our reducing agent tests, however, ferric iron has not been completely eliminated. Even when zinc and hydrogen, powerful reducing agents, were added to synthetic brine, ferric iron was not eliminated and ferric silicate scale resulted(11). This result suggests that reducing agents will not be applicable to scale inhibition based on Reaction (3) alone. Reducing agents must diffuse

through the high ionic strength medium and contact the ferric iron specie before electron transfer can occur. Also, a continuous sink of iron remains in the brine with which to contend. Furthermore, most agents that reduce ferric iron require neutral or basic pH. They often lose reducing power as the pH is decreased. Since the brine is naturally acidic, even more so downhole, reducing agents will not be effective generally in controlling ferric iron production in brine. We would not expect reducing agents to be entirely effective downhole corrosion inhibitors (of oxidative corrodants), either. If hydrogen ion is the oxidant or corrodant, a very powerful reducing agent would be required. Several of the best reducing agents are also basic, which presents a brine incompatibility problem. We have observed, however, scale and corrosion inhibition employing a reducing agent in the field(16). It appears that the reducing agent, sodium formate, may have exhibited some inhibition character by reduction or another mechanism, such as dispersion. Reducing agents stronger than hydrogen, such as iron and zinc, may be beneficial in inhibiting scale formation. We plan to field test these metals in this application in the near future. We expect that reducing agents will not mitigate scale to the extent observed employing pH modification.

Dispersants have been pilot field tested for control of iron silicate scale(17). To date, none of the dispersants has effectively controlled the amount of deposit. Dispersants have made the scales softer and more like sludge. Dispersants are designed to disperse scale precipitates and to inhibit deposition at pipe walls. Many of the reducing agents we have examined potentially exhibit structures capable of inhibiting particle growth.

The tenacity with which the scale adheres to steel piping may also be explained chemically. The iron piping appears to initially corrode before scale deposition occurs. Many times scale chipped away from pipe walls exhibits a corrosion product layer adjacent to the pipe. Since corrosion product consists of magnetite or hematite, both of which contain ferric iron, iron-silicate scale is attracted to the iron oxide surface. Apparently, the scale becomes chemically bound to the corrosion product. Thus, iron silicate precipitates on a preferred surface containing iron compounds. This binding to piping follows a precipitation theorem that similar compounds precipitate or prefer each other. This explains recent observations in pilot scale test units where more scale deposited on steel surfaces than on alumina surfaces. This observation also implies that iron silicate scale may bind less tightly and to a lesser degree on high alloy or cement surfaces (containing low iron contents) now under consideration for corrosion control in the steam gathering systems.

As described above, there exists a link between scaling and corrosion. Not only do the apparent mechanisms of scaling and corrosion involve hydrogen ion as an oxidant, but also corrosion of iron piping appears to be the optimal surface on which scale would prefer to grow. This might suggest that iron in the scale derives from steel piping. Material balance calculations show, however, that only 2-4 ppm of iron in piping are dissolved away by brine. This is equal to only about 10% of the total iron calculated for scale. If all of the iron in scale originated from steel, material balance calculations would predict that all casing and surface equipment in a 10 MW steam gathering system would dissolve in one to two years.

Based on the dissolution of 2-4 ppm of steel piping by geothermal brine, we would expect to observe 4 to 6 ppm of the corrosion products, magnetite and/or hematite, in scale deposits. Generally, we cannot account for this quantity of resultant corrosion product (~ 5 ppm calculated vs ~ 1 ppm observed). Thus, it appears that some of the iron dissolved from steel piping remains in the brine or is precipitated as silicate scale, consistent with Mossbauer tracer studies described above.

We have also noted recently that very little corrosion or corrosion products exist on high alloy production casing at the Salton Sea (18). No magnetite or hematite remains on the high alloy casing, in contrast to carbon steel or low alloy casing. However, the thin scale remaining on the high alloy casing consists of iron arsenide, FeAs_2 , and iron bismuthide, FeBi_2 . We do not know the oxidation state of iron in these scales. It is assumed that the iron, arsenic and bismuth are present as free metals (alloys). Mossbauer spectroscopy will be employed to confirm the oxidation state of iron. If iron is present as the free metal, this will be the first instance of reduced iron detected in scale. This iron will obviously not exhibit the oxidation deposition mechanism described above for iron silicate, indicating that iron reduction and oxidation can occur simultaneously in the system, but not at the same location.


D. L. Gallup

DLG:ss
Attachments

ACKNOWLEDGEMENT

I greatly appreciate the many valuable suggestions from and discussions with J. W. Jost, L. D. Krenzke, W. C. Lieffers, and M. M. Wong.

REFERENCES

1. D. L. Gallup, Tech. Memo., REF: 81-021M, Feb. 20, 1981.
2. G. A. Gritters, Geothermal Div. Memo. 1805p, Mar. 14, 1984.
3. V. Stubican and R. Roy, J. Am. Ceram. Soc. 44, 625 (1962).
4. G. E. Maciel and D. W. Sindorf, J. Am. Chem. Soc., 102, 7607 (1980).
5. L. Greenwood and W. Gibb, "Mossbauer Spectroscopy," Chapman and Hall, London, 1971.
- 5b. M. M. Wong, communication.
6. T. D. Palmer, LLL, UCRL-51976, Dec. 15, 1975.
7. G. R. Andersen, Tech. Memo., REF: 84-61M, July 10, 1984.
8. D. L. Gallup, Tech. Memo., REF: 82-32M, Feb. 25, 1982.
9. E. F. Wahl, Workshop on Materials Problems, 1976, p.15.
10. W. L. Marshall and C. Chen, Geochim. Cosmochim Acta, 46, 289 (1982).
11. D. L. Gallup, Tech. Memo., REF: 85-02M, Jan. 14, 1985.
12. J. W. Cobble, Int. Sym. on Corrosion and Scaling in Geothermal Systems, Jan. 17, 1983.
13. D. L. Gallup, Prog. Report, REF: 83-236R, Dec. 8, 1983.
14. G. A. Marsh, Pure Oil Prog. Report, 3-713, Dec. 23, 1963.
15. C. R. Omelia and W. Stumm, J. Colloid and Inter. Sc., 23, 437 (1967).
16. D. L. Gallup, Prog. Report, REF: 83-30R, Jan. 25, 1983.
17. D. G. Samuelson, et.al., Tech. Memo., PD-20M81, Apr. 13, 1981.
18. Results forthcoming.

RECENT UNION BRAWLEY WELLS - TABLE I

<u>Well</u>	<u>Veysey 11</u> <u>(ppm)</u>
Date	10/14/80
Reference	PD-10M-81
Ag	1.2
Al	.55
Ba	1,149
Ca	22,543
Cr	<0.5
Cs	15.6
Cu	1.4
Fe	3058
K	12,549
Li	248
Mg	113
Mn	1.5
Na	46,665
Pb	254
Rb	66
Si (SiO ₂)	172 (370)
Zn	427.6
Cl-	135,260
F-	.63
I-	4.6
SO ₄ ²⁻	3.6
NH ₃	693
TDS	250,500
CO ₂	19,726
CH ₄	130
H ₂	2
N ₂	17.9
H ₂ S	55.8

TABLE 2

Scale Composition

Al ₂ O ₃	0.50
Ca	0.53
FeO	40.98
Mn ₂ O ₃	0.62
SiO ₂	42.77
<u>H₂O</u>	<u>~12.50</u>
Total	97.90
Fe-Si (mol)	0.80

TABLE 3

Iron-Silicon Ratio vs Temperature

<u>Fe-Si (mol)</u>	<u>Temperature, °F</u>
0.25	220
0.49	260
0.53	280
0.61	310
0.75	350
0.90	425

TABLE 4**Iron-57 Tracer Studies**

<u>Experiment</u>	Solution, ppm		Solid, Wt%		Mossbauer
	<u>Fe³⁺</u>	<u>Fe²⁺</u>	<u>FeO</u>	<u>SiO₂</u>	<u>Fe-57</u>
Fe-57 Foil (Steel)	12	750	0.22	89.88	Trace-Fe ₃ O ₄ and Iron Silicate enriched in Fe-57
Fe-57 Chloride (Brine)	6	760	1.42	79.18	Major-Ferric Silicate enriched in Fe-57

FIGURE 1. IR SPECT M

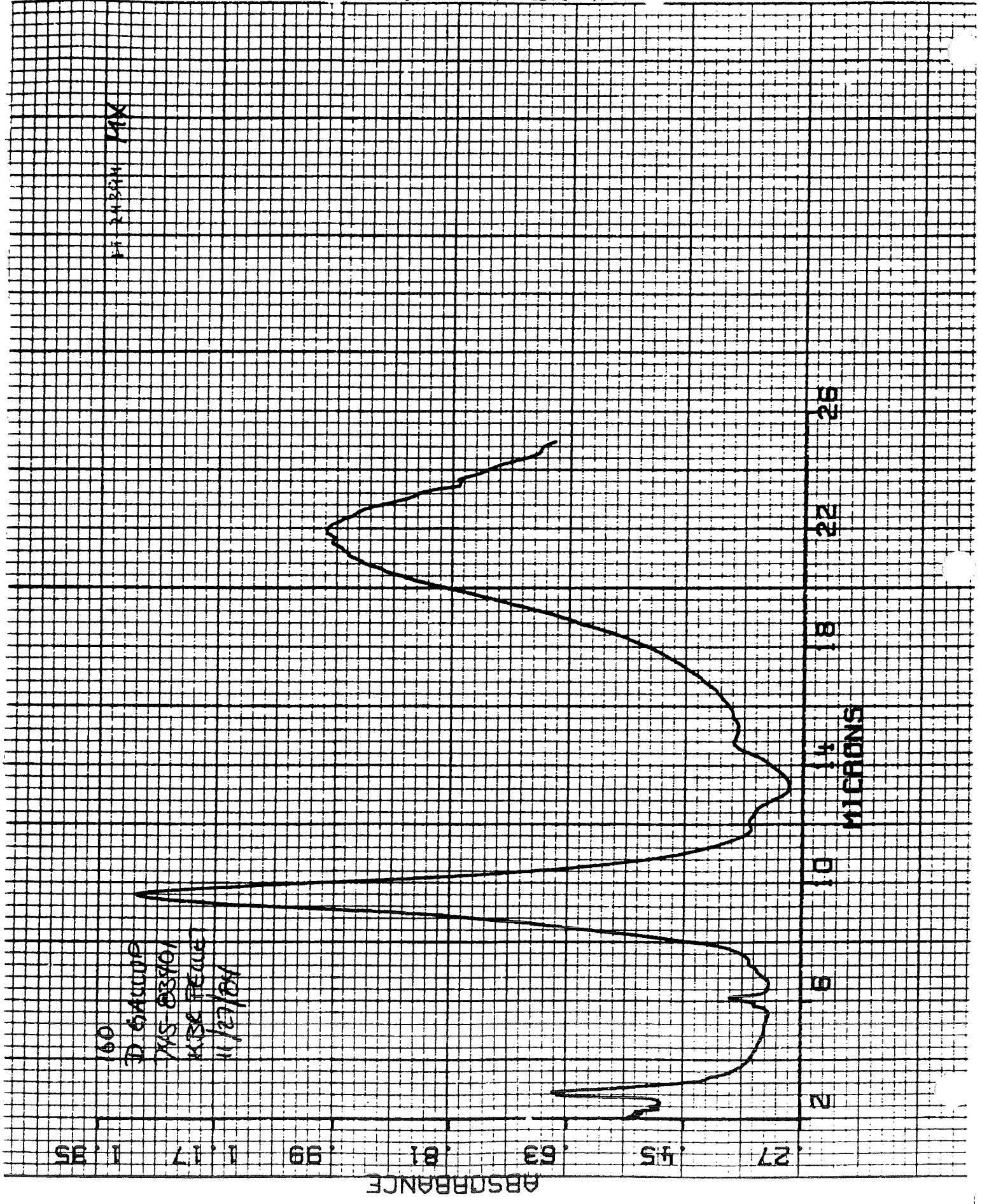


FIGURE 2 IR SPECTRUM

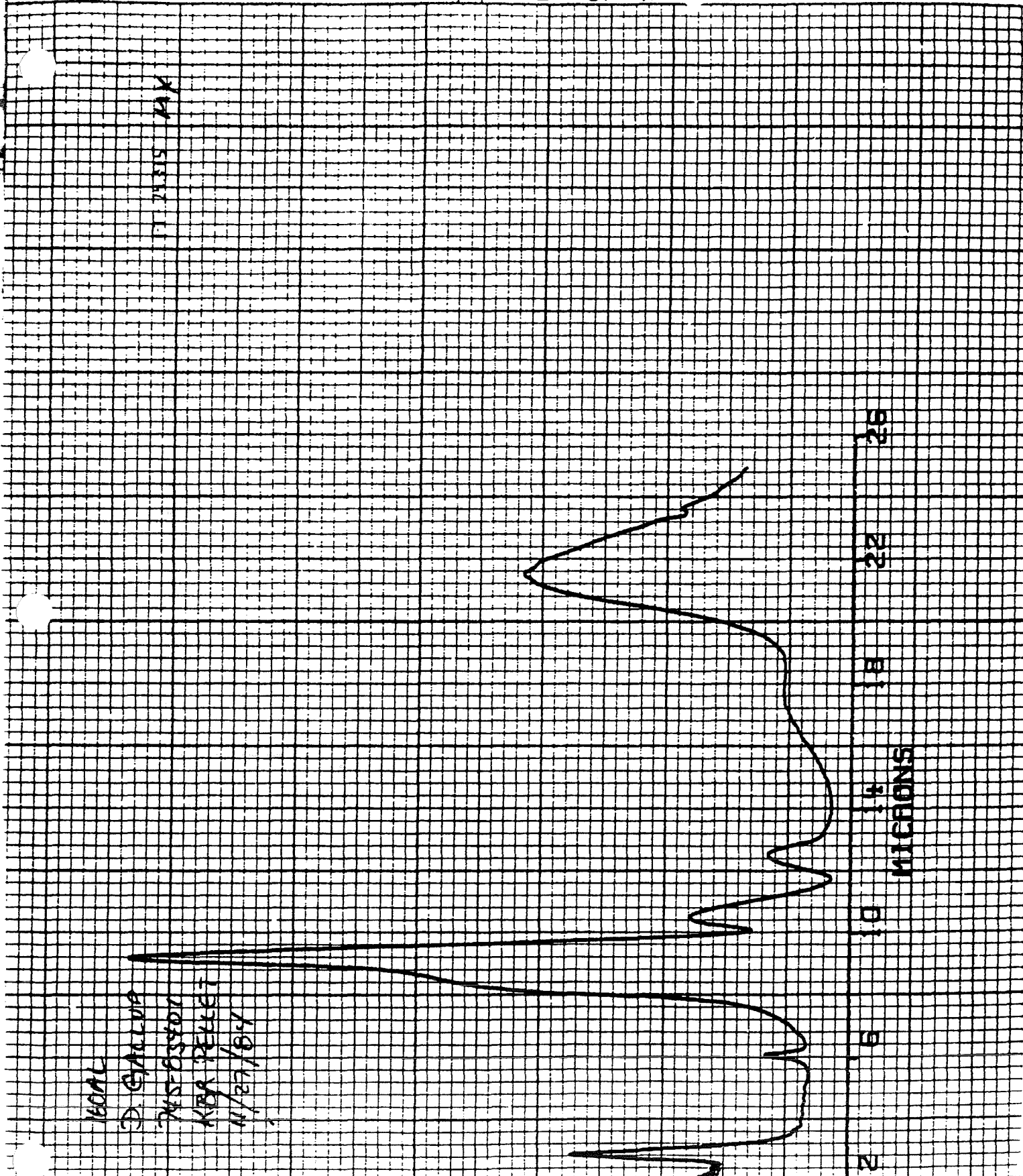
IR SPECTRUM

16006
D. GALLUS
MUSCIVOR
KBR PELLET
11/27/64

1.11
.95
.79
.63
.47
.31
.15
N
6
10
14
18
22
26

ABSORBANCE

MICRONS



CALC10. 001 CER
AL 2657-160
SI-28 CER-NAS

10DEC84

CSU

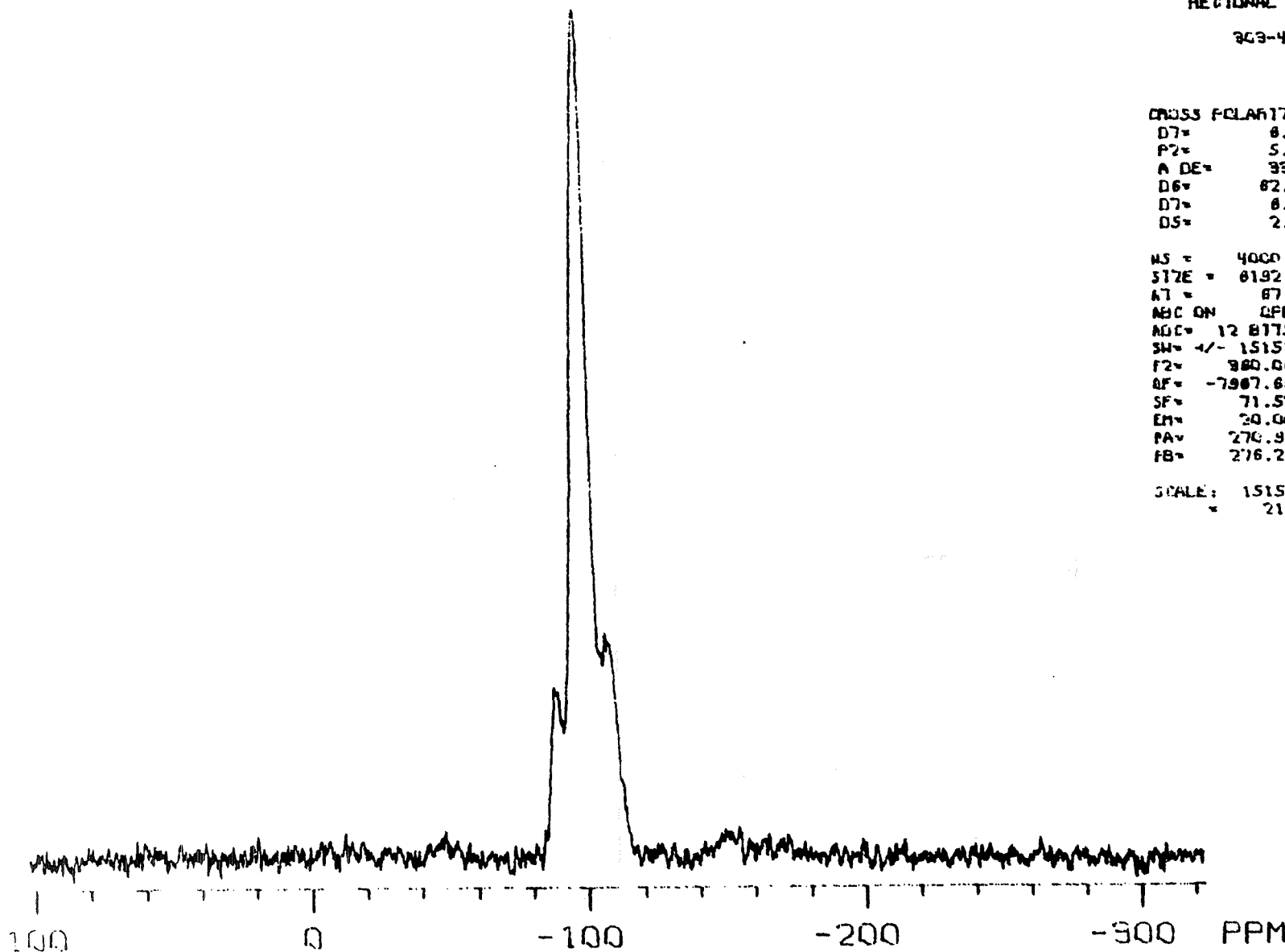
COLORADO STATE UNIVERSITY
REGIONAL NMR FACILITY

303-431-8455

CROSS POLARIZATION
D7= 8.00 USEC
P2= 5.00 MSEC
A DE= 99 USEC
D6= 82.00 MSEC
D7= 8.00 USEC
D5= 2.00 SEC

NS = 4000
SIZE = 8192
AT = 87.62 MSEC
ABC ON QPD ON =
ADC = 12 8175 A1 =
SN = +/- 15151.5 GM =
F2 = 980.062000
RF = -7967.68
SF = 71.528159
EM = 20.00
FA = 270.9
FB = 276.2

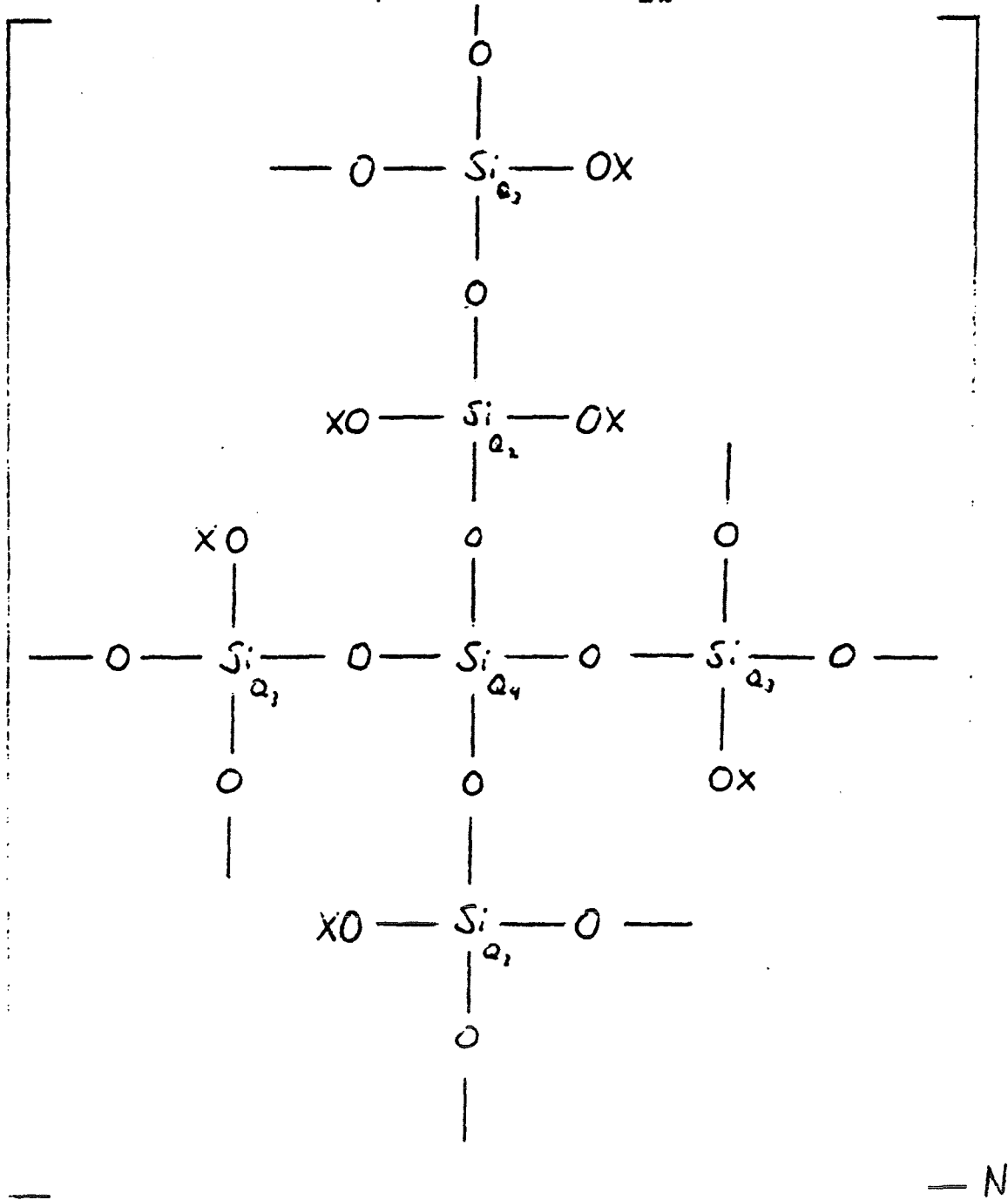
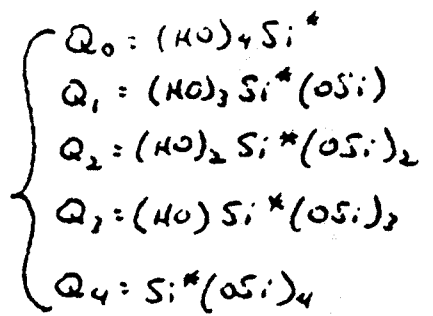
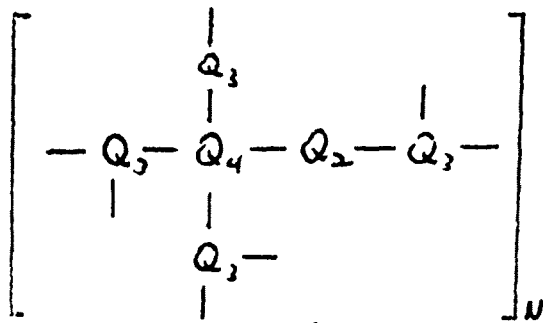
SCALE: 1515.15 HZ/CM
21.1891 PPM/CM



1
4
99

FIGURE 3. 28Si NMR SPECTRUM.

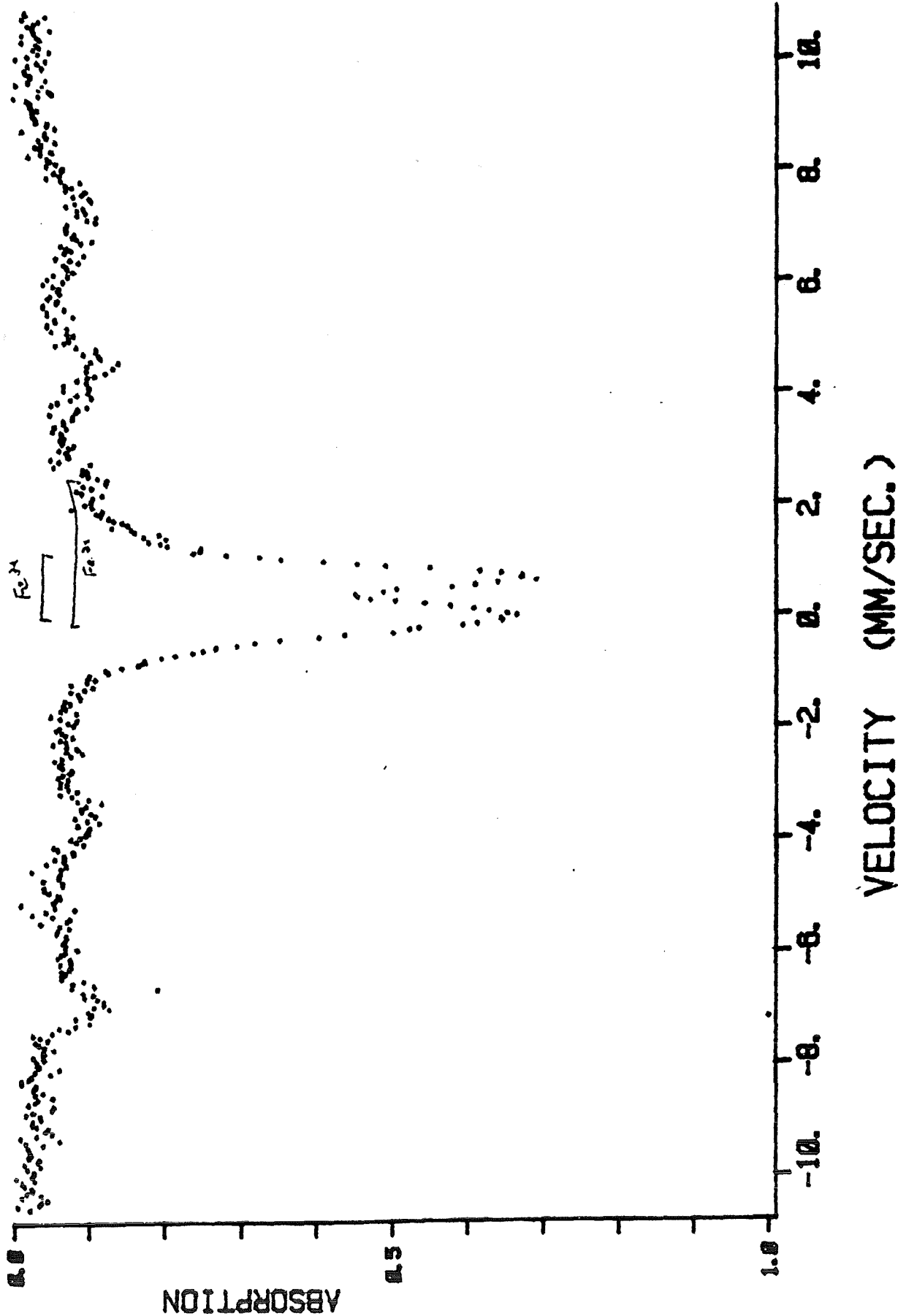
FIGURE 4
IRON SILICATE STRUCTURES



X = Fe, H

FIGURE 5. Mossbauer spectrum - Scale

1210890, SCRU NO 5, 30 MG IN BORON NITRIDE, 1.2X10²⁰, 76K, HOT PZ CHANNELS 0-511



WISCONSIN HIGH SPEEDS "SLUDGE", T-AMBIENT, Q. 4 MOD VS HOT NEN

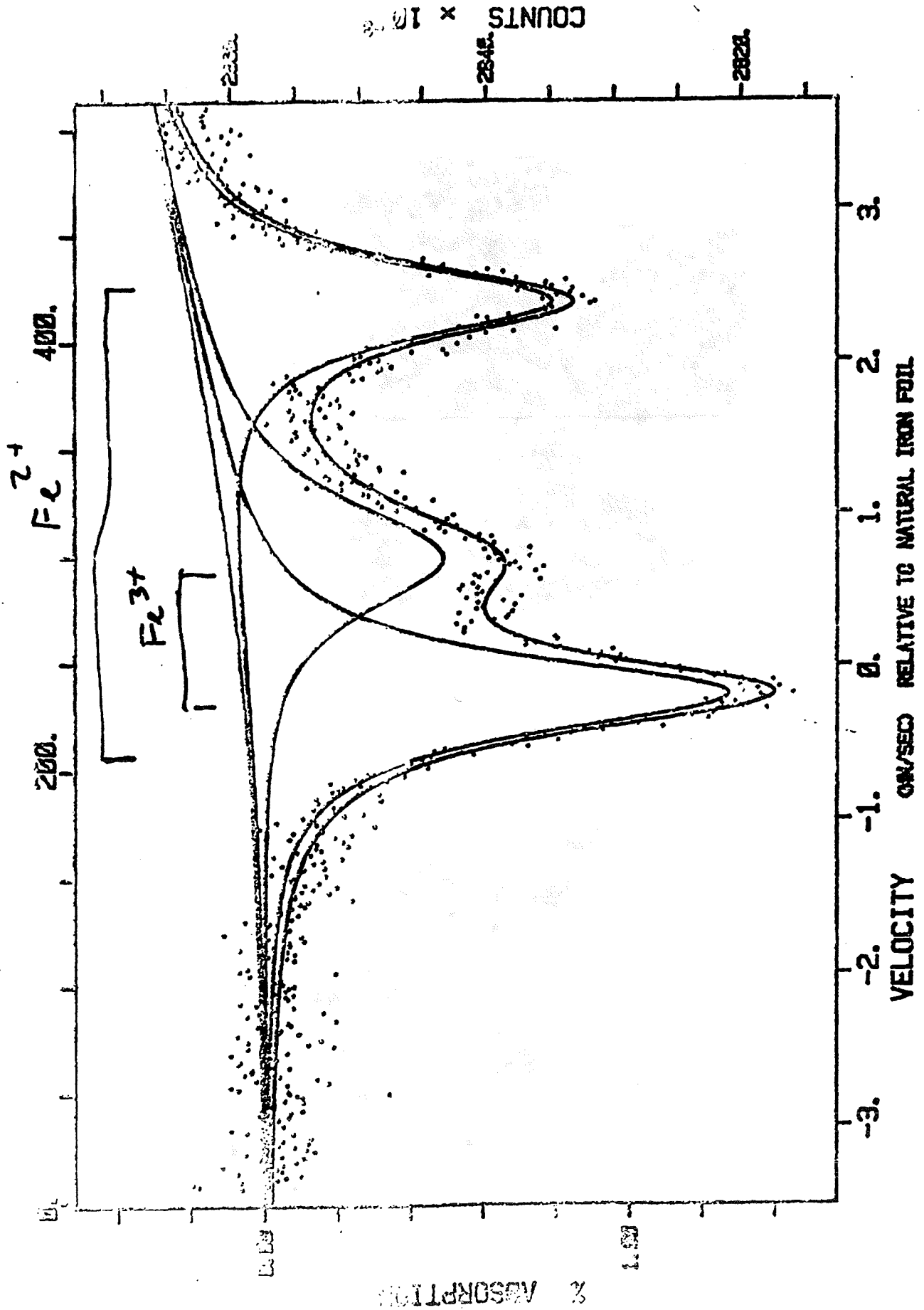


FIGURE 6A. TEM - IRON SILICATE SCALE



X 80,000

FIGURE 6B. TEM - SLUDGE



X 80,000

FIGURE 7. POU-BAIX DIAGRAM

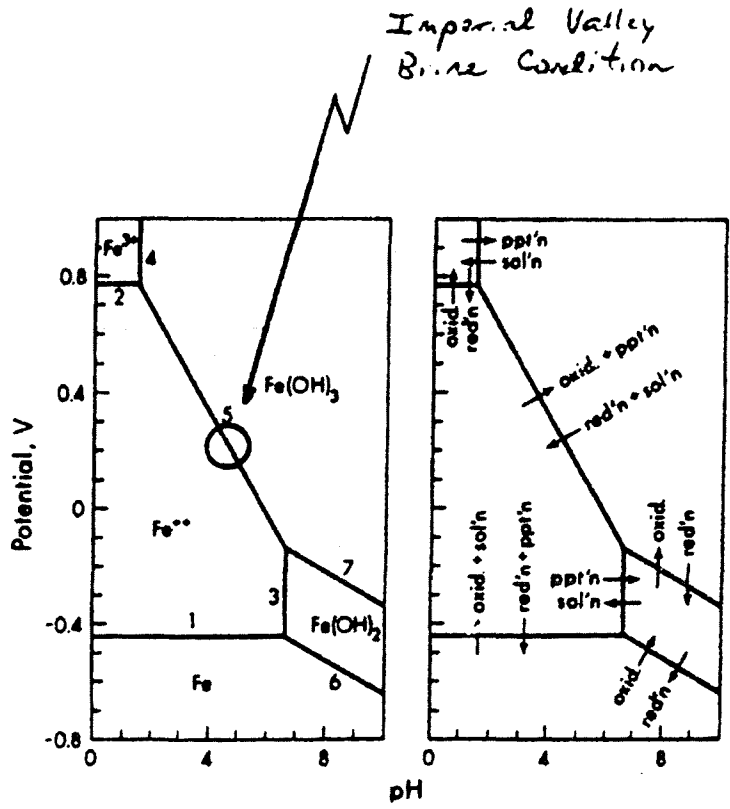
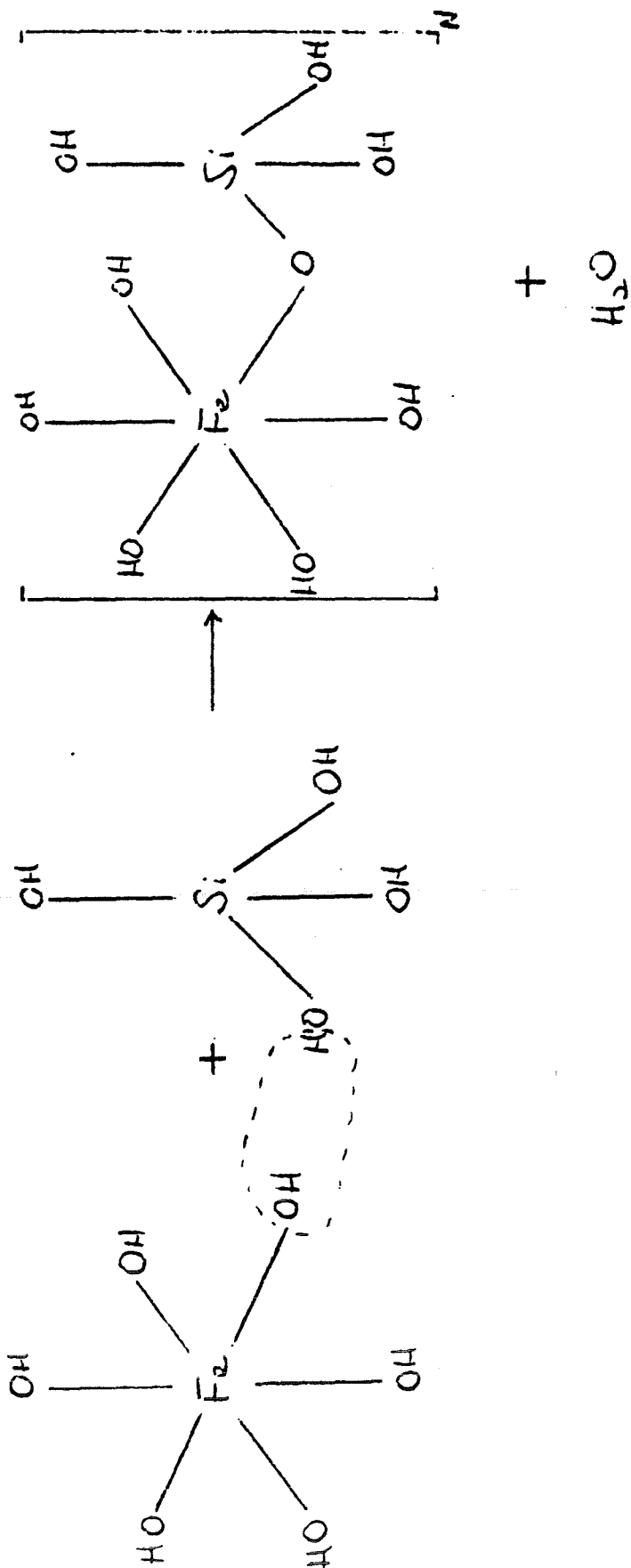


FIGURE 12-1 Simplified predominance-region or potential-pH diagram for the system Fe, Fe(II), Fe(III). Left, predominant species present; right, type of reaction occurring in passing from one region to another.

from HA LAITINEN & WE HARRIS
"CHEMICAL ANALYSIS",
MCGRAW-HILL, N.Y., 1975.

FIGURE 8. IRON-SILICA REACTION



784
0022085 SYN-8 MOD-1.4X100 T-RT

CHANNELS 0-511

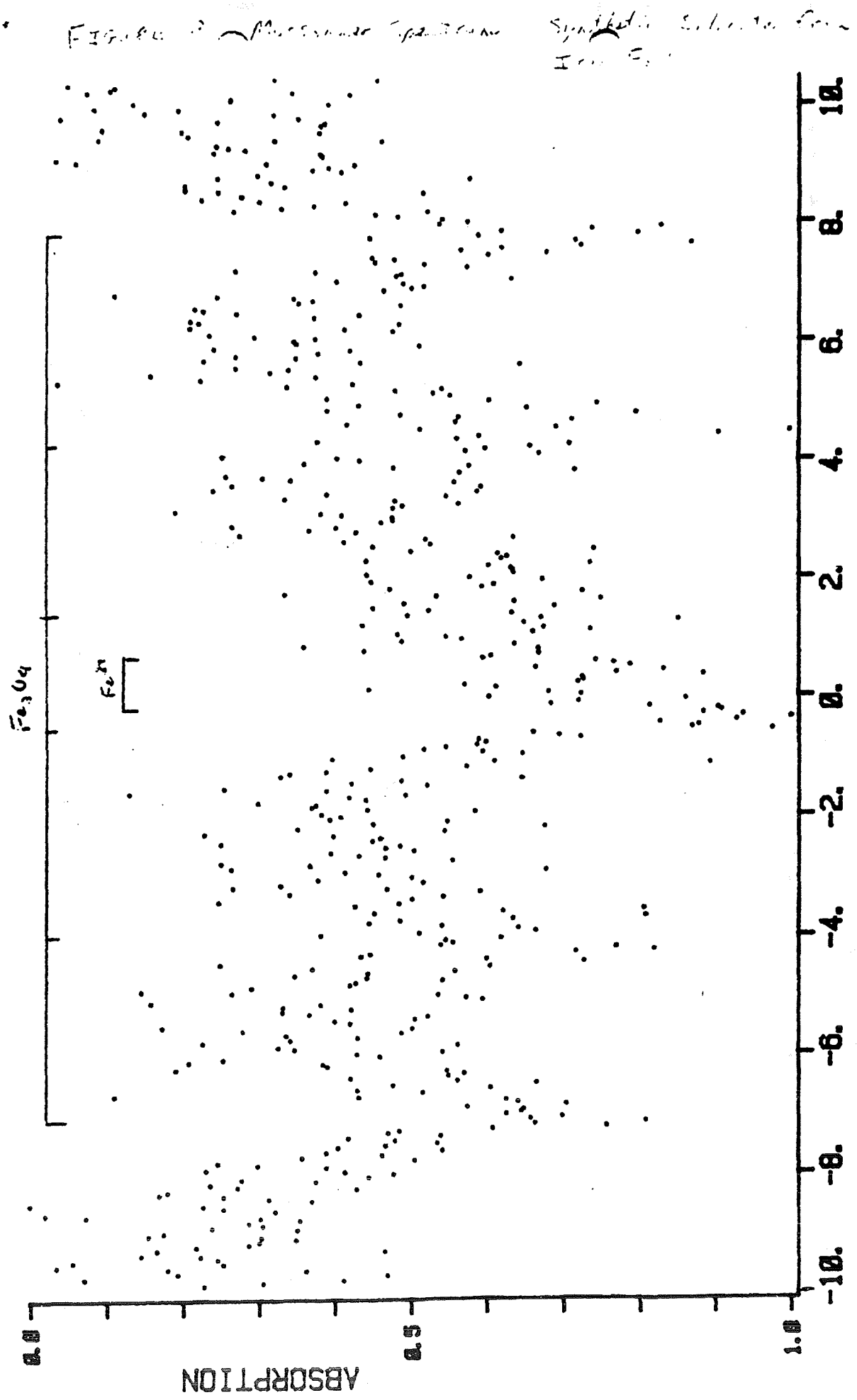
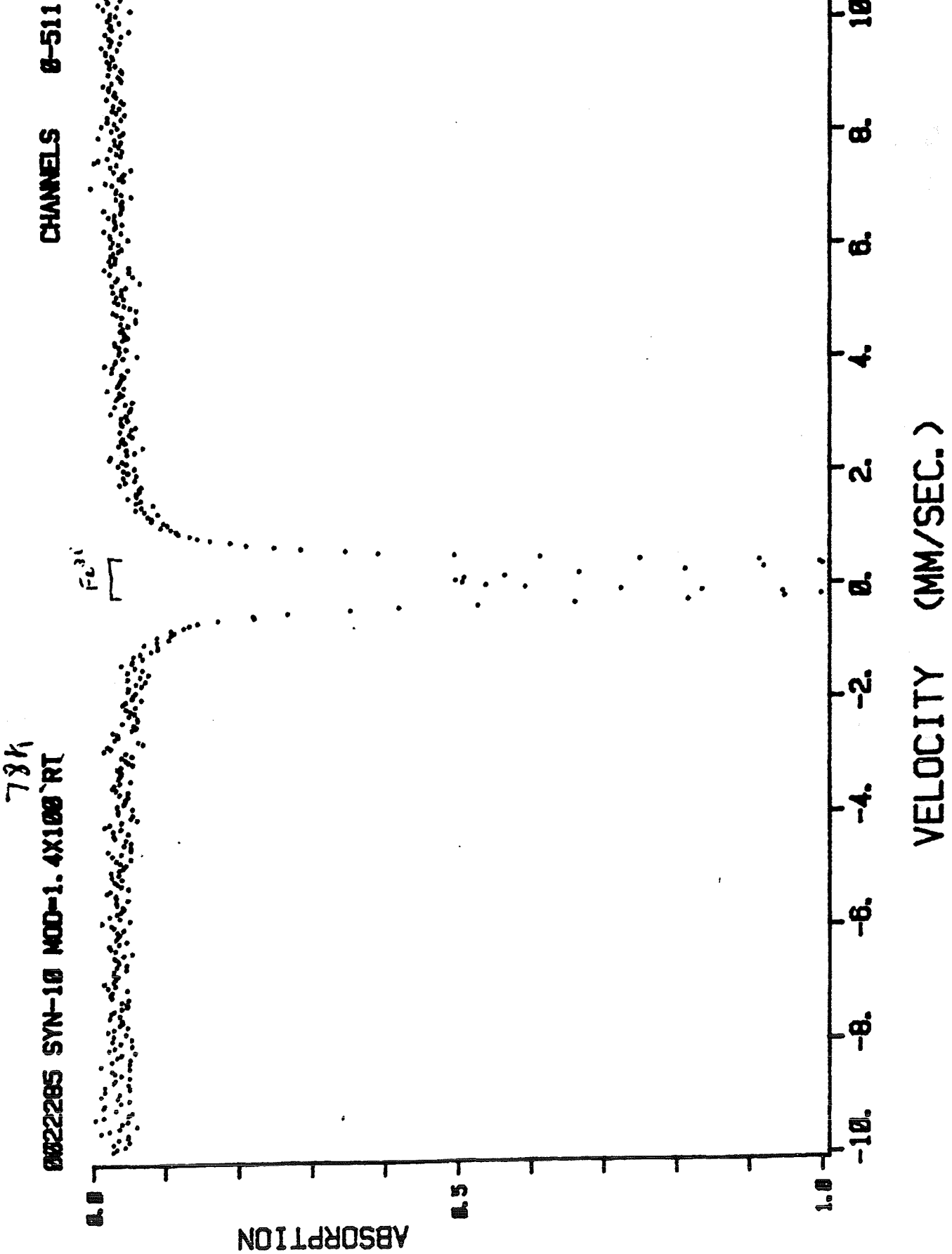


Figure 2 - Mossbauer Spectrum Synthetic Substrate from Han Fe

Figure 10. Mössbauer Spectrum

Synthetic Sulfide film
Fe-57 enriched film



Progress Report

Union Science & Technology Division
Brea, California

UNOCAL 76

Department:

Refining & Products Research

Project:

745-83410

Project Title:

Scale Analysis - Salton Sea

Date:

September 28, 1987

Report Title:

SALTON SEA SCALE REPORT
SEPTEMBER 1987

Report:

REF: 87-158R

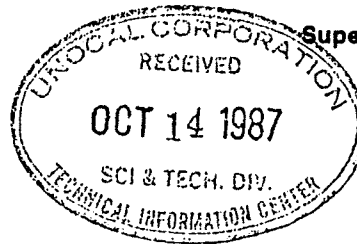
Investigators:

D. L. Gallup, I

Supervisor:

K. Baron, I

**cc: Library (2)
Patent**



S. K. Alley, AD
A. E. M. Barloewen, AD
J. D. Bush, Indio (2)
R. F. Dondanville, Santa Rosa
J. L. Featherstone, Brawley
M. M. Hatter, R
P. F. Helfrey, R
J. W. Jost, AD

L. D. Krenzke, I
C. T. Ratcliffe, I
G. T. Ririe, E-1
D. M. Ruiz, Indio
T. S. Spang, Brawley
J. B. Strong, I
J. W. Ward, A
O. D. Whitescarver, Indio (4)
M. M. Wong, I

SUMMARY

Eleven scale samples obtained from the Salton Sea geothermal field were analyzed this month (Groups 82-85). Deposits retrieved from the Steam Gathering System during the April turnaround (Group 82) consist of iron silicate, fluorite, barite, metal alloys and native silver. Scales deposited in the IID-12 production well consist of iron arsenide, bismuth, gold, copper and magnetite. Scales obtained from brine injection lines consist of copper arsenide and a white layer identified as nearly pure silica.

RESULTS AND DISCUSSION

Tables 1-5 present the results of analyses performed recently on scale samples retrieved from various locations at the Steam Gathering System. The Appendix describes the scales collected by Geothermal Division personnel. Scale groups examined in this study include Groups 82-85.

CONFIDENTIAL

CONFIDENTIAL

Group 82 scales were retrieved from the Steam Gathering System after shutdown in April for a scheduled turnaround. The compositions of these scales are similar to those examined previously from the crystallizer-clarifier system. High temperature deposits (Samples 1 and 3) consist primarily of ferric silicate, $\text{Fe}(\text{OH})_3 \cdot 0.7 \text{SiO}_2$, $\text{Fe}:\text{Si}$ (mol) = 0.7. A trace of the formation mineral, feldspar, is detected in the separator brine outlet (Sample 1), and barite (BaSO_4) and fluorite (CaF_2) appear at the high pressure crystallizer outlet (Sample 3). Sample 4, obtained from the low pressure crystallizer, contains more barite and less iron than Sample 3. Scale deposited in the atmospheric flash tank, Sample 5, consists primarily of fluorite, as expected. Additionally, Sample 5 also contains nearly 8 wt% native silver. Samples 6 and 7, obtained from the brine injection line consist of silver and copper arsenide, respectively, in addition to iron silicate. The deposition of the exotic metals, silver, copper, antimony and arsenic, is believed to be due to galvanic-type reactions in areas of high turbulence that ultimately result in corrosion (iron dissolution).

Group 83 scales were retrieved from the IID-12 production well during a recent workover. Samples 1 and 2, obtained from the bottom joint (titanium) of the hangdown string are metallic in nature. Compounds and elements detected in these scales include arsenic as iron arsenide, copper, bismuth, bismuth oxychloride, antimony, nickel, molybdenum (MoS_2) and surprisingly, gold. Gold could not be quantitatively analyzed due to the small sample size available. This is the first instance of major gold deposition observed in scales deposited from Salton Sea brine. Gold has previously been detected (1), but not as a major (>10 wt%) scale component. This analysis should finally dispel any claims that gold is not present in Salton Sea brines. Special brine analyses have shown that 10 ppb gold is present in IID-12 wellhead separator brine (2). It is recommended that a larger scale sample be retrieved from the bottom joints of the production wells in the future to allow for better quantification of these exotic metals, especially gold. Again, we believe that these metallic scales are deposited via galvanic (reducing) and turbulent conditions. I also recommend that a study be initiated to determine methods to quantitatively precipitate gold from Salton Sea brine and to determine its deposition mechanism on the bottom joints of these production well hangdown liners. Sample 3, obtained from the outside surface of the hangdown liner at 1280 feet, consists primarily of the corrosion product, magnetite. This scale also contains what appears to be copper and iron arsenides.

Group 84 scale was retrieved from the IID-6 injection line meter run after startup of the secondary clarifier. This sample consists primarily of metallic components including copper arsenide and native silver. Also present in the scale is iron silicate. This scale contains <0.5 wt% organic matter (flocculant). I do not believe the higher scaling rate observed is attributed to the presence of flocculant. The metallic nature of this scale suggests that galvanic reactions are responsible for enhanced scaling. Group 85 scale was also retrieved from the injection line at the strainers. This scale also contains <0.5 wt% organic matter. However, it contains only minor amounts of metallic

components and consists primarily of clarifier sludge components--barite, fluorite, iron-poor silica (see Table 5). This scale also does not appear to have been deposited as a result of flocculant addition. Instead, I believe the scaling is due to solids carryover from the clarifier coupled with insufficient brine stabilization with respect to silica. Layers in the scale were examined by scanning electron microscopy. Figures 1 and 2 show the morphology and compositions of a green layer and a white layer, respectively. This SEM study suggests that the green layer composition is similar to clarifier sludge containing iron silicate, fluorite, and barite. The white layer, on the other hand, is enriched in silica. The green layer probably consists of <50 wt% silica, while the white layer appears to be almost pure amorphous silica contaminated with about 5-10 wt% fluorite. That nearly pure amorphous silica is present as a layer in the scale suggests that upsets in silica stabilization by the clarifiers occurred or that the brine cooled and set stagnant in the line during the upset condition described in the Appendix. To reiterate, I find no evidence to suggest that flocculant or polymer concrete injection line caused this scale deposition. Rather, the enhanced scaling appears to be due to upset conditions in the brine clarification system that allowed the brine to be unstable with respect to silica precipitation.

-
1. Ririe, G. T., Tech. Memo, E&P GEOL 87-4M, January 19, 1987.
 2. Gallup, D. L., Tech. Memo, REF: 85-54M, April 4, 1985.



D. L. Gallup
Research Associate

DLG/gs

TABLE 1

X RAY DIFFRACTION

(SALTON SEA SCALE)

	<u>MAJOR (>10%)</u>	<u>MODERATE (1-10%)</u>	<u>TRACE (<1%)</u>
(GROUP 82)			
1 V102 Brine	NC*	---	Feldspar
3 HPC Brine	NC	---	BaSO ₄ , CaF ₂
4 LPC Brine	NC	---	BaSO ₄ , CaF ₂
5 AFT	CaF ₂	Ag	---
6	Ag	NC	---
7 Inj. Line	CuAs ₂	Ag	---
(GROUP 83)			
1	FeAs ₂	(Cu, Fe)As ₂	Bi, BiOCl, MoS ₂
2	FeAs ₂	---	Bi, BiOCl, MoS ₂
3	Fe ₃ O ₄	---	MoS ₂
(GROUP 84)			
1	CuAs ₂	Cu ₂ O, Ag	NaCl
(GROUP 85)			
1	NC	BaSO ₄	CaF ₂ , NaCl

NC* = Non-crystalline

TABLE 2

QUALITATIVE ANALYSIS

(SALTON SEA SCALE)

	MAJOR (>10 Wt%)	MODERATE (1-10 Wt%)	SLIGHT (0.1-1 Wt%)	TRACE (<0.1 Wt%)
	-----	-----	-----	-----
(GROUP 82)				
1	Fe, Si	Mg, Na	Al, Mn	Ag, Ca, Cu, Sr, Ti
3	Fe, Si	Ba	Ca, Mn, Na, Sr	Ag, Al, Cu, Mg
4	Fe, Si	Ba	B, Ca, Mn, Na, Sr	Ag, Al, Cu, Cr
5	Ag, Ca	Fe, Na	Cu, Si	Al, Mn, Sr
6	Ag	Fe, Si	Ba, Ca, Mn, Na	Al, B, Cu, Sr
7	Cu, Fe	As, Sb, Si	Ag, Ca	Cr, Mn, Ni, Sr
(GROUP 83)				
1	As, Au, Bi	Fe, Mo, Ni, Si	Cr, Cu, Pb, Sb	Ag, Al, Ca, Mn, Sr
2	Bi, Cu, Fe	As, Au, Sb, Si	Mo, Ni	Ag, Al, Ca, Mg, Mn
3	Fe	As	Cu, Mo, Si, Zn	Ag, Ca, Mn, Pb
(GROUP 84)				
1	Ag, Cu, Sb	As, B, Fe, K, Na, Si	Mn	Ca, Sr
(GROUP 85)				
1	Fe, Na, Si	As, Ba, Ca, Cu, K, Sb	Ag, B, Mn, Sr	Al, Cr, Ni, Pb

TABLE 3

QUANTITATIVE ANALYSIS (Wt%)

(SALTON SEA SCALE)

No.	Al	Ag	As	Ba	Ca	Cu	Fe	Mg	Mn	Pb	S	Si	Sb
(GROUP 82)													
1	--	--	--	--	0.9	--	25.1	2.6	0.4	--	0.1	18.3	--
3	--	--	--	6.2	2.2	--	18.3	0.1	0.6	--	1.5	17.0	--
4	--	--	--	12.9	1.0	--	8.6	--	0.4	--	3.0	23.4	--
5	--	7.9	--	--	45.0	0.3	0.2	--	--	--	6.0	1.4	--
6	--	19.1	--	--	2.7	0.4	14.0	--	0.4	--	1.1	20.7	--
7	--	0.8	8.7	--	1.8	24.1	16.2	--	0.1	--	1.2	6.5	2.1
(GROUP 83)													
1	0.2	--	15.4	--	0.4	0.2	17.6	0.7	<0.1	<0.1	1.2	1.6	1.5
2	<0.1	--	7.6	--	0.1	1.0	23.1	0.2	<0.1	<0.1	0.6	0.3	1.1
3	<0.1	--	10.1	--	0.1	<0.1	33.1	0.1	0.4	<0.1	0.3	4.6	--
(GROUP 84)													
1	--	17.5	6.7	--	0.9	26.0	4.6	0.1	0.1	0.1	0.7	5.6	0.4
(GROUP 85)													
1	--	--	0.03	10.3	2.8	0.6	4.1	--	0.1	--	2.4	17.5	0.1

TABLE 4

CALCULATED SCALE COMPOSITIONS (Wt%)

GROUP	Al-Si	BaSO4	ALLOY*	CaF2	FeO	MgO	Mn2O3	PbS	SiO2	ZnS	TOTAL
82-1	---		---	1.8	32.3	4.3	0.6	---	39.2	---	78.2
3	---	10.5	---	4.3	23.6	0.2	0.9	---	36.4	---	75.9
4	---	21.9	---	2.0	11.1	---	0.6	---	50.2	---	85.8
5	---		8.2	87.8	0.3	---	---	---	3.0	---	99.3
6	---		19.5	5.3	18.1	---	0.6	---	44.3	---	87.8
7	---		35.7	3.5	20.9	---	0.1	---	13.9	---	74.1
83-1	1.0		30.0	0.8	64.7**	1.2	---	---	3.4	---	101.0
2	---		15.0	0.2	85.0**	0.3	---	---	0.6	---	101.0
3	---		10.0	0.2	42.7	0.2	0.6	---	9.9	0.2	64.0
84-1	---		70.6	1.8	5.9	0.2	0.1	0.1	12.0	---	90.7
85-1	---	17.5	0.7	4.7	5.3	---	0.1	---	37.5	---	75.5

ALLOY* = Ag,As,Au,Bi,Cu,Sb

** = FeAs2

NaCl = 9.9 (For sample 85-1 only)

TABLE 5

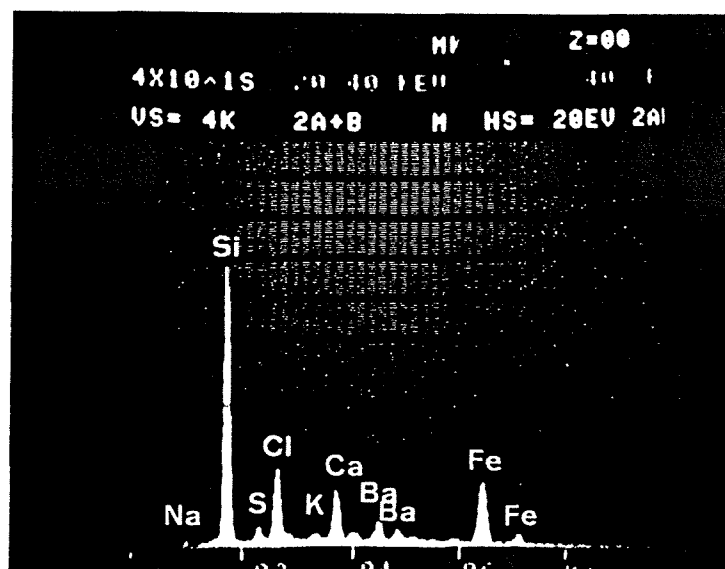
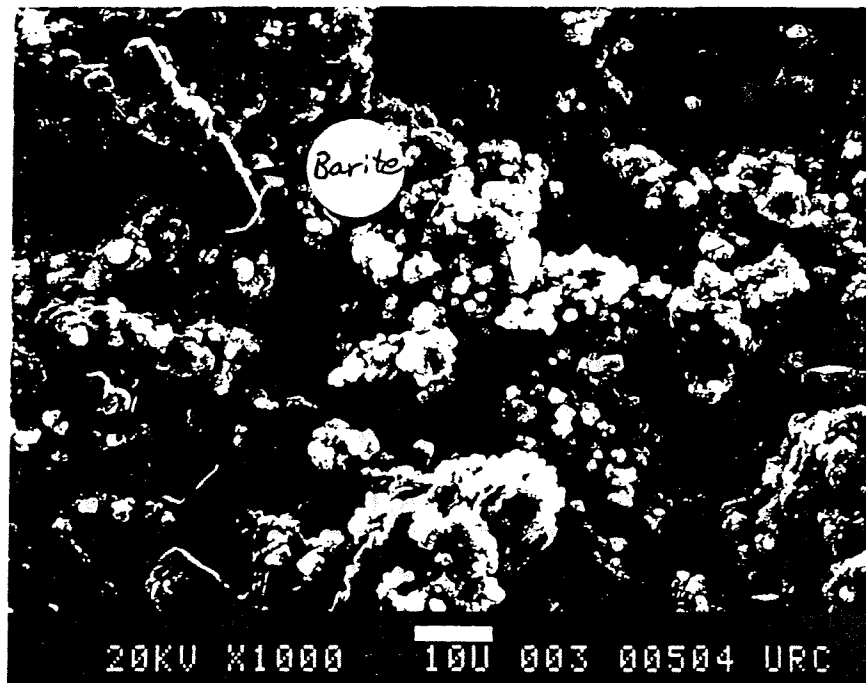
IRON SILICA RATIOS

<u>SAMPLE</u>	<u>MOLE BASIS</u>	<u>WT BASIS</u>
GP 82 1	0.69	1.37
3	0.54	1.08
4	0.18	0.37
5	0.09	0.17
6	0.34	0.68
7	1.25	2.49
GP 83 1	5.50	11.00
2	39	77
3	3.60	7.20
GP 84 1	0.41	0.82

TABLE 5

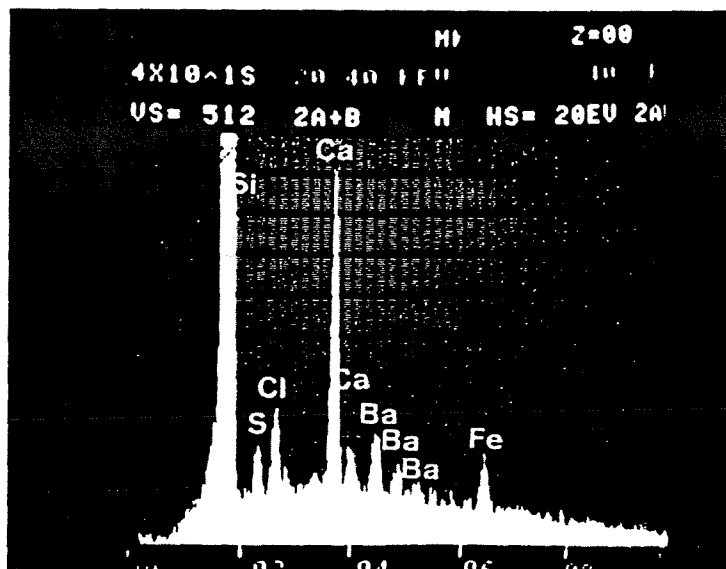
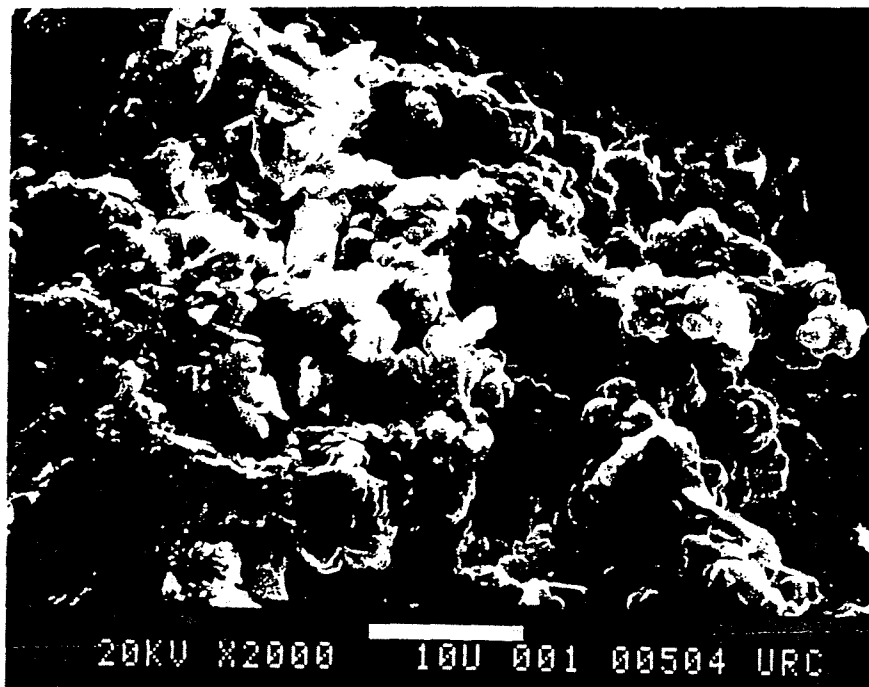
IRON SILICA RATIOS

SAMPLE	MOLE BASIS	WT BASIS
GP 82 1	0.69	1.37
3	0.54	1.08
4	0.18	0.37
5	0.09	0.17
6	0.34	0.68
7	1.25	2.49
GP 83 1	5.50	11.00
2	39	77
3	3.60	7.20
GP 84 1	0.41	0.82



983-12 EDX OFF FIELD @ 50X PHOTO MICROGR. OVER

FIGURE 1. SEM/EDX GREEN LAYER - GP 85



933-12. EDX OF FIELD 2 EDX Photo # 002 OVER

FIGURE 2. SEM/EDX WHITE LAYER - GP 85

APPENDIX

Scale Sample Descriptions


UNOCAL 76

D.L.GALLUP

JUN 15 1987 2406d

June 4, 1987

TO: D. Gallup

FM: D. Holligan 

RE: Group 83 Scale Samples From
IID 12 9-5/8" Alloy Hangdown String

IID 12 was produced for 411 days between December 18, 1985 and February 21, 1987. Total production was 8,719,000 klbs at an average rate of 850,000 lbs/hrs. Wellhead pressure ranged from 290 to 430 psi, and wellhead temperature ranged from 440°F to 460°F.

Metallic scales similar to those seen in the past were found on the bottom joint at 1520'. The remainder of the string had little scale accumulation with the exception of black brittle scale patches found in spots on the outside surface just above and below couplings from 1200' to 1500'.

Please analyze for the usual constituents.

cc: J.Bush/IID 12 well file
G.Gritters

TABLE 1

Scale Description
Group No. 83

Field: Salton Sea
Well: IID 12
Casing String: 9-5/8" Alloy Hangdown
Total Exposure: 12/18/85 to 2/21/87 - 425 Days
Production Time: 12/23/85 to 2/12/87 - 411 Days

Productivity: Average Rate: 850,000 lbs/hr
Total Mass: 8,719,000 klbs
WHP: 290 psi - 400 psi
WHT: 420°F - 461°F

<u>SAMP NO.</u>	<u>JT NO.</u>	<u>APPROX DEPTH FT</u>	<u>SCALE THICK. (IN)</u>	<u>SCALING RATE (IN/YR)</u>	<u>DESCRIPTION</u>
1	1	1520	1/8	.11	Hard, brittle gray scale, relatively high density similar to samples retrieved from the bottom of the hangdown in the past.
2	1	1520	3/64	.042	Similar to Sample 1
3(1)	8	1280	3/16		Black, crumbly scale from outside surface.

(1) Outside diameter sample.

Scaling rate based on production time.



July 22, 1987

TO: Darrell Gallup
FM: David Ruiz *DR*
RE: IID 6 Meter Run Scale Sample
Group 84

Scale Sample

A scale sample taken from the IID 6 meter run is enclosed for analysis. This sample represents scale formed during the 43 days following the April, 1987 turnaround. During this start-up period, there was evidence of polymer flocculant in the secondary clarifier overflow. The flocculant, American Cyanamid's Superfloc 107+, is a very low anionic, dry polymer.

Please analyze the sample for polymer and the usual constituents.

Operating Conditions

The IID 6 meter run was in service for 43 days, between May 28 and July 9. As expected following a plant startup, the operating conditions in the reactor-clarifier system were not stable for much of the 43 day period. During the first ten days following the startup, while the solids inventory was building up, the suspended solids concentration in the primary clarifier reaction well was below eight weight percent. This generally results in increased silica precipitation in the downstream piping. Also, it is suspected that polymer flocculant was present in the secondary clarifier overflow for at least 16 of the 43 days. One or both of these upset conditions may be responsible for the high scaling rates. The typical operating conditions for this period are contained in Table 1.

Darrell Gallup
July 22, 1987
Page Two

Scale Description

The scale removed from the IID 6 injection line was black in color with a high concentration of nodules. There were also some reddish-brown and turquoise surface colors. The scale thickness varied between 1/16" and 3/16", resulting in scaling rates of 0.5 and 1.6 inches per year.

DR/pl/ec

cc: Greg Gritters
File: SS-F-105

TABLE 1

Typical Operating Conditions

<u>Date</u>	<u>Pressure (psig)</u>	<u>Temperature (F°)</u>	<u>Flow Rate (Klb/hr)</u>
6/28/87- 7/09/87	10	222	500



5221p

August 12, 1987

D. L. GALLUP
AUG 14 1987

TO: Darrell Gallup
FM: David Ruiz *DR*
RE: North Injection Pad Strainer Scale Sample, Group #85

Scale Sample

A scale sample taken from the outside of the injection strainer is enclosed for analysis. This is a multilayered, high deposition sample with large quantities of white material. Please analyze this sample for polymer concrete, polymer flocculent (Cyanamid Superfloc 107+), and the usual constituents.

Scale Description

The scale removed from the injection strainers was deposited in several gray, green, and white colored layers. The scale thickness varied between 1/4" and 3/4", resulting in scaling rates of 1.8 and 5.5 inches per year.

Operating Conditions

The injection strainers were in service for 50 days, between June 16 and August 4, 1987. The typical operating conditions for this period are listed in Table 1.

Between June 23 and July 8 (16 days), a high concentration of sheared polymer flocculant was being recirculated in the secondary clarifier. This upset condition may have resulted in the carryover of flocculant into the injection system. The

Darrel Gallup
August 12, 1987
Page 2

flocculant, and possibly polymer concrete from the injection line, may have contributed to the high solids deposition on the injection strainers.

DR/ec

Enclosure

cc: Greg Gritters
File: SS-F-105

TABLE 1

Typical Operating Conditions

Injection Fluid, Group #85

<u>Date</u>	<u>Pressure (psig)</u>	<u>Temperature (°F)</u>	<u>Flow Rate (K lb/hr)</u>
6/16/87-	0-50	222	500-600
8/4/87			

Sea Geothermal Field from

<i>S/ton</i>	<i>Value (\$ millions/yr)</i>
50	144 ^a
32	106 ^a
60	30 ^a
120	9.5 ^a
175	6.0 ^d
450	5.7
640	7.4 ^a
100	1.1
550	1.3 ^a
2,800	1.12
300	0.72
600	0.038
1,300	0.034
250,000 ^f	2.5
	21

market value of min-
geothermal power
uld be cogenerated
oing (and very pro-
ion, a recent pilot
Table 17.2) utilized
yvesteyn, 1992).
ells may place con-
brines (McKibben
wells and in sur-
te phase similar to
and Reiff, 1991),
: al., 1990). Scales
int of initiation of
tite and loellingite
rt % Au, as well as
l 17.7) (McKibben

et al., 1990; M. A. McKibben, unpublished data). The large mass through-put of brine in a typical SSGS geothermal well (typically 10^5 – 10^6 kg/hr) is sufficient to produce such dramatic metal enrichments in the scales, even though the concentrations of most metals in the brines are at ppm to ppb levels (Tables 17.2 and 17.8). These flashpoint deposits suggest that significant fractions of the trace Au and U in the brines are transported as complexes that become rapidly destabilized by gas loss during phase separation, such as Au-HS⁻, U-CO₃²⁻, and possibly Au-As or Au-NH₃ complexes.

TABLE 17.6 Chemical Composition of Magnetite-Loellingite Downhole Liner Scales Formed at or Near the Flashpoint in Two SSGS Wells^a

<i>Element</i>	<i>CW-11, Header Isolation Valve</i>	<i>CW-11, Downhole Liner Joint #55</i>	<i>CW-14, Downhole Liner Joint #60</i>
Ca	395	5608	5080
Mg	727	1368	3405
Na	323	5629	7125
K	63	1479	1990
P	34.7	749	1180
Si	5840	649	1064
B	1.97	46.0	50.9
Ba	2.36	38.4	25.2
Sr	6.04	54.0	78.2
Li	0.0	15.5	27.8
Ti	2.42	67.4	66.2
Al	502	508	1130
Fe	9840	47610	51230
Mn	528	2900	547.7
Cu	169	1123.2	2886.7
Zn	261	152	49.5
Cd	40.6	1333	5410
Pb	24200	3110	375
Ag	208	0.0	0.0
V	0.0	0.0	17.1
Mo	0.294	26.1	538
Ni	1.42	571	1289.7
Co	36.6	1038.6	1058.9
Cr	0.0	882	3530
Be	1.16	186.8	111.1
Tl	27.6	13.3	17.8
Ga	0.0	178.4	67.0
Au	0.000011	0.000013	460
U	103	9020	5726
Sc	0.0	0.0	0.0
Hg	0.000047	6366	313

TABLE 17.6 (Continued)

Element	CW-11, Header Isolation Valve	CW-11, Downhole Liner Joint #55	CW-14, Downhole Liner Joint #60
Se	44.7	0.0	4.70
Ge	0.000019	0.000023	0.000023
Sn	0.0	0.0	0.0
As	989	104300	402300
Sb	149	205.3	717.6
Bi	219	573.6	18222
Te	0.0	180.2	88.8
W	32	69.7	48.2
Y	0.0	1.08	0.511
La	0.0	276	162
Zr	0.0	0.0	0.0
Th	0.0	15.7	5.89

^aAnalyses by inductively coupled argon plasma optical emission spectrometry. Recombined analyses of HNO₃ and HCl soluble fractions of 0.1 g of scale. All data given in ppm wt.

Although platinum group elements (PGE) are present in the brines at concentrations similar to Au (up to 2 ppb, Table 17.8) they are not found in the flashpoint scales at similar levels (Table 17.7). This difference suggests that PGE are transported by complexes that are not strongly affected by gas loss (e.g., Cl⁻) and/or that PGE precipitation is inhibited kinetically compared with Au (McKibben et al., 1990), although the latter explanation seems unlikely at high temperatures and salinities. Experimental data were recently used by Gammons et al. (1992) and Gammons and Bloom (1993) to argue that transport of PGE by HS⁻ complexes could be important in the SSGS brines and that PGE-Cl⁻ complexes are insignificant under such conditions. However, their experimental data predict transport of only 0.01 ppb PGE in the SSGS brines as HS⁻ complexes and would require relative abundances of Au > Ag ≫ PGE for transport of precious metals exclusively as HS⁻ complexes. Their experimental results, derived from experiments conducted mostly at pH < 2, are inconsistent with the observed PGE concentrations and relative abundances of Ag ≫ PGE = Au in the neutral pH SSGS brines. (In addition, the standard state free energy data listed by these authors for PGE compounds at high temperatures cannot be reproduced from the literature sources that they cite.) The contrasting behavior of Au and PGE at the flashpoint in SSGS wells remains as strong empirical evidence that very different complexes are transporting these two types of metals in the SSGS brines.

TABLE 17.7 P

Well
Downhole liner
CW-2, J-23 ^c
CW-2, J-24
CW-2, J-55 ^t
CW-3, J-49 ^c
CW-3, J-56 ^c
CW-4, J-52
CW-4, J-60 ^a
Wellhead valve
CW-2
CW-2
CW-2
CW-4
Flow-line valve
S2-14
S2-14
S2-14

^aJ = joint.

^bNext to last joint.

^cScale disrupted.

^dLast joint, bottle.

Source: McKibben.

Age of the SSGS

The age of mine recent studies mined that the based on U-T isochron method ing vein types calcite separated 138,000 ± 37,000 years; these 1 veins; these 1

Technical Memorandum
Unocal Science & Technology Division
Brea, California



To: D. L. Carrier, Indio **Memo:** ENV 92-196
From: D. L. Gallup, I **Date:** July 31, 1992
Department: Environmental Technology **Project:** 180-55001
Subject: ANALYSES OF SINCLAIR 21 RD **Manager:** M. M. Hatter, I
SCALE DEPOSITS

cc: **Library (2)**
Patent

CONFIDENTIAL

C. J. Cron, A
J. L. Featherstone, Calipatria
D. Hopgood, D
D. C. Jacobs, E1
P. G. Mogen, Indio
circ cc: E.T. Professionals

D. S. Pye, UOC
A. Schriener, Indio
A. Sutiono, Indio
R. N. Upadhyay, A
O. D. Whitescarver, Indio (3)

Per your request, we have analyzed eleven scale samples retrieved during the recent cleanout/workover of the Sinclair-21 RD injection well at the Salton Sea geothermal field. The Appendix includes your description of the samples. Tables 1 - 4 present the results of the "bulk" scale analyses. Petrologic analyses of the deposits will be reported separately by Dr. David Jacobs, Exploration Research.

In general, the scales collected from this well consist of iron silicate, iron corrosion products, barite, fluorite and formation minerals. Traces of heavy metals (silver, copper, antimony, arsenic, and lead are also present in these deposits. Phosphorus (assumed to be present as calcium phosphonate pseudo-scale from NORMs inhibition) is barely detected in these samples.

The presence of barite and fluorite in the scales is typical for pre-NORMs inhibitor treatment of brine. Barite was a major component in scale deposited in this well in 1990.¹ The scales are slightly radioactive - radium-226 concentrations have not been determined by gamma spectroscopy, but

¹ D. L. Gallup and M. E. Obando, Tech. Memo. PMR 90-178M, November 27, 1990

OLIND WHITESCARVER

AUG 10 1992

RECEIVED

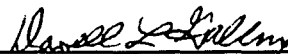
AUG 06 1992

gamma ray exposure rate measurements suggest that they range from 15 - 100 pCi/g. Now that the NORMs inhibition process is commercialized at Salton Sea, barite, fluorite and radium in injection well scales collected in the future should be nearly absent. Heavy metals are present in the scales in relatively low concentrations compared to injection line scales due in part to their removal at the surface in the Line Mine process. The highest concentrations of heavy metals in the deposits are found in Samples 4, 10 and 11.

Phosphorus detected in the scales is possible evidence for deposition of traces of NORMs inhibitor, Nalco 3919, a phosphonoalkylamine compound. The inhibitor is known to precipitate with calcium in the brine as a pseudo-scale. It is estimated that < 0.1 wt% of the wellbore deposits consist of inhibitor-related scale. This result implies that the NORMs inhibitor is probably not entirely responsible for the loss of brine injectivity observed in early 1992 for this well. That the injectivity of the well was so easily restored in a flowing cleanout and acid job also suggests that the NORMs inhibition process had little adverse effect on formation damage.

The phosphonate inhibitors we have been testing in the NORMs reduction process appear to soften existing scales deposited from Salton Sea brines. It is believed that some of the observed injectivity decline in Sin-21 RD resulted from wellbore scale softening and sloughing. Wellbore scale likely fell to the bottom of the well and restricted brine disposal into reservoir fractures and matrix. Disposal of brine from the NORMs process into cleaned wells will be required to fully determine the effect of the inhibitor on injectivity.

Iron silicate deposited in this well results from minor instability of crystallized/clarified injectate. Magnetite and siderite detected in Samples 4, 6 and 7 are assumed to be steel casing corrosion products. Formation minerals (quartz, feldspars, calcite, dolomite, plagioclase and clay) found in the scales likely result from reaming of the open hole section of the well.



Darrell L. Gallup
Principal Scientist

DLG/pah
Attachments

TABLE 1

X-Ray Diffraction Studies					
Sample	Depth, ft	Major	Moderate	Minor	Trace
1	550	BaSO ₄			Quartz, CaF ₂
2	2878	BaSO ₄		Quartz, K-feldspar	CaF ₂
3	4350	BaSO ₄			CaF ₂
4	4835	BaSO ₄		Ag-Sb, Ag, FeCO ₃ , NaCl	Quartz, CaF ₂ , Dolomite
5	5365	BaSO ₄		Quartz, CaF ₂	Calcite, Clay
6	5616	BaSO ₄	Fe ₃ O ₄		Calcite, Quartz, CaF ₂
7	5861	BaSO ₄		Fe ₃ O ₄	Quartz, CaF ₂
8	6108	BaSO ₄	Calcite	Quartz, K-Feldspar	Plagioclase, CaF ₂
		Dolomite			
9	6358	BaSO ₄		Dolomite	CaF ₂
10	6638	BaSO ₄		CaF ₂	Calcite, Dolomite, Quartz
11	6854	BaSO ₄		CaF ₂ , Dolomite	Calcite, Quartz

TABLE 2

Sample	Depth, ft	Emission Qualitative Analyses			
		Major (>10%)	Moderate (1-10%)	Slight (0.1-1%)	Trace (<0.1%)
1	550	Ba, Fe, Si	Ca, Sr	Ag, Cu, Mn, Na	B, Cr
2	2878	Ba, Si	Ca, Fe	Ag, Mn, Na, Sr	Al, B, Cr, Cu, Mo, Ni, Pb
3	4350	Ba, Ca	Fe, Si, Sr		Ag, Al, B, Cr, Cu, Mn, Na, Ni
4	4835	Ag, Ba, Cu, Fe, Si	As, Sb	Al, Mn, Na, Sr	B, Cr, Ni, Pb
5	5365	Ba, Fe, Si	Ca	Ag, Al, Cu, Mn, Na, Sr	Cr, Mg, Ni, Pb, Ti
6	5616	Ag, Ba, Fe, Si	Cu	Al, As, B, Ca, Mn, Na, Sb, Sr	Cr, Ni, Pb, Zn
7	5861	Fe, Si		Ag, Ba, Cu, Mn, Na	B, Ca, Cr, Ni, Sb, Sr
8	6108	Ba, Fe, Si	Ca, Mg	Al, Cu, Mn, Na	Cr, Ni, Pb, Sb, Sr
9	6358	Ba, Fe, Si	Ag, Ca, Cu	Mg, Mn, Na, Sr	Al, B, Cr, Ni, Sb
10	6638	Fe, Si	Ba, Ca, Cu	Ag, Mn, Na, Sr	Al, B, Mg, Sb
11	6854	Ca, Fe, Si	Ba, Cu	Ag, Al, As, Mn, Na, Sb, Sr	B, Cr, Mg, Ni, Pb

TABLE 3

Quantitative Analyses (wt%)																	
#	Depth, ft	Ag	Al	As	Ba	Ca	Cu	F	Fe	Mg	Mn	Na	P	Pb	S	Sb	Si
1	550	0.13	0.1	<0.1	20.6	2.76	0.24	4.9	11.1	<0.1	0.32	0.46	0.02	<0.1	6.88	<0.1	12.5
3	4350	0.11	<0.1	<0.1	27.7	2.49	0.15	0.76	8.5	<0.1	0.22	0.35	0.02	<0.1	10.05	<0.1	8.3
5	5365	0.56	0.88	<0.1	11.9	4.3	0.76	3.03	13.5	0.17	0.35	0.47	0.02	1.45	4.98	<0.1	14.5
7	5861	0.19	0.26	<0.1	8.3	2.4	0.25	1.88	22.3	<0.1	0.45	0.49	0.02	<0.1	3.24	<0.1	16
9	6358	0.51	0.2	1	14.3	3.11	1.34	1.81	9.6	0.18	0.32	0.42	0.01	<0.1	4.37	0.5	19.3
11	6854	1.08	0.47	1.94	12.2	5.8	3.8	3.63	10.3	0.19	0.61	0.54	0.02	<0.1	3.89	1.06	16.6

TABLE 4


Calculated Mineral Modes (wt%)													
Calcite													
Sample	Depth, ft	Ag3Sb	Al-Silicate	BaSO4	CaF2	Dolomite	CaPhos	Cu3As	FeOy	Mn2O3	Na2O	SiO2	TOTAL
1	550	0.2	0.5	35	9.8	<0.1	0.09	0.3	17.6	0.5	0.6	26.8	91.4
3	4350	0.2	<0.5	47.1	1.5	4.3	0.09	0.2	13.5	0.3	0.5	17.8	85.5
5	5365	0.8	4.5	20.2	6.1	3.8	0.09	1.1	21.5	0.5	0.6	31	90.2
7	5861	0.3	1.3	14.1	3.8	1.3	0.09	0.3	35.5	0.6	0.7	34.2	92.2
9	6358	1	1	24.3	3.6	3.9	0.04	2.3	15.3	0.5	0.6	41.3	93.8
11	6854	2.2	2.4	20.7	7.2	6.2	0.09	5.7	16.4	0.9	0.7	35.5	98

APPENDIX

UNOCAL

July 7, 1992

To: Darrell Gallup

Fm: Dan Carrier 

Re: Scale samples from Sinclair-21 Rd cleanout

I have processed the scale samples collected during the cleanout of Sinclair-21 Rd and have sent to you a split of the samples. The samples were collected during the time period of June 16 to June 22, 1992 and the sample set consists of scale samples collected from both the open hole and the casing. Nitrified brine was the medium used to lift the samples out of the well.

Except for the two scale samples collected in the casing, the scale samples were collected by Drilling Department personnel at roughly 200 feet intervals beginning at 4350'. A preliminary visual description of the scale samples is attached. The field collected samples were stored unwashed and wet in zip locked air-tight plastic bags until they were processed on June 31, 1992. Each sample was washed in tap water to remove as much pipe dope, paint flakes, and other miscellaneous particles as possible.

Two splits of samples have been made. One split was sent to you and the other remains in the hands of Geology. If it turns out that the quantity of the samples I have sent to you is too small for your analyses, please call and I will send you more.

Finally, I recommend you send a portion of the sample to Dave Jacobs for petrologic analysis.

pc. A. Schriener

**A Preliminary Visual Description of Scale Samples Collected
from a Clean-out of Sinclair-21 Rd on June 16 to June 22, 1992.**

<u>DEPTH</u> (feet)		<u>VISUAL DESCRIPTION</u>	<u>COMMENTS</u>
550	80% 20%	dark brown, medium hard, brittle, platy scale	from inside casing
2878	100% cm	dark brown to ochre colored scale as above medium gray, massive scale	from inside casing at top of the cement plug
4350	100% trace	dark brown to ochre colored, medium hard to soft, brittle, platy scale massive white scale	from open hole
4835	100% trace	dark brown to ochre colored scale as above massive white scale	from open hole
5365	100% trace	dark brown to ochre colored scale as above massive white scale	from open hole
5616	100% trace	dark brown to ochre colored scale as above massive white scale	from open hole
5861	100% trace	dark brown to ochre colored scale as above massive white scale	from open hole
6108	100% Ab	med. gray scale, massive, moderate hardness dark brown to ochre colored scale as above	from open hole
6358	80% 20%	med. gray scale, massive, moderate hardness dark brown to ochre colored scale as above	from open hole
6638	90% 10%	med. gray scale, massive, moderate hardness dark brown to ochre colored scale as above	from open hole
6854	80% 20%	med. gray scale, massive, moderate hardness dark brown to ochre colored scale as above	from open hole



Technical Memorandum
Unocal Science & Technology Division
Brea, California



UNOCAL

To: F. L. Wilson, Indio
From: D. L. Gallup, I
M. E. Obando, I
Department: Products, Processes & Materials Research
Subject: SINCLAIR-21 SCALE ANALYSES

Memo: PMR 90-178M
Date: November 27, 1990
Project: 745-84370
Manager: C. T. Ratcliffe, I

CONFIDENTIAL

cc: Library (2)
Patent

S. K. Alley, AD
K. Baron, AD
D. L. Carrier, Indio
J. L. Featherstone, Calipatria (2)
M. M. Hatter, I
P. H. Messer, Indio

D. S. Pye, UCC
A. Schriener, Indio
H. D. Simpson, I
R. J. Swanson, Indio
R. N. Upadhyay, AD
J. W. Ward, A
O. D. Whitescarver, Indio (4)

SUMMARY

CONFIDENTIAL

Scales collected from the cleanout of the Sinclair-21 injector at the Salton Sea geothermal field have recently been analyzed. Scales scraped from the casing and open hole sections consist primarily of iron-rich silica (Fe-SiO₂), barite (BaSO₄), and fluorite (CaF₂) that appear to be present as cemented suspended solids from the brine. Scales reamed from the open hole additionally contain formation minerals, as expected. In contrast to injection line scales, the deposits from the well contain very low concentrations of heavy metals (silver, copper, arsenic and antimony). Cuttings of the alloy casing are also found in many of the scale samples.

To mitigate scaling of the casing and formation damage in the open hole, we recommend continued processing of the injection brine through "Line Mine". We also recommend treating the injection brine with a scale inhibitor. Upon shutin of injectors, the wellbore should be purged with acidified condensate also treated with scale inhibitor.

SCALE CHARACTERIZATION STUDIES

Thirty-one scale samples were retrieved from the cleanout of the Sinclair-21 injector at the Salton Sea geothermal field. A description of the samples, well history and well workover provided by Mr. Robert Swanson, Imperial District, is attached as an Appendix. In general, the samples collected from the casing consist of brown scale chips and shiny flecks of alloy casing cuttings. The open hole samples, on the other hand, consist of light tan chips of formation minerals and scale.

Tables 1 - 3 present the results of the scale analyses. To save time and money, not all of the scales were analyzed quantitatively (see Table 3). As shown in Table 1, x-ray diffraction detected several crystalline scale compounds including barite and fluorite. Formation minerals detected by x-ray diffraction include quartz, feldspar, plagioclase, calcite and clays. Elemental analyses of the scales show the presence of significant concentrations of barium (BaSO_4), iron and silicon (iron-rich amorphous silica) and calcium (CaF_2). Surprisingly, the samples contain very low concentration of heavy metals - copper, silver, arsenic and antimony. In contrast, these metals are found in high concentrations in injection line scales at the surface. Chromium and nickel in the samples are evidence for the presence of alloy casing cuttings.

Figures 1 - 6 show scanning electron micrographs of selected samples. In general, these micrographs show dark materials consisting of "true" scale components and light materials consisting of formation minerals. The scale chips appear as subrounded, cemented agglomerates of barite, fluorite and iron silicate. Figures 2 and 3 show samples containing smooth casing chips. As expected, dark scale chips predominate the deposits removed from the casing section, while formation minerals are more prevalent in the samples obtained from the open hole section. Still, a significant amount of what appears to be scale is found in the samples reamed from the open hole.

SCALE DEPOSITION MECHANISMS

Chips of scale are comprised of typical low temperature brine precipitates - barite, fluorite, and iron silicate. These species are normally present as suspended solids in the injection brine. That these species are deposited as hard scales suggests that they are cemented together with silica that has not fully stabilized in the brine. It is also believed that the brine sent to the injection well is not entirely stabilized with respect to barium sulfate precipitation. This may explain why strontium-barium sulfate is the major scale component from the surface to the bottom of the well.

The analyses of the samples indicate that scaling not only occurs on the casing, but also in the open hole. The deposition of scale on the casing and in the open hole is likely responsible for the slow loss of brine injectivity observed during 1989. Scaling in the formation (skin damage) may be responsible for injectivity losses observed during shutin of the well. Barite and silica deposition appear to be the primary culprits for scaling on the casing and in the open hole.

As described in the Appendix, this well suffered severe damage after shutin for one month in April 1990. Without the benefit of sidewall core samples to confirm scale invasion into the reservoir, we can only speculate on the cause of the drastic loss of injectivity as a result of shutting in the well. Since barite appears to be continuing to deposit from brine all the way down the wellbore, we suspect that it may be partly responsible for formation damage during shutin.

Barite begins to precipitate from brine at the Salton Sea field below about 250°F. If the brine remaining in the wellbore upon shutin cools, barite will rapidly precipitate. Based on our brine analyses in support of studies of the deposition of NORM (naturally-occurring radioactive material) at Units 1 and 3, there remains sufficient barium and sulfate in the injectate to deposit massive quantities of barite in the open hole section of the well and into the near-wellbore formation. Scales retrieved from low temperature injectors are radioactive due to co-precipitation of radium with barite.

In the injection piping to the well and in the "Line Mine" brine processing facility just upstream of Sinclair-21, scales are deposited that not only contain barite, fluorite and iron silicate, but also heavy metal alloys of copper, silver, arsenic and antimony, *vide supra*. These heavy metals are nearly absent in the well scales, by contrast. Although the injection line piping and the well casing are constructed of essentially the same material (duplex stainless steels), as soon as the brine enters the well, the heavy metal deposition significantly diminishes. We attribute the heavy metal deposition in surface piping to replacement reactions. For example, dissolved silver "displaces" iron in piping to form native silver according to the reaction:



Copper, antimony and arsenic react similarly with piping in accordance with the "activity series" of metals.

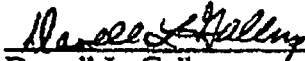
In the "Line Mine" process, we enhance the replacement reactions on poultry wire to recover the corrosive heavy metals. Brine injected into Sinclair-21 was processed through "Line Mine" for only a short period of time before the well workover was required. Thus, at the present time, we cannot explain why heavy metal deposition suddenly diminishes once the brine enters the wellbore.

RECOMMENDATIONS FOR SCALE INHIBITION AND FORMATION DAMAGE CONTROL

The following recommendations, based on the current study of Sinclair-21 scales, are made to control scale deposition and formation damage in low temperature injection wells at the Salton Sea geothermal field:

1. To improve our understanding of the mechanism of wellbore scaling and injectivity losses, sidewall core samples need to be obtained at the next workover of a low temperature injector. Standard scale samples should also be collected to assist in interpretation of scale deposition data.
2. Low temperature injection brines should be processed through "Line Mine" to further stabilize the brine with respect to scaling. "Line Mine" has been shown to filter up to 25% of the remaining suspended solids in the brine after clarification to remove unwanted barium, calcium and silica scales, and to reduce the corrosivity of the brine.
3. We will be pilot testing the use of barite and fluorite scale inhibitors in the framework of our "Line Mine" process within the next few weeks. Assuming that an effective inhibitor will be found, treatment of injection brine with the inhibitor at or upstream of "Line Mine" should be initiated at Units 1 and 3 to mitigate barite/fluorite scaling in the wellbore.

4. To diminish the potential for loss of injectivity during shutin of wells, brine should be "chased" with acidified condensate. This will purge the wellbore of brine that can cool and form more deposits in and around the casing and formation. Condensate should be acidified with HCl to pH 5.0. Since air-exposed condensate contains some sulfate ion, this condensate "chaser" cocktail should also be treated with the barite/fluorite inhibitor to ensure that brine-condensate mixing will not produce more scale.
5. Acid injection into the brine processed through "Line Mine" should be continued to inhibit silica from cementing precipitates as scale in the wellbore.
6. Scales collected from workovers of low temperature injection wells should be handled with care and properly disposed due to the presence of up to 500 picoCuries of radium-226 per gram of scale.



Darrell L. Gallup
Sr. Research Associate



Manuel E. Obando
Research Technician

DLG/MEO/ss
Attachments

TABLE 1
X-RAY DIFFRACTION

Sample No.	Date	Description	Major (>10%)	Minor (<5%)	Minor (5-25%)
1	1-Jun-90	50 Feet Inside Casing	BaSO ₄	-	CaF ₂
2	1-Jun-90	500 Feet Inside Casing	BaSO ₄	-	CaF ₂
3	1-Jun-90	250 Feet Inside Casing	BaSO ₄	-	CaF ₂
4	1-Jun-90	750 Feet Inside Casing	BaSO ₄	-	CaF ₂
5	1-Jun-90	1000 Feet Inside Casing	BaSO ₄	-	CaF ₂
6	1-Jun-90	1250 Feet Inside Casing	BaSO ₄	-	CaF ₂
7	1-Jun-90	1500 feet Before sweep Inside Casing	BaSO ₄	-	CaF ₂
8	1-Jun-90	1500 feet After sweep Inside Casing	BaSO ₄	-	Quartz, Plagioclase
9	1-Jun-90	1750 feet Before sweep Inside Casing	BaSO ₄	-	CaF ₂
10	1-Jun-90	1750 feet After sweep Inside Casing	BaSO ₄	-	CaF ₂
11	1-Jun-90	2000 feet Before sweep Inside Casing	BaSO ₄	-	CaF ₂
12	1-Jun-90	2000 feet After sweep Inside Casing	BaSO ₄	-	CaF ₂
13	1-Jun-90	2250 feet Before sweep	BaSO ₄	-	CaF ₂

TABLE 1
X-RAY DIFFRACTION

Sample No.	Date	Description	Major Phase (>10%)	Minor Phases (<10%)	Other (Trace)
		Inside Casing			
14	1-Jun-90	2250 feet After sweep Inside Casing	BaSO ₄	-	Feldspar, CaF ₂
15	1-Jun-90	2500 feet Inside Casing	BaSO ₄	-	CaF ₂
16	1-Jun-90	2750 feet Inside Casing	BaSO ₄	-	CaF ₂
17	1-Jun-90	2917 feet before sweep at Shoe	BaSO ₄	-	Quartz, CaCO ₃ , CaF ₂ , Clay
18	1-Jun-90	4418 feet Open Hole	BaSO ₄	-	Quartz, Plagioclase, Feldspar
19	1-Jun-90	4650 feet Open Hole	BaSO ₄	-	Quartz, Plagioclase, Feldspar
20	1-Jun-90	4900 feet Open Hole	BaSO ₄	-	CaF ₂
21	1-Jun-90	5150 feet Open Hole	BaSO ₄	-	Quartz, CaF ₂ , Plagioclase, Feldspar
22	1-Jun-90	5400 feet open hole	BaSO ₄	-	Quartz, CaF ₂ , Plagioclase, Feldspar
23	1-Jun-90	5650 feet Open Hole	BaSO ₄	-	Quartz, Plagioclase
24	1-Jun-90	5900 feet Open Hole	-	BaSO ₄ , Clay	Quartz, CaCO ₃ , Plagioclase, Feldspar
25	1-Jun-90	6150 feet Open Hole	-	BaSO ₄ , Clay	Quartz, CaCO ₃ , Feldspar, Plagioclase

TABLE 1
X-RAY DIFFRACTION

Sample No.	Date	Description	Major (1-10)	Minor (1-20)	Notes
26	1-Jun-90	6400 feet Open Hole	-	BaSO ₄ , Clay	Quartz, CaCO ₃ , Feldspar, Plagioclase
27	1-Jun-90	6650 feet Open Hole		BaSO ₄ , Quartz, Feldspar, Clays	CaCO ₃ , Plagioclase
28	1-Jun-90	6850 feet Open Hole	BaSO ₄	Quartz, Clays	CaCO ₃ , Plagioclase, Feldspar
29	1-Jun-90	3150 feet Outside Casing	Quartz	Feldspar	BaSO ₄ , CaCO ₃ , Plagioclase
30	1-Jun-90	3575 feet Outside Casing	BaSO ₄	-	Plagioclase, Quartz, Feldspar
31	1-Jun-90	4100 feet Outside Casing	BaSO ₄	Clays	CaCO ₃ , Plagioclase, Quartz, Feldspar

TABLE 2
QUALITATIVE ANALYSES

Sample No.	Date	Description	Major (>10%)	Minor (1-10%)	Trace (0.1-1%)	Other (<0.1%)
1	1-Jun-90	50 Feet Inside Casing	Ba, Sr	Ca, Fe, Si	Mn	Ag, Al, Cu, Na, Pb
2	1-Jun-90	500 Feet Inside Casing	Fe	Ba, Cr, Ni, Si	Ca, Cu, Mn, Sr	Ag, Pb
3	1-Jun-90	250 Feet Inside Casing	Sr	Ba, Fe, Si	Ag, Ca, Cr, Cu, Mn	Al, Na
4	1-Jun-90	750 Feet Inside Casing	Fe	Ba, Cr, Si	Ca, Mn, Ni, Sr	Ag, Cu, Mo, Pb
5	1-Jun-90	1000 Feet Inside Casing	Fe	Ba, Cr, Si, Sr	Ca, Cu, Mn, Ni	Ag, Al, Mo, Pb
6	1-Jun-90	1250 Feet Inside Casing	Fe	Ba, Si, Sr	Ca, Cr, Mn, Ni	Ag, Cu, V
7	1-Jun-90	1500 feet Before sweep Inside Casing	Ba, Fe	Cr, Ni, Si, Sr	Ca, Cu, Mn, Mo, Ni	Ag
8	1-Jun-90	1500 feet After sweep Inside Casing	Fe	Ba, Cr, Ni, Si	Al, Ca, Cu, Mn, Na, Sr	Ag, Mo
9	1-Jun-90	1750 feet Before sweep Inside Casing	Fe	Ba, Cr, Ni, Si	Ca, Cu, Mn, Ni, Sr	Ag, Al, Mo
10	1-Jun-90	1750 feet After sweep Inside Casing	Fe	Ba, Cr, Si, Sr	Ca, Mn, Ni	Ag, Cu, Mo
11	1-Jun-90	2000 feet Before sweep Inside Casing	Fe	Ba, Cr, Cu, Si	Ca, Mn, Ni, Sr	Ag, Mo, V
12	1-Jun-90	2000 feet After sweep Inside Casing	Fe	Ba, Cr, Si, Sr	Ca, Cu, Mn, Ni	Ag, Mo, Na
13	1-Jun-90	2250 feet Before sweep Inside Casing	Fe	Ba, Si, Sr	Ca, Cr, Cu, Mn, Ni	Ag, Mo, Ni

TABLE 2 QUALITATIVE ANALYSES						
Sample No.	Date	Description	Major (>10%)	Moderate (1-10%)	Minor (0.1-1%)	Trace (<0.1%)
14	1-Jun-90	2250 feet After sweep Inside Casing	Ca	Ba, Fe, Si, Sr	Ag, Cu, Na	Al, Mo
15	1-Jun-90	2500 feet Inside Casing	Fe	Ba, Cr, Ni, Si, Sr	Ca, Cu, Mn, Mo	Ag
16	1-Jun-90	2750 feet Inside Casing	Fe	Ba, Cr, Ni, Si, Sr	Ca, Cu, Mn, Mo	Ag, Mo, Sn
17	1-Jun-90	2917 feet before sweep at Shoe	Ca	Ba, Si	Cr, Fe, Mg, Mn, Ni, Sr	Ag, Al, Cu, Mo, Na
18	1-Jun-90	4418 feet Open Hole	Ca, Fe, Si	Al, Ba, Cu, Cr, K, Na	Ag, Mg, Mn, Mo, Ni, Sr	Pb, Sb
19	1-Jun-90	4650 feet Open Hole	Fe, Na	Ba, Ca, K, Si	Al, Cu, Mg, Mn, Sr	Ag, Cr
20	1-Jun-90	4900 feet Open Hole	Ba	Ca, Fe, Na, Si, Sr	Al, Cu, Mn	Ag, Mg
21	1-Jun-90	5150 feet Open Hole	Ba	Ca, Fe, Si	Al, Cu, Mn, Sr	Ag, Na, Na, Ti
22	1-Jun-90	5400 feet Open hole	Ca	Ba, Cu, Fe, Si, Sr	Al, Mg, Mn	Ag, Na, Pb
23	1-Jun-90	5650 feet Open Hole	-	Ba, Ca, Fe, Si	Al, Cu, Mg, Mn, Sr	Ag, Na, Pb, Ti
24	1-Jun-90	5900 feet Open Hole	Ca, Cu, Fe, K	Ag, Na, Sb, Si, Zn	Al, Cr, Pb, Mg, Mn, Pb	Sr
25	1-Jun-90	6150 feet Open Hole	Al, Ca, K, Si	Cu, Fe, Mg, Na	Ag, Cr, Mn, Pb, Sb, Sr, Ti	Ba, Mo
26	1-Jun-90	6400 feet Open Hole	Ca, Si	Al, Fe, Mn	Cr, Mn	Ag, Cu, Mo, Na, Ni, Pb, Sr, Ti

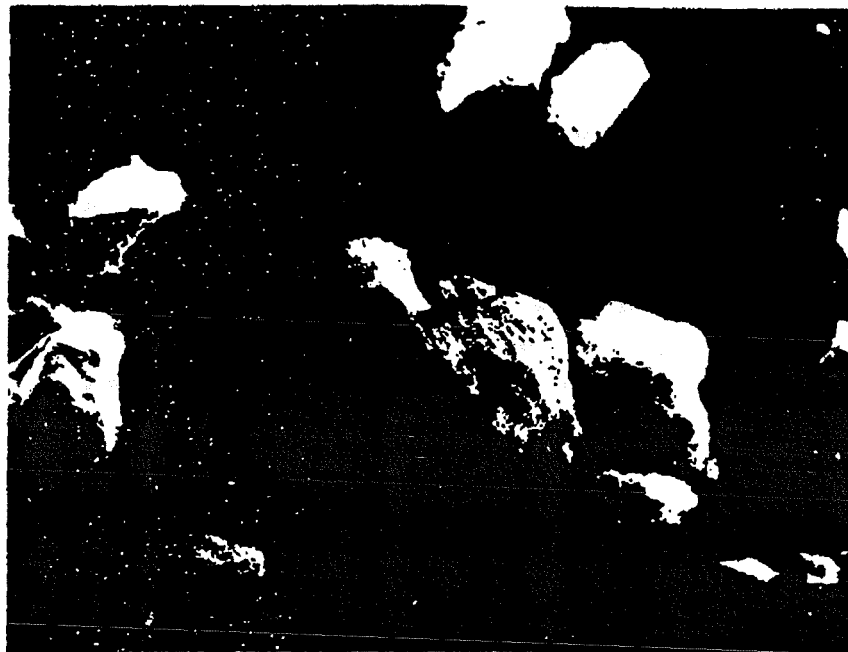
TABLE 2 QUALITATIVE ANALYSES						
Sample No.	Date	Description	Major ($\times 10^6$)	Minor (1-10)	Trace (0.1-1)	Other
27	1-Jun-90	6650 feet Open Hole	Ca, K, Na, Si	Al, Ba, Fe, Mg	Cr, Mn, V	Ag, Cu, Mo, Ni, Pb, Sr, Ti
28	1-Jun-90	6850 feet Open Hole	Fe, K, Na, Si	Al, Ba, Ca, Cu, Mg	Ag, Cr, Mn, Ni, Sr	Pb, Sb, Ti, V
29	1-Jun-90	3150 feet Outside Casing	Ca, K	Al, Ba, Cu, Fe, Na, Si	Ag, Cr, Mo, Pb	Hg, Mn, Ni, Sb, Ti
30	1-Jun-90	3575 feet Outside Casing	Ca	Al, Ba, Fe, Na, Si	Cr, Cu, Mg, Mn, Sr	Ag, Mo, Ni, Ti
31	1-Jun-90	4100 feet Outside Casing	Fe	Ba, Ca, Cu, Si	Ag, Al, Cr, Mn, Na, Ni, Sr	Hg, Mn, Pb, Sb

TABLE 3
QUANTITATIVE ANALYSES (wt %)

Sample No.	Date	Description	Al	Ag (ppm)	Ba	Ca	Cl	Fe	Hg	Mn	Ni	Pb	Si	Zn
1	Jun-90	50 Feet Inside Casing	< 1.0	63.00	8.40	1.32	< 1.0	5.10	< 1.0	< 1.0	0.14	< 1.0	3.50	< 1.0
2	Jun-90	500 Feet Inside Casing	< 1.0	-	6.90	1.05	0.25	15.20	< 0.1	0.20	< 1.0	< 1.0	3.14	< 1.0
3	Jun-90	250 Feet Inside Casing	< 1.0	58.00	8.40	1.25	< 0.1	3.60	< 0.1	< 0.1	< 0.1	< 0.1	3.40	< 0.1
4	Jun-90	750 Feet Inside Casing	< 1.0	94.00	6.00	1.30	0.20	13.80	< 0.1	0.19	< 0.1	< 0.1	4.80	< 0.1
5	Jun-90	1000 Feet Inside Casing	< 1.0	48.00	7.20	1.13	< 0.1	8.10	< 0.1	0.12	< 0.1	< 0.1	4.40	< 0.1
6	Jun-90	1250 Feet Inside Casing	< 1.0	40.00	8.10	1.18	< 0.1	6.20	< 0.1	< 0.1	< 0.1	< 0.1	3.70	< 0.1
7	Jun-90	1500 feet Before sweep Inside Casing	< 1.0	27.00	7.70	1.19	< 0.1	7.80	< 0.1	0.12	0.14	< 0.1	3.90	< 0.1
8	Jun-90	1500 feet After sweep Inside Casing	0.38	45.00	6.50	1.44	0.12	11.20	< 0.1	0.18	0.29	< 0.1	5.00	< 0.1
9	Jun-90	1750 feet Before sweep Inside Casing	< 1.0	140.00	6.00	1.14	0.15	13.90	< 0.1	0.20	0.10	< 0.1	4.50	< 0.1
10	Jun-90	1750 feet After sweep Inside Casing	< 1.0	94.00	6.20	1.25	0.15	11.80	< 0.1	0.18	0.11	< 0.1	4.90	< 0.1
11	Jun-90	2000 feet Before sweep Inside Casing	< 1.0	63.00	6.60	1.14	0.23	12.70	< 0.1	0.18	0.14	< 0.1	4.30	< 0.1
12	Jun-90	2000 feet After sweep Inside Casing	< 1.0	35.00	7.00	1.22	0.11	9.50	< 0.1	0.15	0.29	< 0.1	4.80	< 0.1

TABLE 3														
QUANTITATIVE ANALYSES (wt %)														
Sample No.	Date	Description	Al	As ppm	Ba	Ca	Cd	Cr	Pb	Hg	Mn	Ni	Pb	Zn
13	Jun-90	2250 feet Before sweep Inside Casing	< 1.0	12 ppm	7.60	1.19	< 0.1	8.20	< 0.1	0.12	< 0.1	< 0.1	4.10	< 0.1
14	Jun-90	2250 feet After sweep Inside Casing	< 1.0	27.00	7.90	1.21	< 0.1	5.60	< 0.1	0.10	0.10	< 0.1	4.40	< 0.1
15	Jun-90	2500 feet Inside Casing	< 1.0	19.00	6.90	1.21	< 0.1	6.90	< 0.1	0.13	0.12	< 0.1	4.40	< 0.1
16	Jun-90	2750 feet Inside Casing	< 1.0	31.00	4.30	1.10	0.14	11.70	< 0.1	0.16	0.15	< 0.1	4.30	< 0.1
17	Jun-90	2917 feet before sweep at Shoe	0.57	26.00	7.20	11.70	< 0.1	4.30	0.35	< 0.1	0.16	< 0.1	10.30	< 0.1

FIGURE 1. SAMPLE #1 (50'-CASTING)



LOW MAGNIFICATION OVERVIEW OF SCALE CUTTINGS

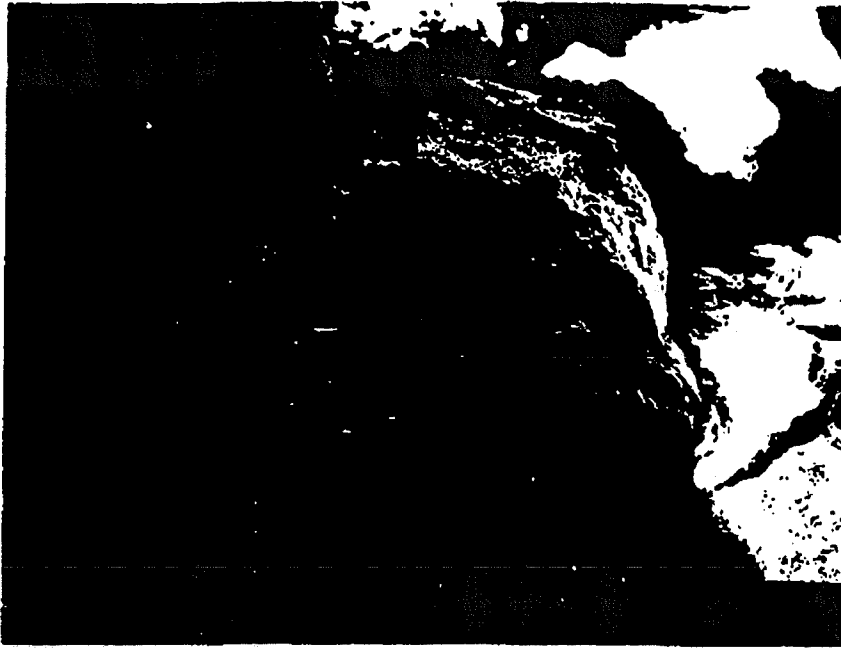
EDAX

Major: Ba, Ca, Si, Fe

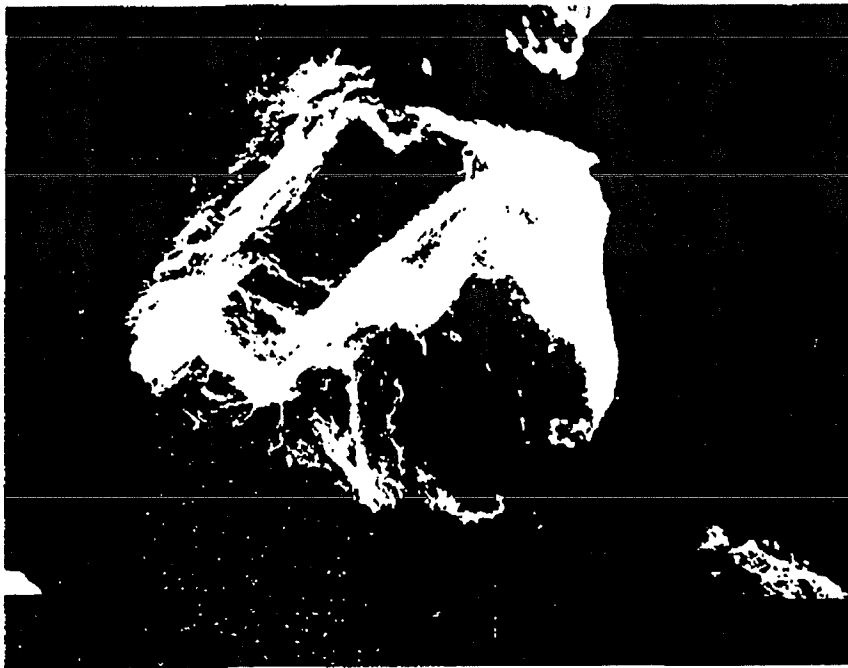
Minor: Al, K

Trace: Cu, As

FIGURE 1. SAMPLE # 1



DARK MATERIAL - SCALE (1.5 CM, Co. F., S. D.)

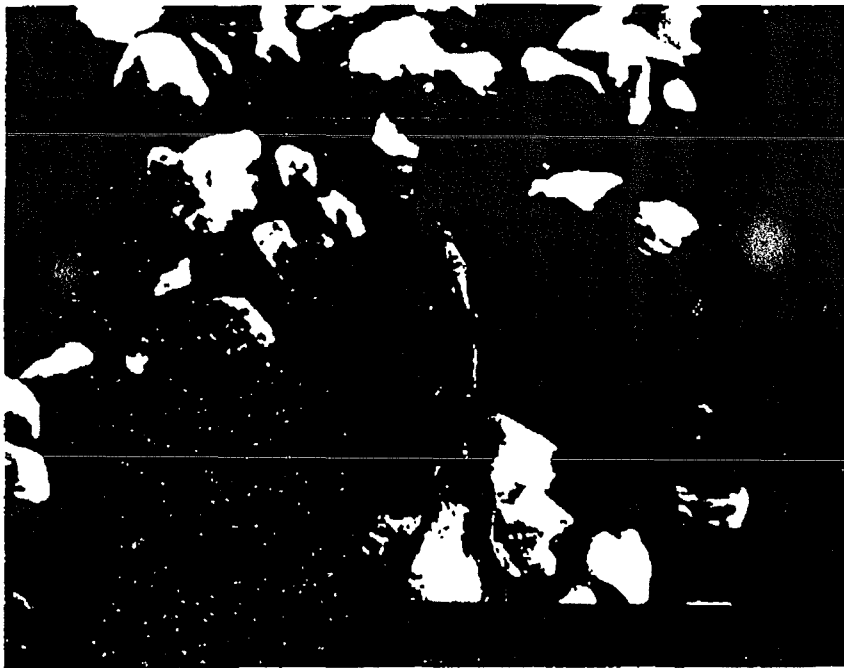


LIGHT MATERIAL - FORMATION (0.5 CM, K. H. D. PAR)

FIGURE 2. SAMPLE #7 (1500^{psi} CASING)



SCALE CHIPS (BaSO_4 , CaF_2 , Iron Silicate)



ALLOY CUTTINGS (Cr, Ni, Mn)

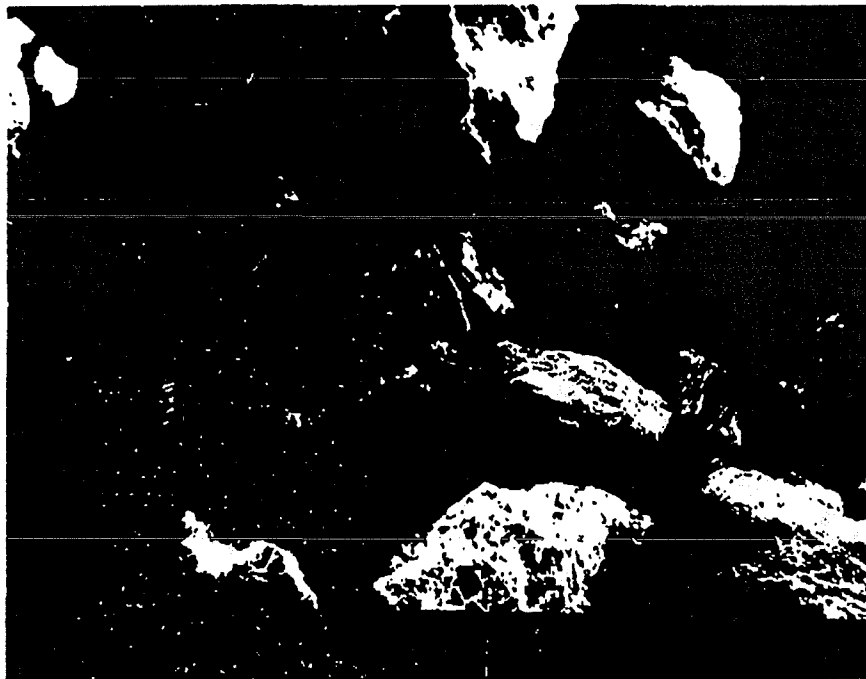
FIGURE 3. SAMPLE # 13 (2250' - CASING)

ALLOY CASING CUTTING



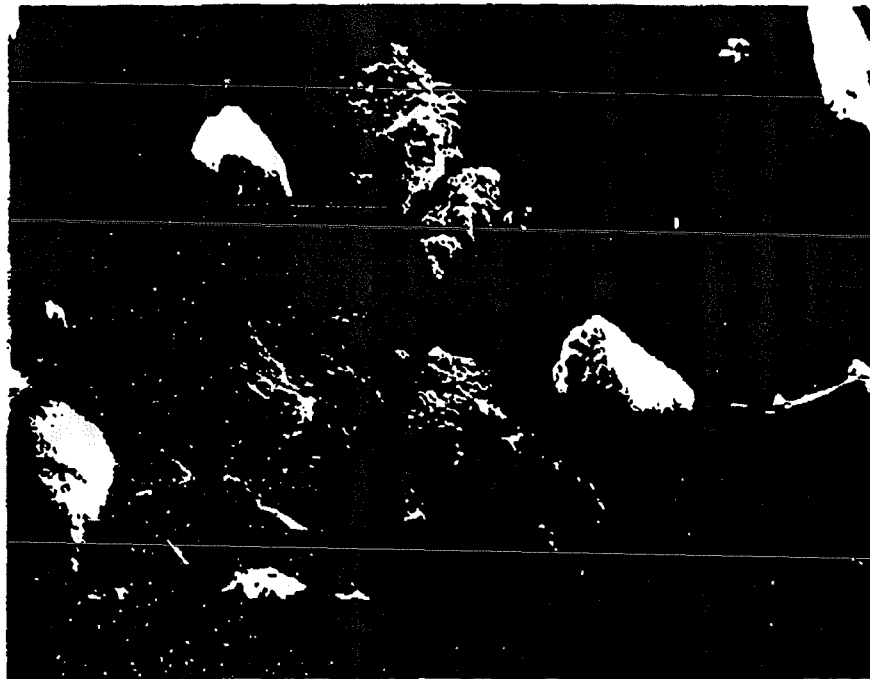
SLURRY CHIPS (3BaSO_4 , CaF_2 , SiO_2)

FIGURE 4. SAMPLE #19 (4650' OPEN HOLE)



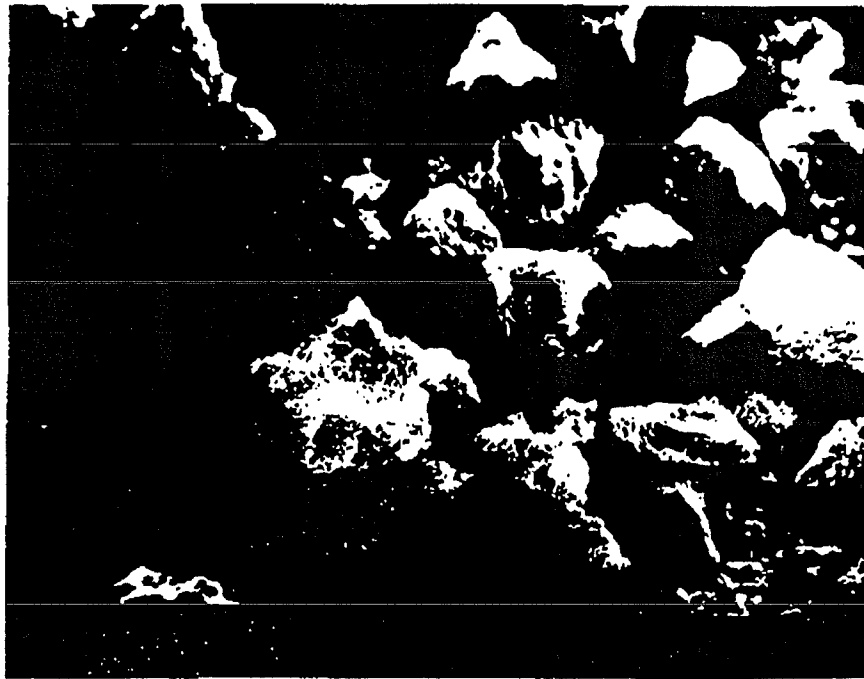
LIGHT MATERIAL - QUARTZ, FELDSPAR
DARK MATERIAL - SCALE ($BaSO_4$, SiO_2)

FIGURE 5. SAMPLE #25 (6150' - OPEN HOLE)



PRIMARY FORMATION (QUARTZ, FELDSPAR)
MINOR SCALE ($BaSO_4$, SiO_2)

FIGURE 6. SAMPLE #31 (4100' OUTSIDE CASING)



LIGHT MATERIAL - FORMATION (QUARTZ, FELDSPAR)

DARK MATERIAL - $BasO_4$ Scale + Amorphous SiO_2

APPENDIX

Scale Sample Descriptions

UNOCAL

October 3, 1990

Darrell Gallup
Unocal Corporation
Science and Technology
Division
Rm. I-105
P.O. Box 76
376 S. Valencia
Brea, CA 92621

Dear Mr. Gallup:

Scale samples retrieved from the casing and cuttings from the open hole section of Sinclair 21 are enclosed. Chemical analysis of the samples by X-ray diffraction and SEM would prove useful in studying our injection process and could lead to a possible decrease in workover frequency. The operating history and sample collection process are discussed below.

Sinclair 21 was originally drilled and completed in May, 1988 in the Salton Sea Field in Imperial County California. Commercial injection commenced on February 14, 1989. The initial performance of the well was determined to be 1575 (Klb/hr) with a well head pressure of 0 (Psi) from a high rate test performed in March 1989 (See Figure 1). The well was on line continuously until April 4, 1990 when it was shut in for the Unit 3 turnaround. The well was put back on line May 1, 1990 following completion of the turnaround with a significant reduction in injection capacity. Also, on May 1, 1990 the line mine was put into operation including acid injection upstream of the line mine. Injection continued until June 6, 1990 at which time the well was shut in for a clean out.

A total of 11,333 MMBbls of brine have been injected into Sinclair 21 over an operating period of 487 days. Injection rate vs time and wellhead pressure vs time for Sinclair 21 are shown in Figure 2. Periodically samples of the injection brine are collected and analyzed. The chemical data is summarized in Tables 1 and 2.

The clean out began on June 14, 1990. A plug was set in the 9-5/8 inch casing at 2920 feet to insure complete recovery of the scale while scraping the casing. All samples were collected from the

shale shaker and depths were approximated. Samples were collected every 250 feet from the cased portion of the well to 2917 feet and every 250 feet from the open hole section to 6850 feet (See Table 3). The samples were prepared by Alex Schriener and have been washed with tap water and air dried.

If any further information is required please contact me in Indio at (619) 342-4723.

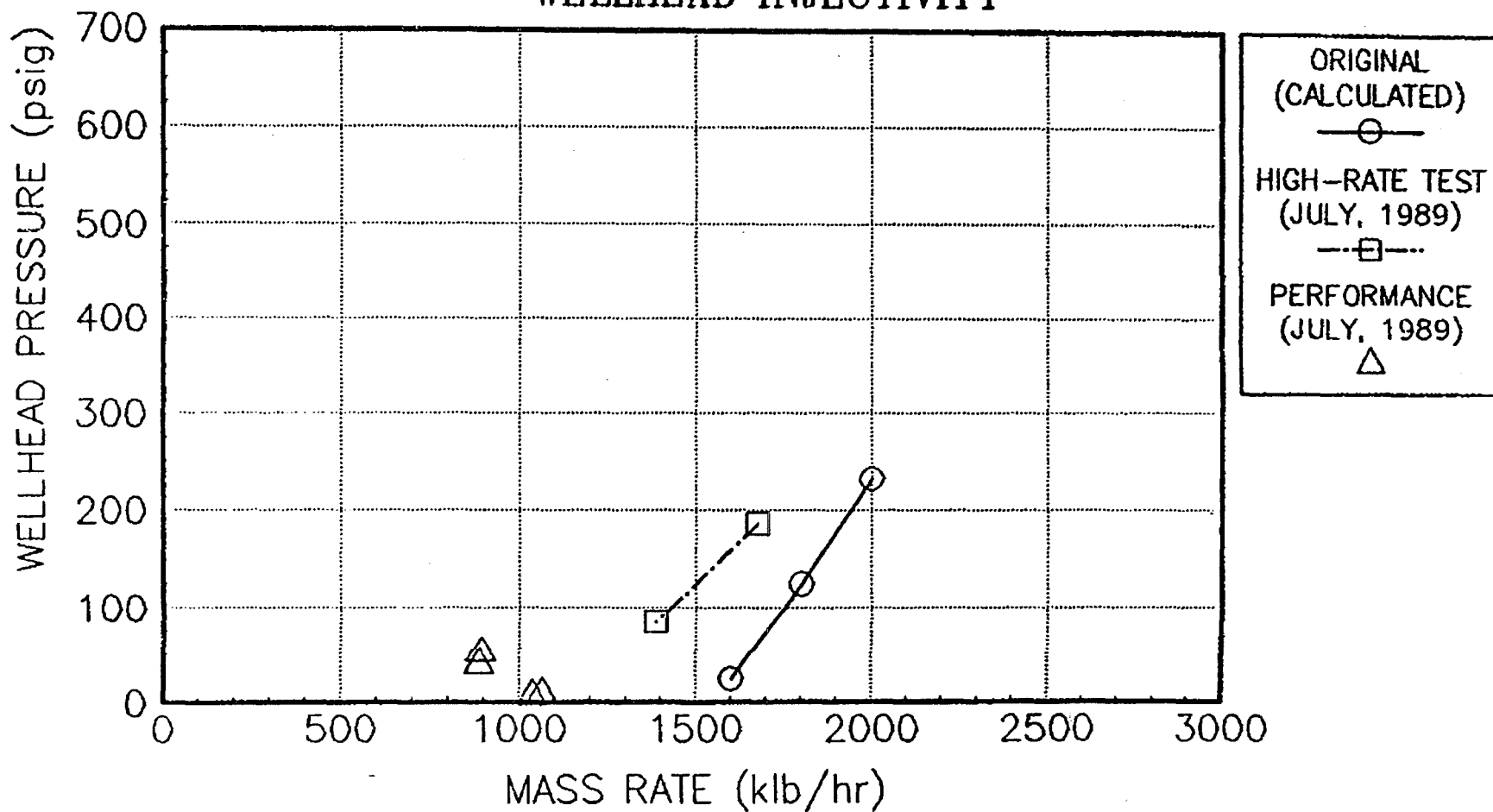
Sincerely yours,

Robert J. Swanson

Robert J. Swanson

RJS:rjs
Attachments

FIGURE 1
SINCLAIR 21
WELLHEAD INJECTIVITY



Conditions for calculated injectivity
 csg ID:8.84 Shoe:3064 Hole ID:8.75 MPI:5020
 Visc:.42 kh:122000 sg:1.21 PWS:2093 Date:3-89

MATCHED DATA FROM HIGH RATE TEST
 PERFORMED MARCH, 1989.

FIGURE 2

Sinclair 21

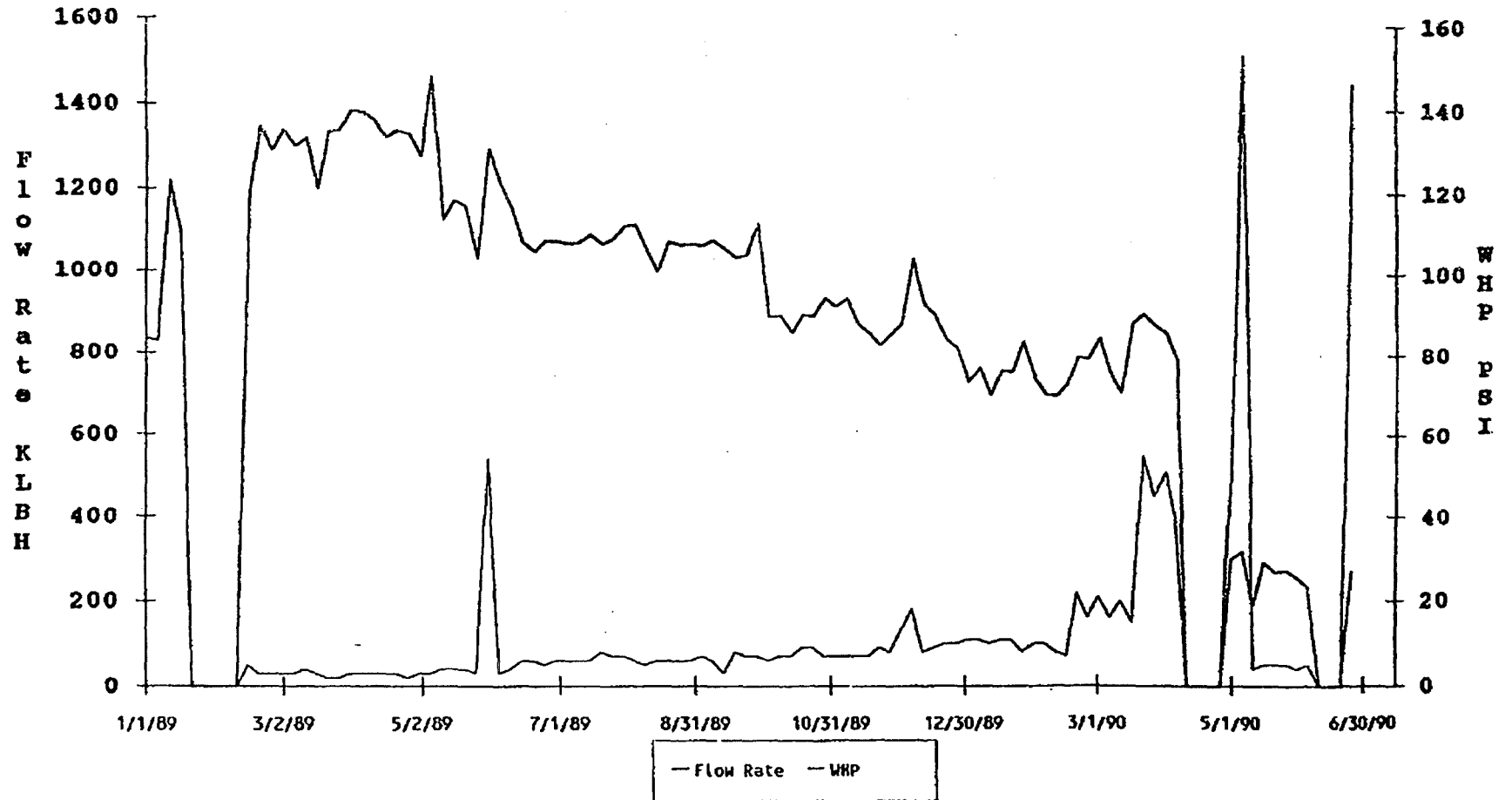


TABLE 1

SINCLAIR 21 INJECTION BRINE
 CHEMICAL ANALYSIS ADJUSTED TO PPM
 FLASH CORRECTED

DATE	2/24/89	6/9/89	9/8/89	11/2/89	3/19/90
S.G.	1.23	1.235	1.233	1.232	1.241
TDS	310199	303459	296497	302384	291853
Ag	1.02	1.01	0.84	1.25	1.241
As	19.8	15.7	18.4	17.7	14.8
B	422	294	407	414	396
Ca	32114	30668	31130	32011	31807
Cs	NA	NA	NA	NA	NA
Cu	4.02	3.62	4.45	5.11	4.43
Fe	1156	1102	1065	1055	1009
K	17975	17645	17123	17631	17052
Li	240	233	227	229	222
Mg	46.5	43.5	49.3	46.8	45.8
Mn	1163	1121	1089	1093	1042
Na	69385	68573	67750	67877	66504
Ba	281	267	263	265	253
Pb	103	102	99	101	97
Rb	NA	NA	NA	NA	NA
Sr	565	559	546	555	536
Zn	422	412	406	399	382
Br	115	130	114	128	109
Cl	184610	181700	175588	179951	171797
F	9.7	12.6	9.7	7.6	3.7
I	16.3	12.1	6.5	4.9	7.7
SO4	41.5	30	17.2	8.1	1
NH4	356	380	410	406	428
SiO2	153	155	167	179	149

TABLE 2

TABLE 3
SAMPLE DEPTHS

<u>SAMPLE No.</u>	DEPTH OF CASING SAMPLES	<u>SAMPLE No.</u>	DEPTH OF OPEN HOLE SAMPLES
1	50'	29	3150'
2	250'	30	3575'
3	500'	31	4100'
4	750'	18	4418'
5	1000'	19	4650'
6	1250'	20	4900'
7	1500' B	21	5150'
8	1500' A	22	5400'
9	1750' B	23	5650'
10	1750' A	24	5900'
11	2000' B	25	6150'
12	2000' A	26	6400'
13	2250' B	27	6650'
14	2250' A	28	6850'
15	2500'		
16	2750'		
17	2917' B		
-	2917' A		

B = BEFORE SWEEP
A = AFTER SWEEP



UNOCAL

Department: Products, Processes &
Materials Research

Project: 745-73410

Project Title: Geothermal Scale
Characterization

Date: October 20, 1989

Report Title: SALTON SEA SCALE
ANALYSES - OCTOBER 1989

Report: PMR 89-159R

Investigators: D. L. Gallup, I
M. E. Obando, M-TR

Manager: K. Baron, AD

CONFIDENTIAL

cc: Library (2)
Patent

S. K. Alley, AD
J. L. Featherstone, Calipatria
M. M. Hatter, R
P. F. Helfrey, R
L. D. Krenzke, I
B. J. Kelly, R
M. D. Mosby, Indio

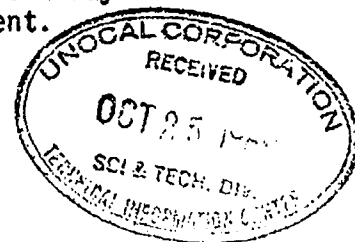
C. T. Ratcliffe, I
A. Schriener, Indio
H. D. Simpson, I
R. N. Upadhyay, AD
J. W. Ward, AD
O. D. Whitescarver, Indio (4)
M. M. Wong, I

Eight scale samples collected from the Salton Sea geothermal field were recently analyzed. This group of scales was collected from the Sinclair 15 and Sinclair 25 injection wells. The attached Appendix describes the scales collected by Geothermal Division personnel. The attached Tables present the results of the standard elemental and mineral analyses.

Samples 1 through 4 were retrieved from the Sinclair 15 hangdown string. Samples 1 through 3 are similar in composition and consist primarily of barite, fluorite, and non-crystalline iron silicate. Sample 4 is different from samples 1-3. In addition to the above compounds Sample 4 contains silver, copper, arsenic and antimony. Calcium sulfate was also detected in low concentrations.

Samples 5 through 8 were extracted from the Sinclair 25 hangdown string. Analysis of Sample 5 revealed moderate amounts of barite, fluorite, non-crystalline iron silicate and elemental silver. Arsenic is also present in low concentrations. Samples 6 and 7 are similar in composition consisting of barite, fluorite and non-crystalline iron silicate. Arsenic is not present and just traces of silver were found. Sample 8 consists primarily of dyscracite (Ag_3Sb) and domeykite (Cu_3As). X-ray diffraction showed that barite, calcite and quartz are also present.

CONFIDENTIAL

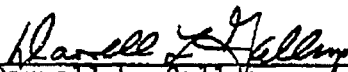


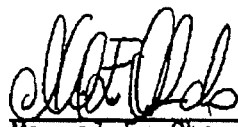
October 20, 1989

Figures 1A through 1D consist of scanning electron micrographs and x-ray fluorescence analyses of a shale pebble retrieved from plugged drill pipe in Sinclair 25. These formation-scale samples were collected by Mr. Alex Schriener, Geothermal Division. The analyses show that the shale is non-porous and consists of alumino-silicate and brine evaporites. Scale deposited on the surface of the shale consists of brine suspended solids cemented with silica scale. The suspended solids consist of iron silicate, barite and fluorite.

Figures 2A through 2F show scanning electron micrographs and x-ray fluorescence analyses of a sandstone pebble also retrieved from Sinclair 25. The sandstone matrix is porous and contains clays. The sandstone exhibits an iron to silicon ratio of about one to nine, and also contains traces of alumino-silicates and what appears to be sphalerite (ZnS). Scale coating the sandstone again consists of cemented suspended solids exhibiting an iron to silicon ratio of 1:1.3. There is no evidence to suggest that the suspended solids plugged the matrix porosity. Figures 2E and 2F show a very thin scale coating consisting of iron silicate (iron:silicon ratio = 1:5).

The scale is tightly bound to the rock samples. This suggests that flowing cleanouts of injection wells may not remove these scales to restore injectivity. It appears that these scales can only be removed by acid dissolution. It may be interesting to determine the extent of scale deposition in the reservoir by obtaining sidewall cores in these wells in the future.


Darrell L. Gallup
Sr. Research Associate


Manuel E. Obando
Research Technician

DLG/MEO(ss)
Attachments

TABLE 1

X-RAY DIFFRACTION RESULTS

<u>SAMPLE NO.</u>	<u>DESCRIPTION</u>	<u>(>20%)</u> <u>MAJOR</u>	<u>(5-20%)</u> <u>MODERATE</u>	<u>(<5%)</u> <u>TRACE</u>
1	Sin-15 #1		BaSO ₄ , CaF ₂ , Non-crystalline	
2	Sin-15 #2		BaSO ₄ , CaF ₂ , Non-crystalline	
3	Sin-15 #3		BaSO ₄ , CaF ₂ , Non-crystalline	
4	Sin-15 #4		BaSO ₄ , CaF ₂	CaSO ₄ , Non-crystalline
5	Sin-25 #1		Ag, BaSO ₄ , CaF ₂ , Non-crystalline	
6	Sin-25 #2		BaSO ₄ , CaF ₂	Non-crystalline
7	Sin-25 #3		BaSO ₄ , CaF ₂ , Non-crystalline	
8	Sin-25 #4	Ag ₃ Sb, Cu ₃ As	Quartz, CaCO ₃	BaSO ₄

TABLE 2
QUALITATIVE ANALYSIS

<u>SAMPLE NO.</u>	<u>(>10%) MAJOR</u>	<u>(1-10%) MODERATE</u>	<u>(0.1-1%) SLIGHT</u>	<u>(<0.1%) TRACE</u>
1	Ca, Si	Ba, Fe	Cu, Mn, Sr	Ag, Al, B, Cr, Mo, Na, Pb
2	Ca, Si	Ba, Fe	Cu, Mn, Na	Ag, Al, Cr, Cu, Pb, Zn
3	Ca	Ba, Fe, Si	Mn, Sr	Ag, Al, Cr, Cu, Mo, Na, Pb, Zn
4	As, Cu	Ag, Fe, Si, Sb	Mn, Na	Ca, Pb, Sr
5	Ag, Ba, Fe, Si	Ca, Cu, Sb	Al, As, Cr, Mn, Na, Sr	B, Pb
6	Ca	Ba, Fe, Si	Cu, Mn, Sr	Ag, Al, Cr, Na
7	Ca	Ba, Fe, Si	Mn, Sr	Ag, Al, B, Cu, Na
8	Ag, As, Cu, Sb	Fe, Si	Na	B, Ca, Mn, Pb, Sr

TABLE 3
QUANTITATIVE ANALYSIS (wt%)

<u>SAMPLE NO.</u>	<u>As</u>	<u>As</u>	<u>Ba</u>	<u>Ca</u>	<u>Cu</u>	<u>Fe</u>	<u>Mg</u>	<u>Mn</u>	<u>Na</u>	<u>S</u>	<u>Sb</u>	<u>Si</u>
1	0.005	0.11	6.3	3.9	<0.1	10.3	<0.1	0.3	0.2	1.5	0.1	25.6
2	0.003	<0.1	6.7	4.0	<0.1	10.1	<0.1	0.3	0.1	1.6	0.1	25.4
3	0.002	<0.1	7.1	4.3	<0.1	10.6	<0.1	0.3	0.1	1.7	0.1	20.0
4	1.6	4.3	4.9	3.3	13.7	17.7	0.3	0.5	0.6	1.1	4.4	11.5
5	12	0.83	4.3	7.0	2.6	9.0	<0.1	0.3	0.2	1.0	1.0	18.0
6	0.04	<0.1	4.9	6.6	0.2	14.9	<0.1	0.5	0.3	1.1	0.1	20.2
7	0.008	<0.1	5.7	6.0	<0.1	16.0	<0.1	0.5	0.3	1.3	0.1	20.1
8	10	3.9	1.9	1.2	41.0	3.6	<0.1	0.1	0.2	0.4	18.0	4.8

TABLE 4
SCALE CALCULATED COMPOSITIONS (wt%)

<u>NO.</u>	<u>Pb3Sb</u>	<u>BaSO4</u>	<u>CaF2</u>	<u>Cu3As</u>	<u>Fe3O4</u>	<u>Mn2O3</u>	<u>SiO2</u>	<u>TOTAL</u>
1	0.1	10.7	7.6	0.2	14.2	0.4	54.8	88.1
2	0.1	11.4	7.8	0.2	13.9	0.4	54.4	88.2
3	0.1	12.1	8.4	0.2	14.6	0.4	51.4	87.2
4	6.0	8.3	6.4	18.0	24.4	0.7	24.6	88.5
5	13.0	7.3	13.7	3.4	12.4	0.4	38.5	88.7
6	0.1	8.3	12.9	0.3	20.6	0.7	43.2	86.2
7	0.1	9.7	11.7	0.2	22.1	0.7	43.0	87.5
8	28.0	3.2	2.3	44.9	5.0	0.1	10.3	93.9

Figure 1A. SEM and EDX of Shale Pebble from Plugged Drill Pipe at 4839 feet-Sinclair-25.

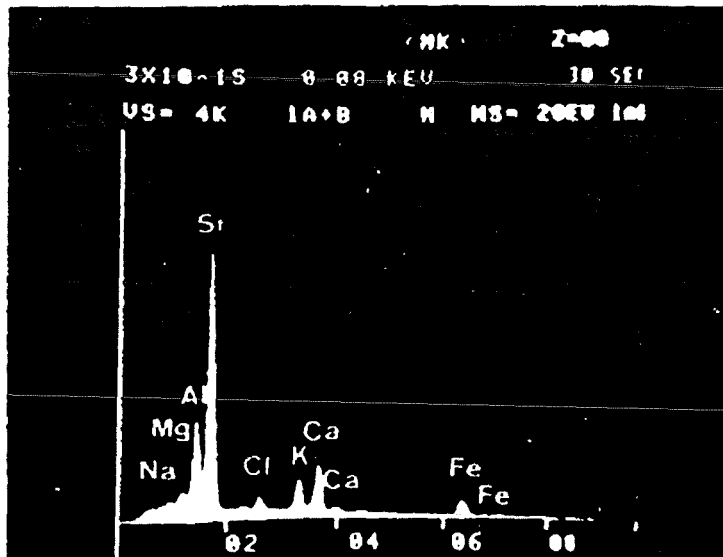
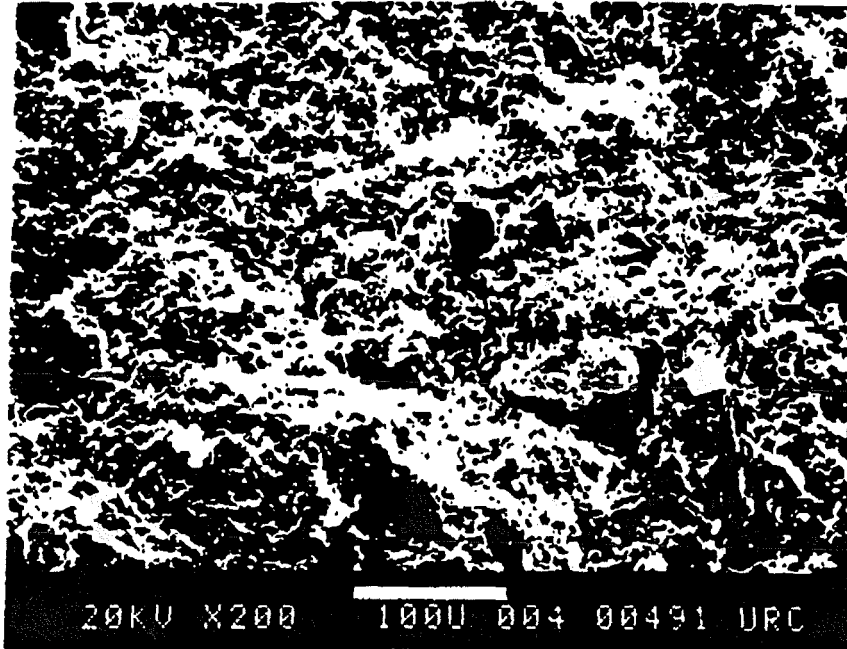
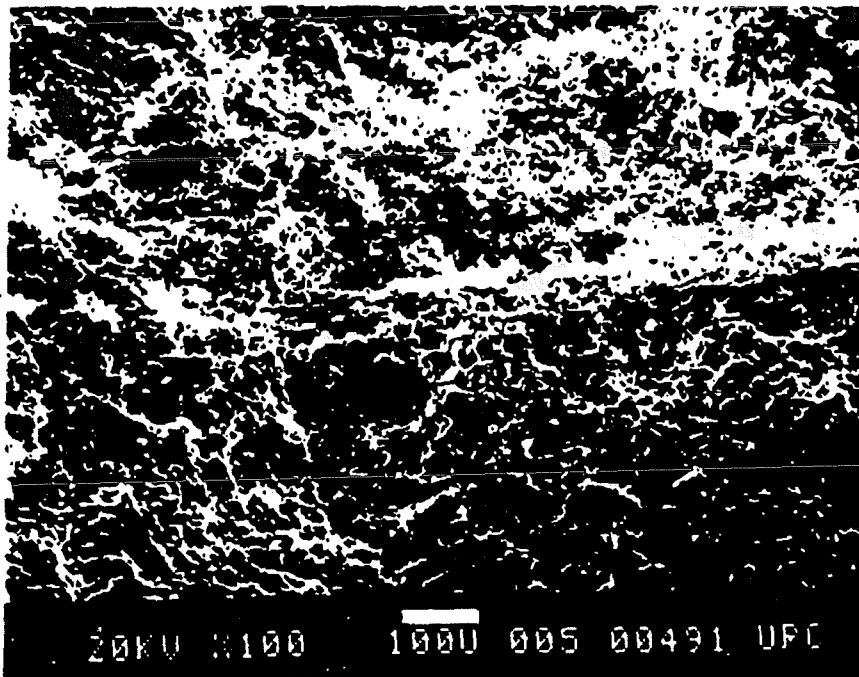
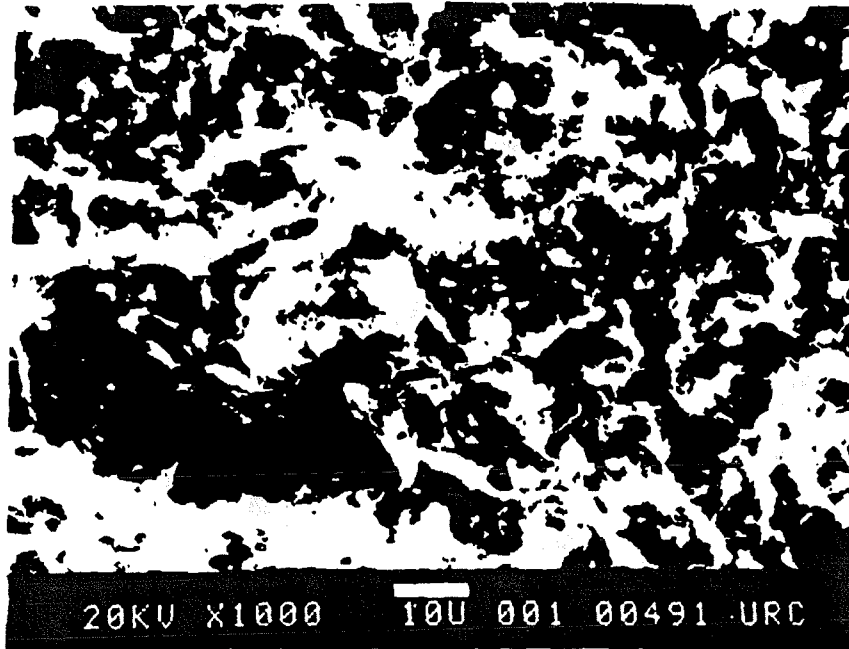


Figure IB. SEMs of Shale Pebble and Scale Coating Interface.



SHALE BLACK SURFACE A SCALE

4-1-73

Figure IC. SEMs of Scale Coating on Shale Pebble.

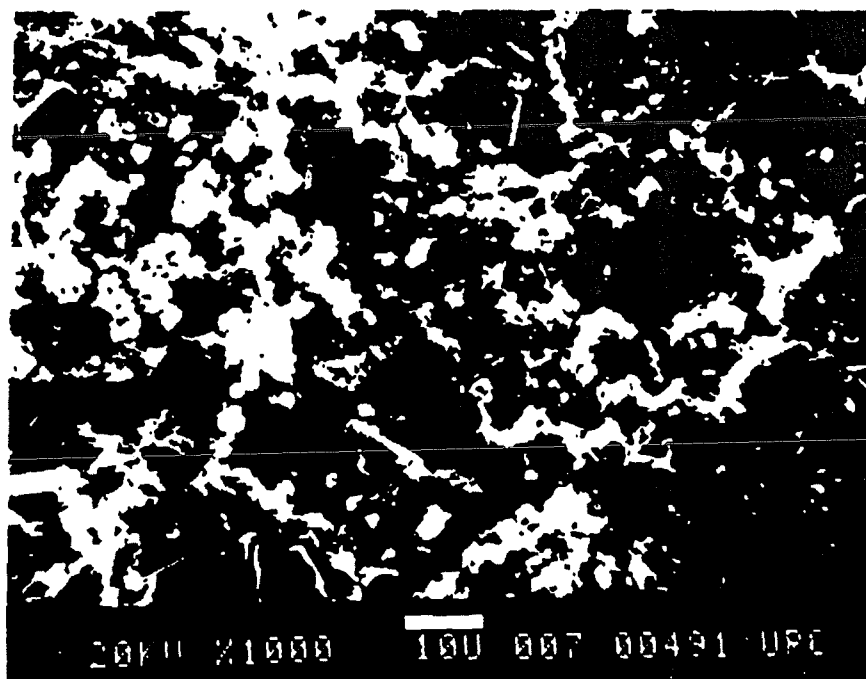
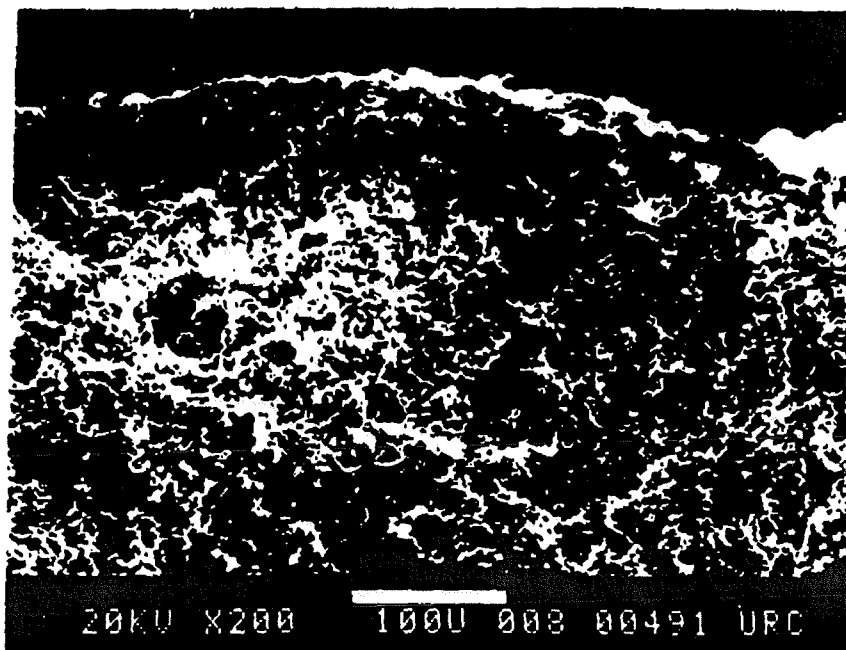


Figure ID. EDX of Scale Coating on Shale Pebble.

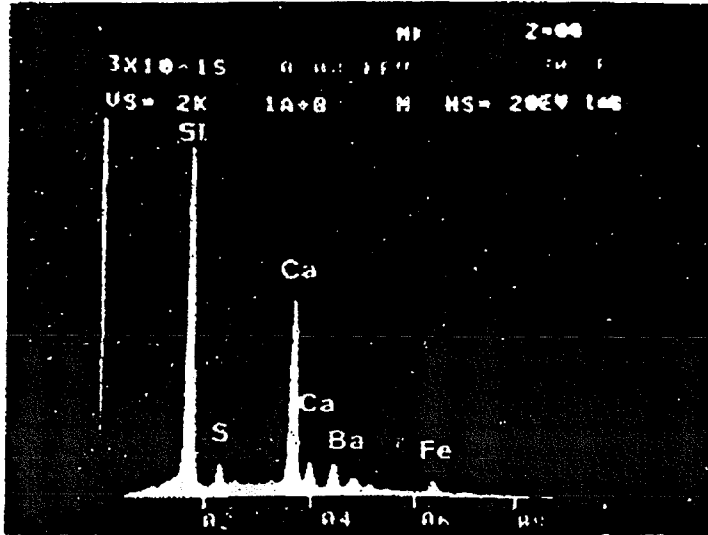


Figure 2B. SEMs of Sandstone with Scale Coating.

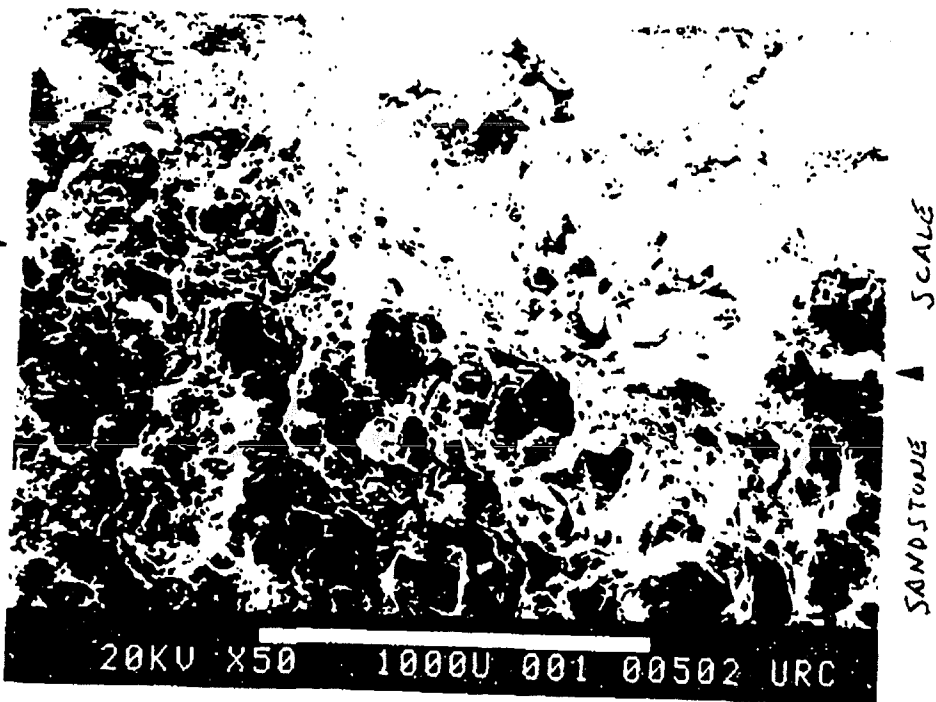
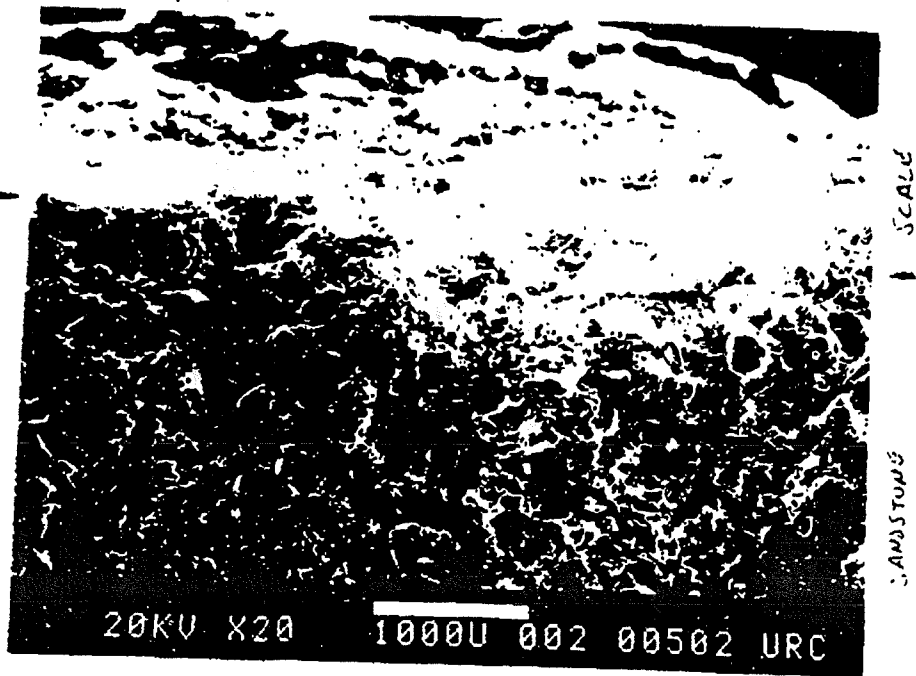
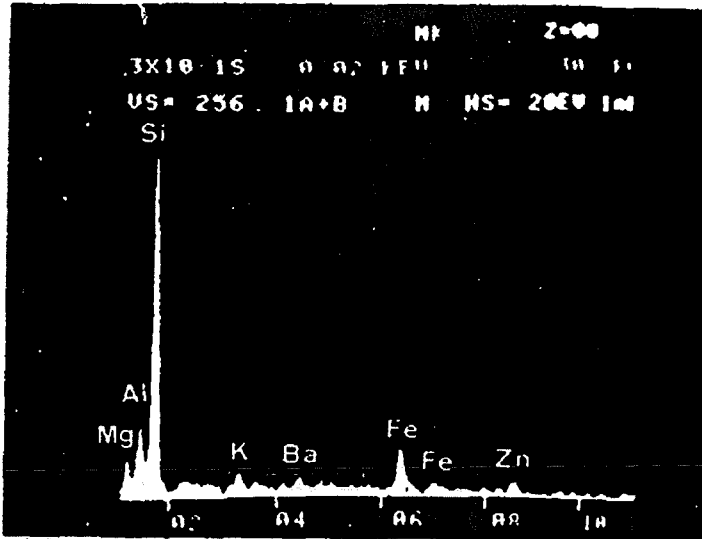


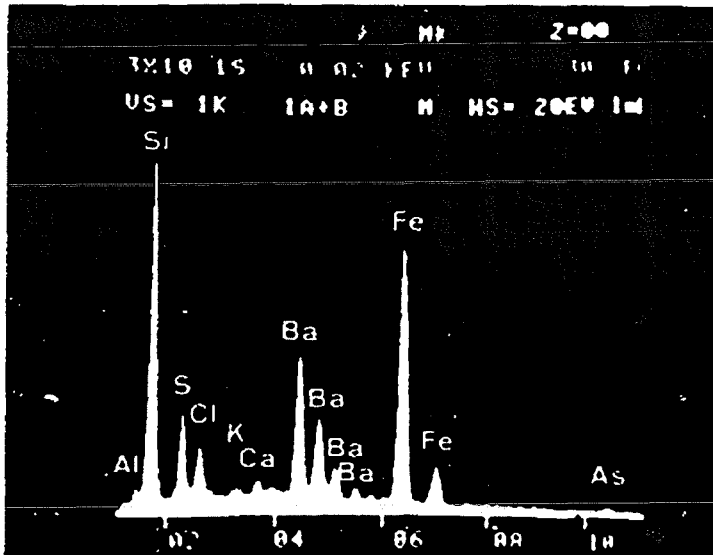
Figure 2C. EDXs of Sandstone and Scale Coating.



Side 1 clean
clays ZnS in
Quartz Matrix
Fe:Si → 1.25:9.0
No scale penetrated
the matrix.

SANDSTONE

SIN-25-A EDX FIELD SIDE 1 (2) @ 50X



Suspended Solids
are counted
together w/ SiO₂
Fe:Si = 7:9

SCALE

SIN-25-A EDX FIELD PHOTO (2) @ 50X

Figure 20. SEMs of Scale Coating on Sandstone Pebble.

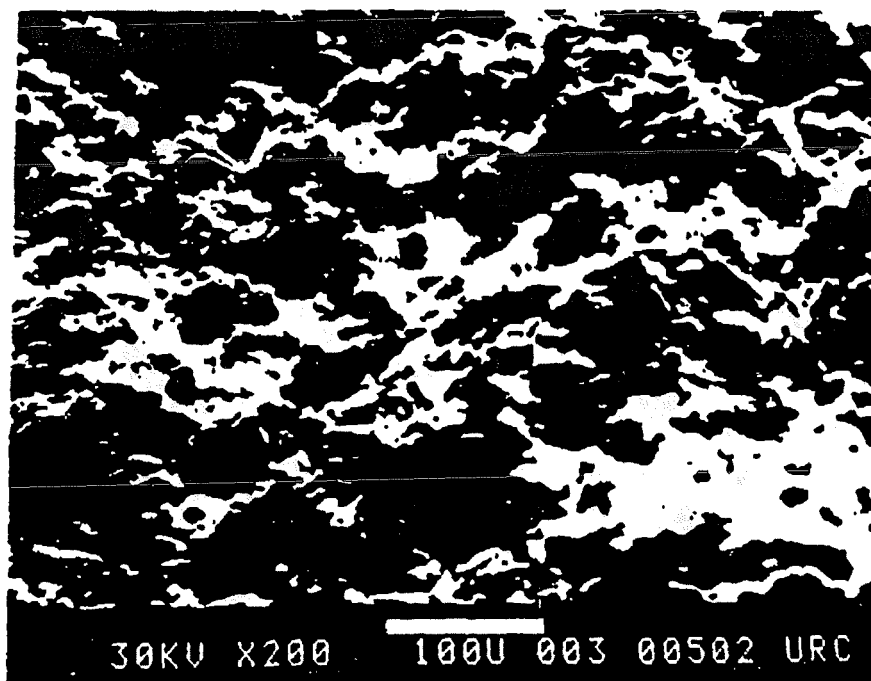
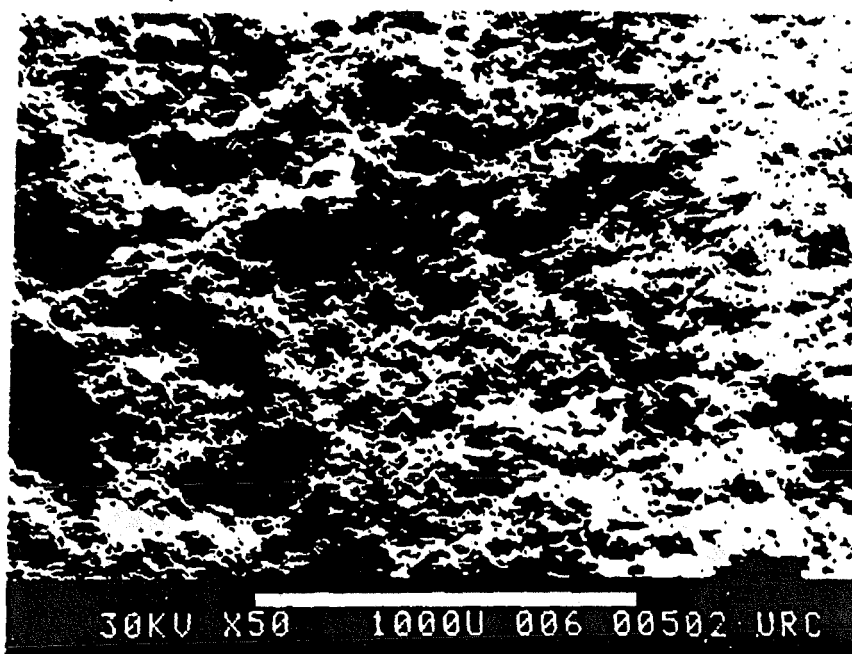
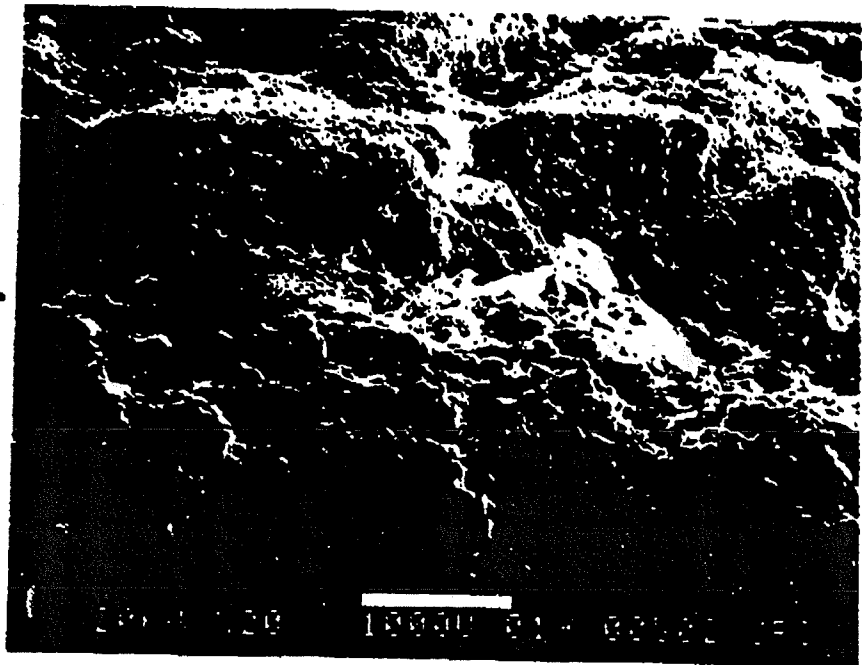
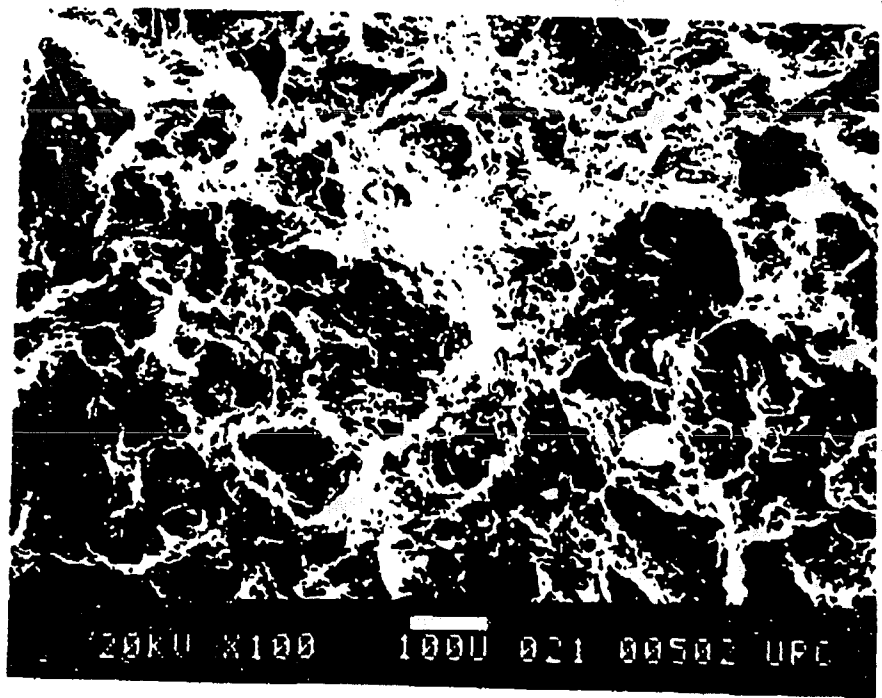


Figure 2E. SEM of Scale Coating on Sandstone Pebble and Sandstone Matrix.

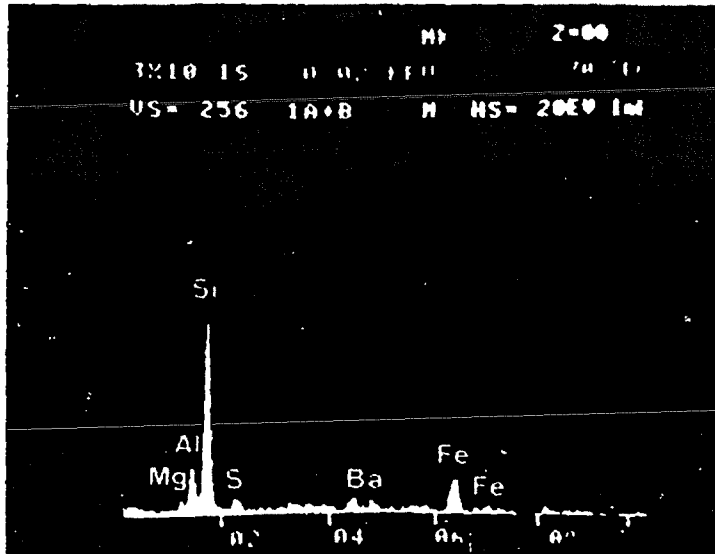
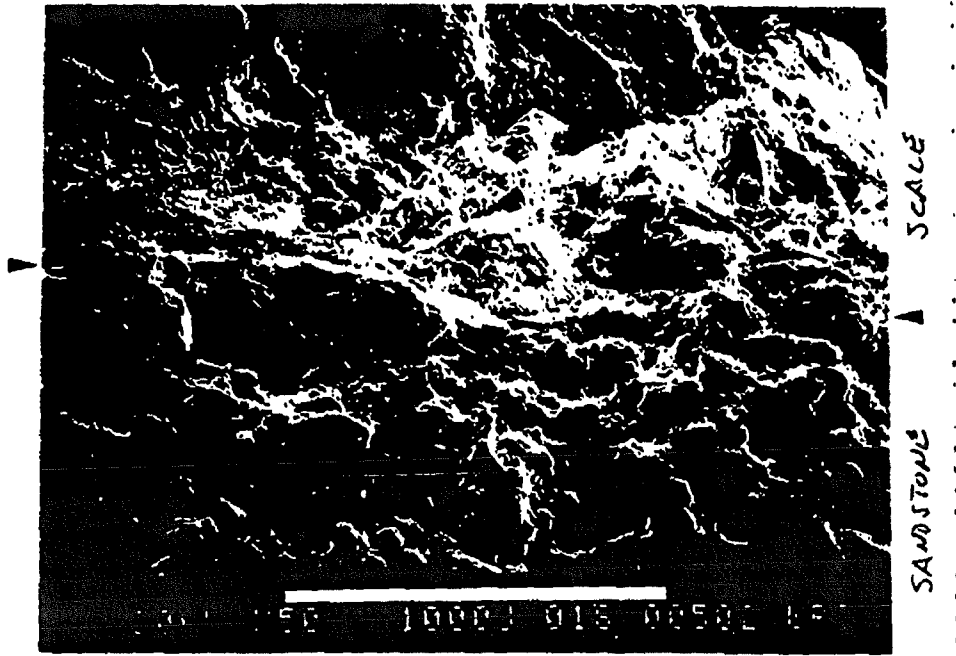


SANDSTONE
SCALE



MATRIX

Figure 2F. SEM and EDX of Scale Coating on Sandstone Pebble.



SIN-75-A FAX FIELD SIDE 2 (:) 50X

15 15:51

SCALE

APPENDIX

Scale Sample Descriptions

September 22, 1989

TO: Darrell Gallup
FM: Mark D. Mosby *MDM/pcl*
RE: Sinclair 15 Scale Samples from the 8-5/8"
Hangdown String: August 1989 Inspection

A high alloy string was installed in well Sinclair 15 for 918 days from February 12, 1987 to August 18, 1989. The well was on injection during this time for 284 days (1987 and 1988). Prior to retrieving the hangdown string the well had been shut-in since December 13, 1988.

A thin, brittle, reddish brown layered scale deposit was present over the entire internal surface. Enclosed are four scale samples taken from different depths. Please analyze these samples for the usual constituents.

Tables 1 and 2 summarize the injection history and chemistry of the fluids being injected into Sinclair 15. The scaling rates for this run are similar to the scaling rates from previous runs. I will appreciate any comments you may have on the mechanism that controls the Sinclair injection wells' scale deposition and possible chemical ways to reduce or remove the wellbore scale deposits.

MDM/pcl
cc: John D. Bush
Greg Gritters
Sinclair 15 Well File (August, 1989)

TABLE 1
WELL SINCLAIR 15
SCALE SAMPLE DESCRIPTION

FIELD: Salton Sea

WELL: Sinclair 15 RD-1

CASING STRING: 8-5/8" Mixed High Alloy

EXPOSURE TIME: 2/12/87 to 8/18/89 - 918 Days

INJECTION TIME: 6/23/87 to 8/07/87 - 45 Days

9/04/87 to 4/15/88 - 223 Days

11/28/88 to 12/13/88 - 16 Days

TOTAL - 284 Days

INJECTION RATE: Average Rate - 300 KPH

WHP - 75 psig

WHT - 220°F

TDS - 27

SCALE SAMPLE DEPTHS AND DESCRIPTION

<u>Sample No.</u>	<u>Joint No.</u>	<u>Alloy Type</u>	<u>Depth</u>	<u>Scale Thickness</u>
1	83	IN 825	49'	1/8"
2	78	SM 3040	163'	1/8"
3	35	SM 25Cr	1818'	1/8"
4	1	SM 2550	3016'	1/8" - 1/2"

MDM/pcl
9/22/89
3932d

Sample Date	Unit 1 Sec. Clarifier	Sinclair 15 Inj. Brine	Sinclair 25 Inj. Brine
89-03-17	89-03-17	88-03-10	89-03-17
Analytes (Mg/lit)			
Ag	1.04	1.25	1.04
As	15.71	16.5	16.1
B	430	491	425
Ca	31,378	36,281	31,066
Cs	N/A	N/A	N/A
Cu	4.25	3.58	3.16
Fe	781	1,020	780
K	17,324	18,841	17,439
Li	240	260	242
Mg	140.3	104	138
Mn	1,028	1,200	1,027
Na	76,037	79,563	76,401
Ba	163	200	160
Pb	95.7	106	94.9
Rb	N/A	N/A	N/A
Sr	549	591	555
Zn	376	438	370
Br	142	24.0	142
Cl	195,300	206,000	193,100
F	13.1	11.0	12.2
I	19.0	13.0	18.0
SO ₄	49	26	47.0
NH ₄	586	475	531
SiO ₂	210	215	256
TDS	324,883	345,881	322,829
Sp. Gravity(g/cc)	1.209	-	1.208

Table 2 - Salton Sea Unit 1 secondary clarifier, Sinclair 15 and Sinclair 25 injection brine chemistry: These are the original analysis from samples taken by David Rohrs.

MDM/pcl
9/22/89
3932d

UNOCAL

3934d

September 22, 1989

TO: Darrell Gallup
FM: Mark D. Mosby *MDM/pcl*
RE: Sinclair 25 Scale Samples from the 7"
Hangdown String: September 1989 Inspection

A 9Cr-1Mo 7" hangdown casing string was installed in well Sinclair 25 for 2,311 days (6.33 years) from May 22, 1983, to September 19, 1989. The well was on injection for approximately 474 days during this period (1988 and 1989). In 1989, from June 21, 1989, through early September 11, 1989 the well was receiving slightly acidified brine (3 gpm) during the injection line mine experiment.

A thin, brittle, reddish brown layered scale deposit was present over the entire internal surface. Enclosed are three scale samples taken from various hangdown string depths. Please analyze these samples for the usual constituents.

Tables 1 and 2 summarize the injection history and chemistry of the fluids being injected into Sinclair 25.

MDM/pcl

cc: John D. Bush
Greg Gritters
Sinclair 25 Well File (September, 1989)

TABLE 1
WELL SINCLAIR 25
SCALE SAMPLE DESCRIPTION

FIELD: Salton Sea

WELL: Sinclair 25

CASING STRING: 7" 9Cr-1Mo

EXPOSURE TIME: 5/22/83 to 9/19/89 - (2,311 Days or 6.33 years)

INJECTION TIME: 4/05/88 to 4/14/88

4/27/88 to 10/29/88

11/03/88 to 4/15/88

5/19/89 to 9/11/89 TOTAL DAYS = 474

INJECTION RATE: Average Rate - 480 KPH

WHP - 0-60 psig

WHT - 210-225°F

TDS - 27

SCALE SAMPLE DEPTHS AND DESCRIPTION

<u>Sample No.</u>	<u>Joint No.</u>	<u>Depth</u>	<u>Scale Thickness</u>
1	80	62'	1/8"
2	40	1570'	1/8"
3	20	2356'	1/8"
4	1	3140'	1/4" - 1/2"

MDM/pcl
9/22/89
3934d

Sample Date	Unit 1 Sec. Clarifier	Sinclair 15 Ini. Brine	Sinclair 25 Ini. Brine
	89-03-17	88-03-10	89-03-17
Analytes (Mg/lit)			
Ag	1.04	1.25	1.04
As	15.71	16.5	16.1
B	430	491	425
Ca	31,378	36,281	31,066
Cs	N/A	N/A	N/A
Cu	4.25	3.58	3.16
Fe	781	1,020	780
K	17,324	18,841	17,439
Li	240	260	242
Mg	140.3	104	138
Mn	1,028	1,200	1,027
Na	76,037	79,563	76,401
Ba	163	200	160
Pb	95.7	106	94.9
Rb	N/A	N/A	N/A
Sr	549	591	555
Zn	376	438	370
Br	142	24.0	142
Cl	195,300	206,000	193,100
F	13.1	11.0	12.2
I	19.0	13.0	18.0
SO ₄	49	26	47.0
NH ₄	586	475	531
SiO ₂	210	215	256
TDS	324,883	345,881	322,829
Sp. Gravity(g/cc)	1.209	-	1.208

Table 2 - Salton Sea Unit 1 secondary clarifier, Sinclair 15 and Sinclair 25 injection brine chemistry: These are the original analysis from samples taken by David Rohrs.

MDM/pcl
9/22/89
3934d